



ΠΑΝΕΠΙΣΤΗΜΙΟ ΙΩΑΝΝΙΝΩΝ  
ΣΧΟΛΗ ΘΕΤΙΚΩΝ ΕΠΙΣΤΗΜΩΝ  
ΤΜΗΜΑ ΦΥΣΙΚΗΣ

Εντοπισμός Anderson και Τοπολογικά  
Φαινόμενα σε Συστήματα Πολλών  
Σωματίων με Αταξία

Γεώργιος Θ. Σταματίου

*ΔΙΔΑΚΤΟΡΙΚΗ ΔΙΑΤΡΙΒΗ*

ΙΩΑΝΝΙΝΑ

2020





UNIVERSITY OF IOANNINA  
SCHOOL OF SCIENCES  
DEPARTMENT OF PHYSICS

# Anderson Localization and Topological Phenomena in Disordered Many-Body Systems

George T. Stamatiou

*Ph.D. THESIS*

IOANNINA

2020



**Advisory Committee:**

- S.N.Evangelou, Professor, Department of Physics, University of Ioannina (supervisor)
- F.Diakonou, Associate Professor, Department of Physics, National and Kapodistrian University of Athens
- A.Karanikas, Associate Professor, Department of Physics, National and Kapodistrian University of Athens

**Examination Committee:**

- S.N.Evangelou, Professor, Department of Physics, University of Ioannina (supervisor)
- F.Diakonou, Associate Professor, Department of Physics, National and Kapodistrian University of Athens
- A.Karanikas, Associate Professor, Department of Physics, National and Kapodistrian University of Athens
- G.N.Throumoulopoulos, Professor, Department of Physics, University of Ioannina
- D.Katsanos, Lecturer, Department of Physics, University of Ioannina
- M.Kamaratos, Associate Professor, Department of Physics, University of Ioannina
- C.J.Lambert, Research Professor, Department of Physics, Lancaster University



# Abstract

The work in this thesis primarily addresses the effect of disorder in certain condensed matter systems. Disorder itself leads to the phenomenon of Anderson localization where the wavefunction due to disorder is confined in a finite region of space characterized by an exponential decay of its amplitude. First, we study the midgap state at energy  $E = 0$  in a lattice with hopping disorder in one and two dimensions. Using the well established methods of energy and wavefunction statistics, we show an even-odd system size asymmetry and the multifractal behavior of the special  $E = 0$  state. Second, we examine the doubly degenerate Majorana states at  $E = 0$  for the case of a topological superconductor in one dimension. In the absence of disorder, the two states are localized at the two ends of the chain. We ask how the disorder affects their behavior for this kind of system proposed for quantum computation. In the presence of disorder, a spreading of the Majorana states in the lattice occurs. Third, we show the interplay of disorder and interactions in a many-body system, namely the quantum XXZ Heisenberg anti-ferromagnet. The motivation is to study how disorder leads to the phenomenon of Many-Body Localization. The energy level statistics shows a distinction between an ergodic and a many-body localized phase and the eigenstate statistics reveals a multifractal behavior near the critical regime. For strong disorder the many-body localized states can be used as potential quantum memories. The significance of this work is that the ubiquitous presence of disorder in quantum systems has not always a negative impact and can lead to a better manipulation of quantum information.

---

# Εκτεταμένη Περίληψη

Ένα από τα πιο ενδιαφέροντα θέματα της σύγχρονης Φυσικής είναι η κατανόηση των κβαντικών ιδιοτήτων της ύλης παρουσία αταξίας όταν η τοπολογία αλλά και οι αλληλεπιδράσεις παίζουν σημαντικό ρόλο. Η ισχυρή αταξία  $W$  οδηγεί στο φαινόμενο του εντοπισμού Anderson και μονωτική συμπεριφορά. Οι καταστάσεις περιορίζονται σε μία πεπερασμένη περιοχή του χώρου ενώ εκτός αυτής χαρακτηρίζονται από εκθετική μείωση. Από την άλλη, η παρουσία της τοπολογίας υποδηλώνει ανοσία ως ένα βαθμό στις τοπικές διαταραχές ενώ ο συνδυασμός αταξίας και αλληλεπιδράσεων οδηγεί στο φαινόμενο του Εντοπισμού Πολλών Σωματίων (Many-Body Localization ή MBL) και την απουσία εργοδικότητας στο σύστημα. Τα κβαντικά φαινόμενα παρουσία αταξίας, τοπολογίας και αλληλεπιδράσεων εμφανίζονται σε νανοδομές -τάξη μεγέθους του 1nm- από την κατασκευή των οποίων αναμένεται νέα φυσική αλλά και τεχνολογική πρόοδος. Η σύνδεση των παραπάνω συστημάτων με την κβαντική πληροφορική και την κατασκευή ανθεκτικών κβαντικών υπολογιστών με πλήθος qubits αποτελεί ένα από τα πιο σπουδαία επιστημονικά θέματα των ημερών.

Η παρούσα διδακτορική διατριβή έχει ως στόχο να ερευνήσει το ρόλο της αταξίας σε συγκεκριμένα συστήματα συμπυκνωμένης ύλης. Η κβαντική περιγραφή των ηλεκτρονίων στα στερεά παρουσία αταξίας γίνεται στην προσέγγιση ισχυρής δέσμευσης (tight binding). Στη διακριτή βάση του πλέγματος η κυματοσυνάρτηση ενός ηλεκτρονίου γράφεται ως κβαντική υπέρθεση στη βάση των πλεγματικών θέσεων ισχυρά εντοπισμένων ατομικών τροχιακών σε κάθε πλεγματική θέση. Η αντιμετώπιση των συστημάτων γίνεται με συνδυασμό αναλυτικών και αριθμητικών τεχνικών στη μία και στις δύο διαστάσεις όπου ξεκινώντας από συστήματα

---

μικρού μεγέθους προσεγγίζουμε τα μεγαλύτερα συστήματα με μια τεχνική γνωστή ως finite size scaling (FSS).

Ειδικότερα, εξετάζεται η στατιστική των ενεργειών και των καταστάσεων τυχαίων πινάκων (random matrices). Η θεωρία τυχαίων πινάκων (Random Matrix Theory) είναι το κατάλληλο μαθηματικό εργαλείο για να εξετάσουμε τη στατιστική των ενεργειών. Ανάλογα με την υπάρχουσα συμμετρία οι τυχαίοι πίνακες κατατάσσονται σε 10 κλάσεις συμμετρίας. Η κατάταξη γίνεται με βάση τη συμμετρία χρονικής αναστροφής (time reversal), τη συμμετρία σωματιούπολης (particle-hole) και τη συμμετρία χειρός (chiral). Η ορθογώνια κλάση για παρουσία τυχαίου δυναμικού, η μοναδιαία για παρουσία μαγνητικού πεδίου που παραβιάζει τη συμμετρία χρονικής αναστροφής και η συμπλεκτική για παρουσία σπιν με σύζευξη σπιν-στροφορμής (spin-orbit coupling). Από τις συνολικά 10 συμμετρίες έχουμε 3 βασικές (Wigner-Dyson), 3 που διατηρούν την συμμετρία χειρός (chiral) και 4 που σχετίζονται με την υπεραγωγιμότητα (Bogoliubov-de Gennes ή BdG). Ένα στατιστικό μέτρο για τη μελέτη των ενεργειών είναι η κατανομή  $P(S)$  των διαστημάτων μεταξύ των διαδοχικών ενεργειών. Στην περίπτωση μεταλλικής-εκτεταμένης συμπεριφοράς οι ιδιοτιμές ενέργειας είναι συσχετισμένες, εμφανίζουν άπωση και ακολουθούν την κατανομή Wigner. Από την άλλη, στη μονωτική-εντοπισμένη συμπεριφορά οι αντίστοιχες ιδιοτιμές ενέργειας είναι μη-συσχετισμένες, τυχαίες και εμφανίζουν έλξη υπακούοντας στην κατανομή Poisson. Οι κατανομές Wigner και Poisson αποτελούν τις δύο οριακές περιπτώσεις.

Εκτός από τις χβαντικές ενέργειες εξετάζεται η στατιστική των χβαντικών καταστάσεων. Μία χαρακτηριστική ποσότητα για τη μέτρηση της χωρικής έκτασης των καταστάσεων είναι ο δείκτης  $IPR$ . Για μία πλήρως εκτεταμένη-μεταλλική κατάσταση σε  $N$  πλεγματικές θέσεις έχουμε  $IPR = N^{-1}$  ενώ για μία πλήρως εντοπισμένη κατάσταση σε μία πλεγματική θέση έχουμε  $IPR = 1$ . Ακόμα, γίνεται διερεύνηση σχετικά με τις μορφοκλασματικές (fractal) ιδιότητες των ιδιοκαταστάσεων. Είναι γνωστό ότι ακριβώς στο κρίσιμο σημείο της μετάβασης μέταλλου-μονωτή οι ιδιοκαταστάσεις δεν είναι ούτε εκτεταμένες ούτε εντοπισμένες αλλά χαρακτηρίζονται

---

από μια κρίσιμη-πολυμορφοκλασματική συμπεριφορά. Ένα πολυμορφοκλασματικό (multifractal) είναι ένα μη-ομογενές μορφοκλασματικό του οποίου η διάσταση δεν χαρακτηρίζεται από έναν αριθμό αλλά έχουμε ένα ολόκληρο φάσμα μορφοκλασματικών διαστάσεων  $D_q$ . Πρόκειται για ένα γενικευμένο μέτρο για τον προσδιορισμό της χωρικής έκτασης των ιδιοκαταστάσεων. Στην ειδική περίπτωση που ο δείκτης  $q$  ισούται με 2, η αντίστοιχη μορφοκλασματική διάσταση είναι η  $D_2$ . Σε ένα μονοδιάστατο σύστημα (1D), μία πλήρως εκτεταμένη, μεταλλική κατάσταση έχει  $D_2 = 1$  ενώ μία πλήρως εντοπισμένη κατάσταση σε μία πλεγματική θέση έχει  $D_2 = 0$ . Τέλος, η διάσταση  $D_2$  για μία πολυμορφοκλασματική κατάσταση παίρνει ενδιάμεσες τιμές μεταξύ του 0 και του 1.

Η διατριβή χωρίζεται σε τρία κύρια μέρη. Στο πρώτο μέρος θεωρούμε την παρουσία αταξίας στους δεσμούς μεταξύ των ατόμων σε ένα στερεό με σκοπό να διατηρείται η υποπλεγματική συμμετρία (sublattice ή chiral). Αυτή η περίπτωση είναι γνωστή ως μη-διαγώνια αταξία (off-diagonal disorder). Επικεντρωνόμαστε στη συμπεριφορά της κατάστασης με ενέργεια  $E = 0$  η οποία εμφανίζεται μόνο σε συστήματα με περιττό αριθμό ατόμων  $N$  και την υπολογίζουμε αναλυτικά και αριθμητικά. Η συγκεκριμένη κατάσταση παρουσιάζει υπο-εκθετική μείωση σε αντίθεση με το φαινόμενο του εντοπισμού Anderson όπου μία κατάσταση χαρακτηρίζεται από εκθετική μείωση. Η κλιμάκωση της ποσότητας  $\ln\langle IPR \rangle$  με το λογάριθμο του αριθμού  $N$  οδηγεί στον υπολογισμό της μορφοκλασματικής διάστασης  $D_2$  η οποία μετρά τη χωρική έκταση της κατάστασης στο  $E = 0$  και αποκαλύπτει το πολυμορφοκλασματικό χαρακτήρα της. Για ασθενή αταξία ( $W \rightarrow 0$ ) η κατάσταση εμφανίζει πιο εκτεταμένη συμπεριφορά ( $D_2 \rightarrow 1$ ) και για πολύ ισχυρή αταξία έχει μία πιο εντοπισμένη εικόνα ( $D_2 \rightarrow 0$ ). Για ενδιάμεσες τιμές της αταξίας, η διάσταση  $D_2$  είναι μεταξύ 0 και 1 αναδεικνύοντας το πολυμορφοκλασματικό προφίλ της κατάστασης για  $E = 0$ . Επιπλέον μελετήθηκε η στατιστική των ενεργειών κοντά στην ενέργεια  $E = 0$  και βρέθηκε μία ταχύτερη προσέγγιση στο όριο της κατανομής Poisson για συστήματα άρτιου  $N$  σε σύγκριση με συστήματα περιττού  $N$ .

Για ένα τετραγωνικό πλέγμα στις δύο διαστάσεις (2D) η κατάσταση για ενέργεια  $E = 0$  εμ-

---

φανίζει πολυμορφοκλασματικά χαρακτηριστικά για συστήματα μικρότερα από το πολύ υψηλό μήκος εντοπισμού. Για ασθενή αταξία ( $W \rightarrow 0$ ) η κατάσταση για  $E = 0$  εμφανίζει πιο εκτεταμένη συμπεριφορά ( $D_2 \rightarrow 2$ ) και για πολύ ισχυρή αταξία έχει μία πιο εντοπισμένη εικόνα ( $D_2 \rightarrow 0$ ). Για ενδιάμεσες τιμές της αταξίας, η διάσταση  $D_2$  είναι μεταξύ 0 και 2. Ακόμα, υπολογίστηκε η στατιστική των ενεργειών κοντά στην ενέργεια  $E = 0$ . Για τα περιττά συστήματα εμφανίζεται η κατανομή Wigner αναλλοίωτη υπό αλλαγή κλίμακας ενώ τα άρτια συστήματα χαρακτηρίζονται από μία κατανομή ενδιάμεση των Wigner και Poisson.

Στο δεύτερο μέρος δείχνουμε το συνδυασμό μεταξύ αταξίας και τοπολογίας. Θεωρούμε έναν μονοδιάστατο p-wave υπεραγωγό παρουσία αταξίας στους δεσμούς μεταξύ των ατόμων. Το συγκεκριμένο μοντέλο έχει προταθεί για χρήση στους κβαντικούς υπολογιστές. Απουσία αταξίας, το σύστημα έχει δύο καταστάσεις Majorana για ενέργεια  $E = 0$  που είναι εντοπισμένες στα δύο άκρα του συστήματος και προστατεύονται από την τοπολογία. Στην περίπτωση αυτή υπολογίστηκε ο αριθμός περιέλιξης (winding number). Το βασικό κίνητρο εδώ είναι η μελέτη των ειδικών καταστάσεων Majorana υπό την επίδραση της αταξίας. Λόγω της εγγενούς συμμετρίας σωματίου-οπής στους υπεραγωγούς το σύστημα αποτελείται από δύο μονοδιάστατα συστήματα, ένα για ηλεκτρόνια και ένα για οπές. Αρχικά βρίσκουμε μία άρτια-περιττή ασυμμετρία μεταξύ των συστημάτων άρτιου και περιττού μεγέθους  $L$ . Τα συστήματα περιττού  $L$  εμφανίζουν διπλό εκφυλισμό στην ενέργεια  $E = 0$ . Επομένως έχουμε δύο καταστάσεις στην ενέργεια  $E = 0$  που αντιστοιχούν στα δύο οiwονεί-σωμάτια Majorana. Από την άλλη, τα άρτια συστήματα χαρακτηρίζονται από την ύπαρξη ενεργειακού χάσματος. Ο υπολογισμός της στατιστικής των ιδιοτιμών της ενέργειας έδειξε και πάλι μία ταχύτερη προσέγγιση στο όριο της κατανομής Poisson για τα άρτια συστήματα σε σύγκριση με τα περιττά. Τα αποτελέσματα αυτά είναι παρόμοια με αυτά που βρέθηκαν στο πρώτο μέρος για την περίπτωση της μη-διαγώνιας αταξίας και απουσία υπεραγωγιμότητας. Επιπλέον, παράγεται μία αναλυτική σχέση για την κατάσταση στο  $E = 0$  μέσω της μεθόδου των πινάκων μεταφοράς (transfer matrix method). Η κλιμάκωση της ποσότητας  $\ln\langle IPR \rangle$  με το μέγεθος του συστήματος  $L$  οδήγησε στον υπ-

---

ολογισμό της μορφοκλασματικής διάστασης  $D_2$ . Απουσία αταξίας οι καταστάσεις Majorana είναι εντοπισμένες στα άκρα και έχουμε  $D_2 = 0$ . Καθώς αυξάνουμε την ισχύ της αταξίας  $W$  οι καταστάσεις αρχίζουν να διαχέονται μέσα στο σύστημα και να εμφανίζουν πολυμορφοκλασματική εικόνα με  $0 < D_2 < 1$ .

Το τρίτο μέρος αφορά το συνδυασμό αταξίας και αλληλεπιδράσεων. Μελετάμε ένα πρόβλημα πολλών σωματίων (many-body problem) σε ένα πλέγμα  $N$  τυχαία αλληλεπιδρώντων φερμιονίων παρουσία τυχαίου δυναμικού στη μία διάσταση. Το συγκεκριμένο πρόβλημα μέσω του μετασχηματισμού Jordan-Wigner είναι ισοδύναμο του μονοδιάστατου χβαντικού μοντέλου Heisenberg που αποτελείται από  $N$  spins-1/2 παρουσία τυχαίου μαγνητικού πεδίου ισχύος  $W$  και τυχαίων αλληλεπιδράσεων ισχύος  $\delta$ . Το βασικό κίνητρο εδώ είναι η μελέτη του φαινομένου που είναι γνωστό ως Εντοπισμός Πολλών Σωματίων (MBL) το οποίο εμφανίζεται παρουσία αταξίας και αλληλεπιδράσεων. Λόγω του εκθετικά μεγάλου μεγέθους του many-body χώρου Hilbert το πρόβλημα αποτελεί μία δύσκολη υπολογιστική διαδικασία. Εκτελούμε ακριβή διαγωνοποίηση (exact diagonalization) και εξετάζουμε το κέντρο του many-body ενεργειακού φάσματος όπου η πυκνότητα ενέργειας είναι μεγαλύτερη. Αρχικά, υπολογίστηκε η στατιστική των many-body ιδιοτιμών της ενέργειας και βρέθηκε μια μετάβαση μεταξύ δύο ξεχωριστών φάσεων. Μίας εργοδικής-εκτεταμένης φάσης που χαρακτηρίζεται από την κατανομή Wigner και μίας many-body εντοπισμένης (MBL) φάσης που χαρακτηρίζεται από την κατανομή Poisson. Για τις τιμές της αταξίας που χρησιμοποιήθηκαν στις δύο παραμέτρους  $W$  και  $\delta$  έγινε μία εκτίμηση των δύο κρίσιμων σημείων μεταβάλλοντας το μέγεθος του συστήματος (scaling). Στη μία περίπτωση για  $\delta = 1$  και μεταβάλλοντας το  $W$  το κρίσιμο σημείο εκτιμήθηκε στο  $W_c \approx 2.4$ . Στη δεύτερη περίπτωση για  $W = 0.5$  και μεταβάλλοντας το  $\delta$  το κρίσιμο σημείο εκτιμήθηκε στο  $\delta_c \approx 7$ . Επιπλέον, μελετήθηκε η στατιστική των many-body καταστάσεων. Η κλιμάκωση της ποσότητας  $\langle \ln IPR \rangle$  με το μέγεθος του συστήματος συμφωνεί στην εκτίμηση των κρίσιμων σημείων με τη στατιστική των ενεργειών. Ακόμα, στα κρίσιμα σημεία μελετήθηκαν οι κατανομές  $P(\ln IPR)$  οι οποίες είναι σχεδόν αναλλοίωτες υπό αλλαγή κλίμακας. Τέλος, υπ-

---

ολογίστηκε η μορφοκλασματική διάσταση  $D_2$ . Για ασθενή αταξία  $W$ , οι καταστάσεις βρέθηκαν πλήρως εργοδικές-εκτεταμένες με  $D_2 = 1$  ενώ κοντά στο κρίσιμο σημείο είναι πολυμορφοκλασματικές με ενδιάμεση διάσταση  $D_2$  μεταξύ 0 και 1. Όμοια, για ασθενή αταξία  $\delta$  οι καταστάσεις εμφανίζουν και πάλι εργοδική-εκτεταμένη συμπεριφορά ενώ κοντά στο κρίσιμο σημείο είναι πολυμορφοκλασματικές. Για ισχυρή αταξία και στις δύο περιπτώσεις οι καταστάσεις είναι πιο εντοπισμένες (MBL) και μπορούν να χρησιμοποιηθούν δυνητικά για κβαντικές μνήμες.

# Acknowledgments

I would like to take this opportunity to thank the people who have been involved with my PhD life during my years in Ioannina. First and foremost, I would like to thank my supervisor, Professor S.N.Evangelou. The seemingly countless hours of our meetings have broadened my knowledge and made my PhD experience an interesting process. I also appreciate that he discussed with me all these fascinating problems and made available his earlier theoretical and numerical work in the many-body Heisenberg chain. I would also like to thank Professor K.Magoutis and Dr.S.Athanasopoulos for their help with the HPC systems during the last two years. In addition, I thank the HPC system "ARIS" in Athens who gave me the opportunity to complete a great amount of my computational work. I also thank D.Manolas for allowing me to have a part of his early stage work prior to publication. At a personal level, my life in Ioannina will not be fulfilled without the companionship of Kelly who was always near me. Also, I thank my friends inside and outside the academic circle for our light-hearted discussions and their unconditional support. Finally, I literally cannot describe with words the contribution of my parents Theofanis and Eleni. Being my main psychological and my only financial supporters, they helped me to pursue my dream for a PhD in Physics during those difficult years. This work is dedicated to them.

---

# Contents

<b>1</b>	<b>Introduction</b>	<b>1</b>
1.1	Anderson Localization . . . . .	1
1.2	Random Matrix Theory . . . . .	5
1.3	Multifractality . . . . .	9
1.4	Interactions . . . . .	11
1.5	Outline . . . . .	12
<b>2</b>	<b>One-electron Disordered Systems</b>	<b>13</b>
2.1	Chiral Disordered Systems . . . . .	13
2.2	1D Off-Diagonal Disorder . . . . .	20
2.3	2D Off-Diagonal Disorder . . . . .	27
2.4	Summary . . . . .	32
<b>3</b>	<b>Topological Disordered Systems</b>	<b>33</b>
3.1	1D p-wave Superconductor . . . . .	36
3.2	Disordered 1D p-wave Superconductor . . . . .	41
3.3	Level Statistics . . . . .	45
3.4	Majorana Mode Multifractality . . . . .	47
3.5	Summary . . . . .	52

<b>4</b>	<b>Many-Body Localization</b>	<b>53</b>
4.1	Thermalization .vs. Localization . . . . .	53
4.2	The Model . . . . .	55
4.3	Level Statistics . . . . .	59
4.4	Statistics of Eigenstates . . . . .	64
4.4.1	Participation Ratio . . . . .	65
4.4.2	Shannon Entropy . . . . .	70
4.4.3	Multifractality . . . . .	71
4.5	Summary . . . . .	73
<b>5</b>	<b>Conclusions</b>	<b>75</b>
	<b>Bibliography</b>	<b>79</b>

# Chapter 1

## Introduction

### 1.1 Anderson Localization

It is known since several decades ago that the presence of disorder in quantum systems drives interesting phenomena. In 1958, P.W.Anderson studied the behavior of electrons in disordered crystals [1]. The Anderson model of localization is the foundation over which our knowledge for the effect of disorder on electronic systems has been established. The quantum mechanics allows electrons to hop from one atom to its neighbors. In a disordered lattice a single electron at each lattice site can feel a random potential. In the second quantization formalism, the Hamiltonian is

$$H_0 = \sum_{n=1}^N V_n c_n^\dagger c_n + t \sum_{n=1}^{N-1} (c_n^\dagger c_{n+1} + c_{n+1}^\dagger c_n), \quad (1.1)$$

where  $c_n^\dagger$  and  $c_n$  are fermionic creation and annihilation operators for the electron on site  $n$ , the total number of lattice sites is denoted by  $N$  and the on-site potential  $V_n$  is an independent random variable uniformly distributed in the interval  $[-\frac{W}{2}, \frac{W}{2}]$  where  $W$  is the strength of disorder. The hopping parameter  $t$  is assumed to have non-zero values only for

nearest neighbors and we set  $t = 1$  defining the energy scale. The tight-binding model with a random on-site potential has been subject of extensive studies also in higher dimensions (see [2] and references therein). It is known that a critical disorder  $W_c$  exists and if the strength  $W$  exceeds this value,  $W > W_c$ , then all the states are exponentially localized. This means that the wavefunction amplitude decays exponentially outside a localization length  $\xi$ . The phenomenon of *Anderson localization* constrains the wavefunction to a finite region of space of the order of  $\xi$ . For  $W > W_c$  in the localized phase, the system loses all of its conductivity properties and becomes an insulator. This implies the absence of diffusion and the states cannot transport current having zero conductivity. This is a completely different behavior from ideal crystals which are always conductors and have a finite conductivity. From the scaling theory of localization [3], in  $1D$  and  $2D$  all states are localized ( $W_c = 0$ ) whereas in  $3D$  we have a metal-insulator transition at  $W_c \sim 16.5$ .

The quantum motion of an electron in dimension  $D$  can be represented in the discrete basis of lattice sites  $\{|n\rangle, n = 1, 2, 3, \dots, N\}$ . The so-called Tight-Binding approximation effectively describes the motion of electrons in solids and can be used to calculate the electronic band structure for  $W = 0$ . The main assumption is that each atomic orbital is strongly localized on its corresponding lattice site  $|n\rangle$  and the wavefunction of an electron can be expressed as a linear combination in the discrete basis of lattice sites  $\{|n\rangle\}$

$$|\Psi\rangle = \sum_{n=1}^N \psi_n |n\rangle, \quad (1.2)$$

where  $N$  is the total number of sites and  $\psi_n, n = 1, 2, \dots, N$  are the corresponding probability amplitudes.

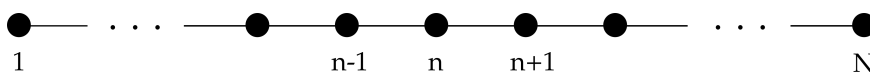


Figure 1.1: 1D chain

For the disordered chain (Fig.1.1) with Hamiltonian of Eq(1.1) the hoppings  $t = 1$  and  $V_n \in [-\frac{W}{2}, \frac{W}{2}]$  is an independent random variable following a uniform distribution. Open boundary conditions are considered. The Hamiltonian in 1D is represented as a simple tridiagonal matrix

$$H = \begin{pmatrix} V_1 & 1 & \dots & 0 & 0 \\ 1 & V_2 & 1 & \dots & 0 \\ \vdots & 1 & \ddots & \ddots & \vdots \\ 0 & \dots & \ddots & V_{N-1} & 1 \\ 0 & 0 & \dots & 1 & V_N \end{pmatrix}.$$

The *Density of States* describing the number of states for a specific energy for  $W = 0$  is

$$\rho(\epsilon) = \frac{1}{\pi} \frac{1}{\sqrt{4t^2 - (\epsilon - V)^2}}. \quad (1.3)$$

For finite small disorder  $W = 1$  and system size  $N = 1000$   $\rho(\epsilon)$  is plotted in Fig.1.2(a) along with the relation of Eq.1.3. A corresponding localized wavefunction at  $\epsilon \approx 0$  can be seen in Fig.1.2(b).

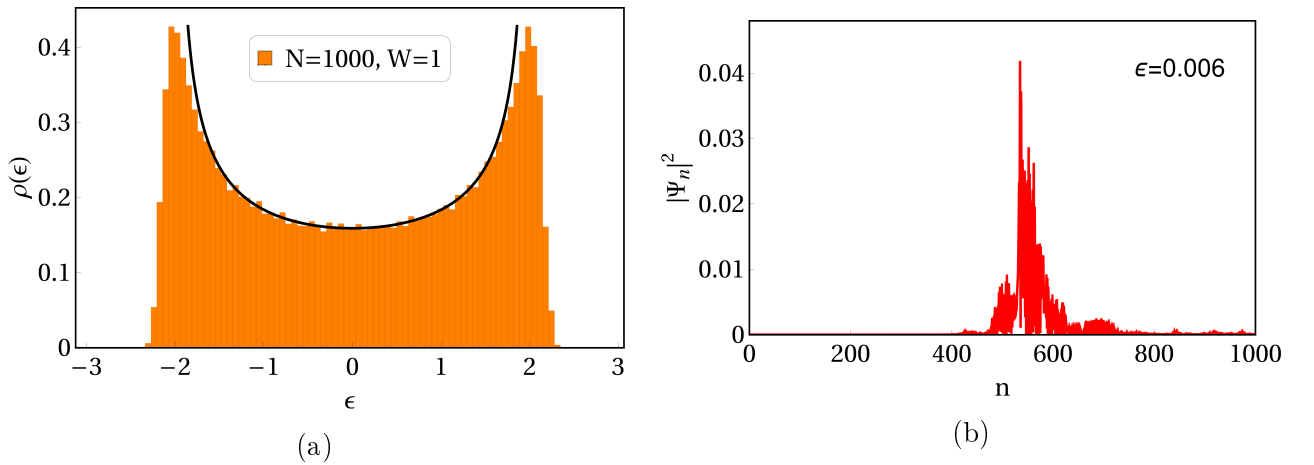


Figure 1.2: (a)  $\rho(\epsilon)$  for a disordered 1D lattice of size  $N = 1000$ ,  $W = 1$  and  $t = 1$ . The solid black line represents  $W = 0$ . (b) The wavefunction for  $\epsilon = 0.006$  and  $W = 1$  is localized.

For a quantum lattice system in the presence of a random potential of strength  $W$  we can explore the correlations between the eigenvalues  $E_n$ . A concise statistical measure which highlights the degree of level correlation is the statistical distribution  $P(S)$  of consecutive energy level spacings, where  $S_n = E_{n+1} - E_n$ . The distribution should be normalized with  $\langle S \rangle = 1$  and  $\int_0^{\infty} P(S) dS = 1$ . The eigenvalues of a localized system are uncorrelated randomly distributed and exhibit attraction. This limit denotes the *Poisson Statistics* and characterizes the insulating behavior and *integrability*. The Poisson distribution of consecutive level spacings

$$P(S) = e^{-S} \tag{1.4}$$

is plotted in Fig.1.3. For  $S \rightarrow 0$  we observe the level attraction with  $e^{-S} \rightarrow 1$ .

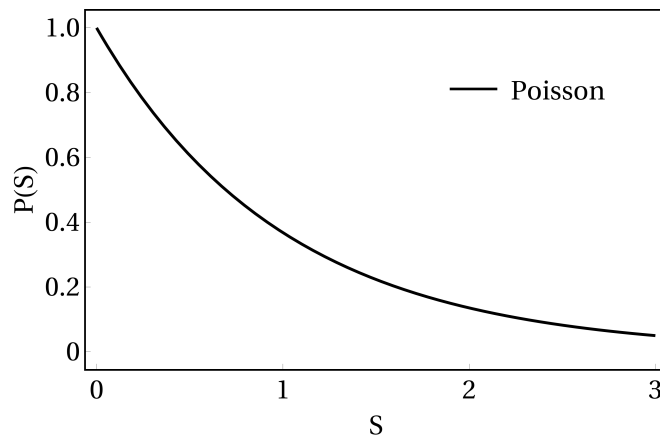


Figure 1.3: The  $P(S)$  Poisson distribution.

The tridiagonal matrix representing a 1D lattice shows localization as electrons can hop to nearest neighbors only. This picture fails to describe extended behavior and this is where Random Matrix Theory takes in with the matrix becoming full as shown in the following section.

## 1.2 Random Matrix Theory

Since the work of E.Wigner [4] and F.Dyson [5], there was a strong interest in studying the energy correlations of quantum spectra for systems with many degrees of freedom such as in complex atomic nuclei. Random matrix theory (RMT) is the appropriate mathematical tool which explores the statistical properties of eigenvalue spectra of  $N \times N$  random matrices which are full with every site connected to all others. In the system we consider only inherent symmetries such as time-reversal and spin rotation. This combination gives the three random ensembles with Gaussian disorder, namely GOE, GUE and GSE.

A  $N$ -dimensional lattice with "all to all" random couplings  $H_{ij}$  can be realized by a random  $N \times N$  Hamiltonian

$$H = \begin{pmatrix} H_{1,1} & H_{1,2} & \dots & H_{1,N-1} & H_{1,N} \\ H_{2,1} & H_{2,2} & H_{2,3} & \dots & H_{2,N} \\ \vdots & H_{3,2} & \ddots & \ddots & \vdots \\ H_{N-1,1} & \dots & \ddots & H_{N-1,N-1} & H_{N-1,N} \\ H_{N,1} & H_{N,2} & \dots & H_{N,N-1} & H_{N,N} \end{pmatrix}.$$

In the limit  $N \rightarrow \infty$  the density of states is the Wigner semi-circle distribution

$$\rho(\epsilon) = \frac{1}{2\pi} \sqrt{4 - \epsilon^2} \quad , \quad -2 \leq \epsilon \leq 2. \quad (1.5)$$

For uniformly (not Gaussian) distributed random variables with  $W = 1$ , the  $\rho(\epsilon)$  for matrix size  $N = 1000$  is plotted in Fig.1.4(a) along with the Eq.1.5. An example of the wavefunction for an energy near the band centre can be seen in Fig.1.4(b). The wavefunctions as opposed to tridiagonal matrices are extended in all available space.

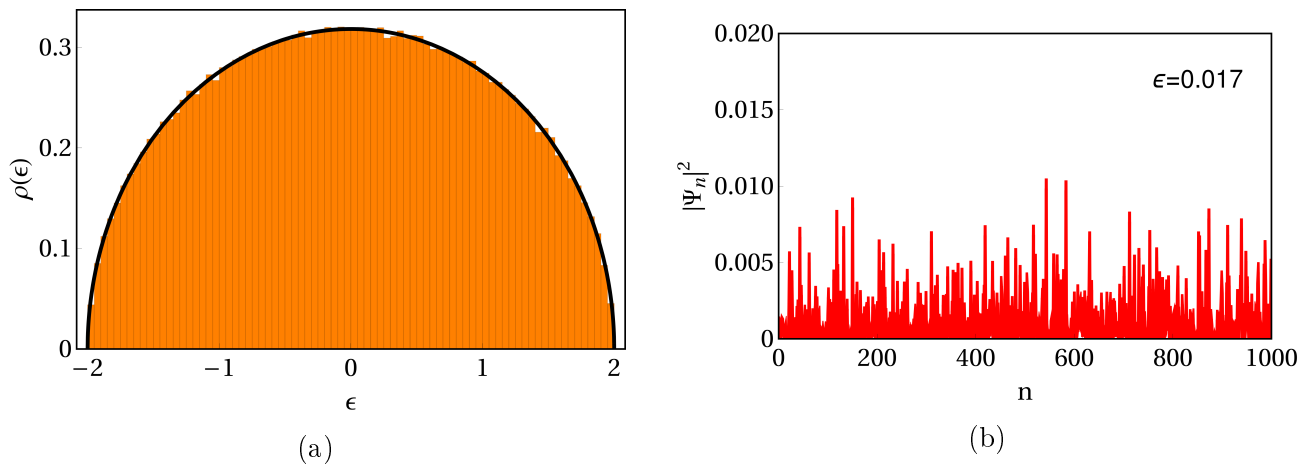


Figure 1.4: (a)  $\rho(\epsilon)$  for a random matrix of dimension  $N = 1000$  and  $W = 1$  uniform. The solid black line represents the Wigner semi-circle. (b) The wavefunction for  $\epsilon = 0.017$  and  $W = 1$  is extended.

Although RMT was originally intended for modelling systems with many degrees of freedom, it is also proved useful for systems with few degrees of freedom as well. Moreover, energy-level statistics provides an indication of the type of motion for a quantum system. In the field of quantum chaos we are interested in the spectral statistics of a quantum Hamiltonian whose classical analogue is chaotic. As Berry-Tabor conjectured [6], the level statistics of a quantum system is in its integrable domain follows the Poisson distribution. This is also seen in 1D disordered systems (Section 1.1) which correspond to integrable motion. On the other hand, Bohigas, Giannoni and Schmidt [7] conjectured that if the system is chaotic then its level statistics follows the Wigner distribution and we have a chaotic behavior.

We consider random  $N \times N$  full matrices with  $H_{ij}$  elements taken from a Gaussian distribution. The three statistical ensembles with the corresponding symmetries of time-reversal and spin-rotation are classified as:

- *Gaussian Orthogonal (GOE)* for real and symmetric random matrices.

The time-reversal symmetry (TRS) is preserved and we can derive the  $P(S)$  level spacing distribution beginning with a  $2 \times 2$  random matrix. We have

$$H_{GOE} = \begin{bmatrix} H_{11} & H_{12} \\ H_{12} & H_{22} \end{bmatrix}.$$

The difference between the eigenvalues is

$$S = E_2 - E_1 = \sqrt{(H_{11} - H_{22})^2 + 4H_{12}^2}. \quad (1.6)$$

If we set  $x = H_{11} - H_{22}$  and  $y = 2H_{12}$ , then  $S = \sqrt{x^2 + y^2}$ . Considering the normalization conditions  $\int_0^\infty P(S)dS = 1$  and  $\langle S \rangle = \int_0^\infty SP(S)dS = 1$ , the probability distribution of the spacing  $S$  is

$$P_{GOE}(S) = \frac{\pi}{2} S e^{-\frac{\pi}{4} S^2}. \quad (1.7)$$

- *Gaussian Unitary (GUE)* for complex Hermitian random matrices. The time-reversal symmetry is broken (e.g. by the presence of a magnetic field) and the  $2 \times 2$  complex random matrix is

$$H_{GUE} = \begin{bmatrix} H_{11} & H_{12} \\ H_{12}^* & H_{22} \end{bmatrix}.$$

The diagonal elements are real and the off-diagonal elements are complex. We have

$H_{12} = H_{12}^{Re} + iH_{12}^{Im}$ . The difference between the eigenvalues is

$$S = E_2 - E_1 = \sqrt{(H_{11} - H_{22})^2 + (2H_{12}^{Re})^2 + (2H_{12}^{Im})^2}. \quad (1.8)$$

If we set  $x = H_{11} - H_{22}$ ,  $y = 2H_{12}^{Re}$  and  $z = 2H_{12}^{Im}$  then  $S = \sqrt{x^2 + y^2 + z^2}$ . In this case, we obtain

$$P_{GUE}(S) = \frac{32}{\pi^2} S^2 e^{-\frac{4}{\pi} S^2}. \quad (1.9)$$

- *Gaussian Symplectic (GSE)* for quaternion self-dual matrices. In this case time-reversal symmetry is preserved but the spin-rotation is not, e.g. in the presence of spin-orbit interaction. The  $4 \times 4$  quaternion random matrix is

$$H_{GSE} = \begin{bmatrix} a & 0 & X & Y \\ 0 & a & -Y^* & X^* \\ X^* & -Y & b & 0 \\ Y^* & X & 0 & b \end{bmatrix},$$

where the diagonal elements  $a, b \in \mathbb{R}$ ,  $X = X^{Re} + iX^{Im}$ ,  $Y = Y^{Re} + iY^{Im}$  and  $X^*, Y^*$  are their complex conjugate. By diagonalizing  $H_{GSE}$  we obtain 4 eigenvalues degenerate by two (Kramers pairs). The difference between the two pairs is

$$S = E_2 - E_1 = \sqrt{(a-b)^2 + (2X^{Re})^2 + (2X^{Im})^2 + (2Y^{Re})^2 + (2Y^{Im})^2}. \quad (1.10)$$

If we set  $x = a - b$ ,  $y = 2X^{Re}$ ,  $z = 2X^{Im}$ ,  $w = 2Y^{Re}$  and  $k = 2Y^{Im}$ , then  $S = \sqrt{x^2 + y^2 + z^2 + w^2 + k^2}$ . The probability distribution of the spacing  $S$  is

$$P_{GSE}(S) = \frac{2^{18}}{3^6 \pi^3} S^4 e^{-\frac{64}{9\pi} S^2}. \quad (1.11)$$

The above universality classes constitute the *Wigner-Dyson* ensemble (or 3-fold way) and the universal index  $\beta = 1, 2, 4$  characterizes the level repulsion for each class such as  $P(S) \sim S^\beta$ , for  $S \rightarrow 0$ . The 3 distributions are plotted in Fig.1.5

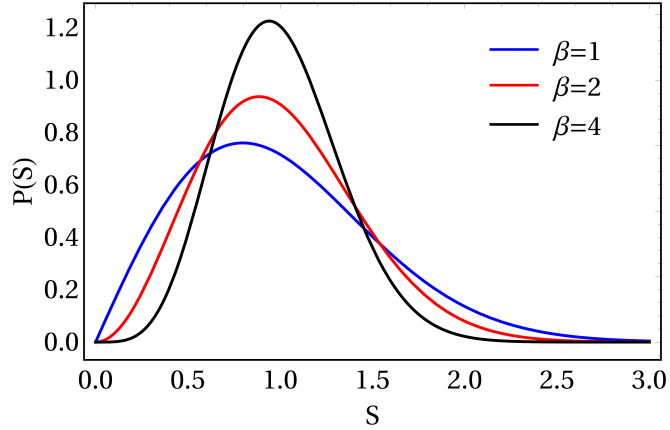


Figure 1.5: The distributions of neighboring energy levels  $P(S)$  for the standard Wigner-Dyson ensembles according to the universal index  $\beta$ . GOE ( $\beta = 1$ ) in blue, GUE ( $\beta = 2$ ) in red, GSE ( $\beta = 4$ ) in black. They show level repulsion which is a characteristic of quantum chaos.

### 1.3 Multifractality

At a metal-insulator transition we have a critical behavior and the eigenvalues follow an intermediate distribution between Wigner and Poisson. At the critical point the eigenstates are neither extended nor localized and exhibit a multifractal behavior [8, 9, 10, 11, 12, 13, 14, 15]. A *multifractal* is a non-homogeneous fractal where the fractal dimension  $D_f$  has a different value if we choose a different starting point [16, 17]. Multifractal measures are used to study distributions of quantities on a geometric support. In a quantum lattice model the geometric support of the wavefunctions is a lattice (e.g. square, honeycomb, kagome etc.) and there is a systematic way to calculate the continuous spectrum of infinite multifractal dimensions. They are defined as

$$D_q = -\frac{1}{q-1} \lim_{L \rightarrow \infty} \frac{\ln \sum_{i=1}^N P_i^q}{\ln L}, \quad q \in (-\infty, \infty), \quad (1.12)$$

where  $P_i = |\Psi_i|^2$  is the probability density of an electron to be found on site  $i$  of the

supporting lattice and is the basic measure of the multifractal formalism.  $N$  and  $L$  are the total number of sites and the linear length scale, respectively. For  $q = 1$  the generalized fractal dimension is

$$D_1 = -\frac{\sum_{i=1}^N P_i \ln P_i}{\ln L} = \frac{S}{\ln L}, \quad P_i = |\Psi_i|^2, \quad (1.13)$$

and measures the scaling of the *Shannon entropy* ( $S$ ) with the length scale  $L$ . The dimension  $D_1$  is called *information dimension*. For  $q = 2$  the generalized fractal dimension is

$$D_2 = -\frac{\sum_{i=1}^N P_i^2}{\ln L}, \quad P_i = |\Psi_i|^2, \quad (1.14)$$

and is called *correlation dimension*.  $D_2$  describes the scaling with size  $L$  of the quantity  $\sum_{i=1}^N P_i^2$  known as *Inverse Participation Ratio (IPR)*, where

$$IPR = \sum_{i=1}^N P_i^2 = \sum_{i=1}^N |\Psi_i|^4 \sim L^{-D_2}. \quad (1.15)$$

This measure is used to characterize the localization properties of a wavefunction. A perfectly extended (ballistic) Bloch wavefunction has probability amplitudes  $\Psi_i = \frac{1}{\sqrt{N}}$  over all lattice sites  $N$ , has  $IPR = \sum_{i=1}^N (\frac{1}{\sqrt{N}})^4 = \sum_{i=1}^N \frac{1}{N^2} = \frac{1}{N}$ , whereas a perfectly localized wavefunction on just one lattice site has  $IPR = 1$ . For disordered states IPR takes values between 0 and 1.

To summarize, the scaling of  $IPR$  (or  $PR = IPR^{-1}$ ) with the system size gives us information about the multifractal character of a wavefunction and its degree of localization. For an equally distributed wavefunction over all lattice sites  $N$ , all generalized dimensions  $D_q$  are represented by the fractal dimension  $D_0$  of the supporting lattice. The wavefunction is fully extended when  $D_q = D_0$ , completely localized when  $D_q = 0$  and has a multifractal behavior for  $0 < D_q < 1$ .

## 1.4 Interactions

The non-interacting Hamiltonians considered previously are simple but effective. However, almost all systems in nature contain interactions as they are complex having many constituents coupled to each other. The general Hamiltonian which includes interactions is

$$H = H_0 + U \sum_i \left( n_i - \frac{1}{2} \right) \left( n_{i+1} - \frac{1}{2} \right), \quad (1.16)$$

$H_0$  is the non-interacting Hamiltonian,  $U$  is the strength of interaction and  $n_i = c_i^\dagger c_i$  is the number operator. In the last 15 years, Basko, Aleiner and Altshuler [18] have carried an extremely challenging and still ongoing research in the field of the so called Many-Body Localization (MBL). This interesting phenomenon can be considered at first as an extension of the single-particle Anderson Localization to interacting systems. An interacting disordered system can be in two possible states, localization (no ergodicity) or thermalization (ergodicity). A quantum phase transition to MBL with the absence of ergodicity means that in this phase the system fails to thermally equilibrate. This feature is of fundamental importance as it is closely related to the foundations of statistical mechanics and the notion of information transfer [19, 20].

A closed quantum system, isolated from the environment and initially in a single (pure) quantum state  $|\Psi_0\rangle$  will evolve unitary in time according to the Schrödinger equation expected to reach a thermal Gibbs state, invariant under future evolution of the system. In order for this to happen, the system has to be able to act as its own reservoir. The thermal state contains no information about the initial state  $|\Psi_0\rangle$  but information itself cannot be erased. The system has no memory and in a sense hides the quantum information. This is not always the case, because the Anderson localized systems cannot act as their own reservoirs and therefore do not exhibit thermalization [21, 22, 23, 24].

## 1.5 Outline

We study the energy and wavefunction statistics in three kinds of disordered systems. First, a lattice with nearest neighbor bond disorder which preserves lattice chiral symmetry. The second case is a superconductor with bond disorder supporting the elusive Majorana modes. Third, a many-body system of qubits with both random potentials and interactions is studied. Our main motivation is to examine the statistics of the energy levels and wavefunctions over the random ensemble near the Fermi level ( $E = 0$ ). Our approach is to initially consider small sizes and reach larger ones in a finite size scaling spirit. The statistical properties of the energy levels can show the ergodic or localized behavior. Moreover, we find at what degree the states have fractal characteristics. We address the following questions. For chiral disordered systems is there an even-odd distinction and what are its ramifications? In the presence of non-trivial topology are the Majorana modes robust to disorder and is there any indication of their multifractality? Finally, how the many-body localization appears and what are its characteristics ?

In Chapter 2, we discuss the presence of off-diagonal disorder in a one and two dimensional lattices. We specifically stress the presence of chiral (or sublattice) symmetry and explore the nature of the special  $E = 0$  state which signifies the even-odd asymmetry in both 1D and 2D. Moreover, we show results for the level statistics and multifractality for this case.

In Chapter 3, we explore the interesting case of a topological superconductor. We introduce the Kitaev toy model for a superconductor in one dimension and study its topological aspects. We show what happens in the presence of off-diagonal disorder.

In Chapter 4, we examine a prototype interacting system. More specifically, we study the XXZ Heisenberg quantum spin anti-ferromagnetic chain with disorder. The disorder combined with interactions gives a new many-body localized phase.

In Chapter 5, we give an overall description of our results and discuss possibilities of future work.

# Chapter 2

## One-electron Disordered Systems

### 2.1 Chiral Disordered Systems

Our motivation is to study the localization peculiarities which arise with the presence of off-diagonal disorder at the band center [25, 26, 27, 28] and to explore the nature of the  $E = 0$  state. We consider a 1D chain with nearest neighbor (NN) hopping  $t$  of random strength and without on-site potential. We assume open boundary conditions in 1D and the Hamiltonian with no diagonal disorder is

$$H = \sum_n t(c_n^\dagger c_{n+1} + c_{n+1}^\dagger c_n). \quad (2.1)$$

We conveniently choose the hoppings  $t = e^V$ , where  $V = \ln t$  are taken from the uniform (box) distribution so that  $V \in [-\frac{W}{2}, \frac{W}{2}]$  with constant probability density function  $P(V) = \frac{1}{W}$ . The mean value is  $\langle V \rangle = \int_{-W/2}^{W/2} V P(V) dV = 0$  and the variance is  $\sigma_V^2 = \langle V^2 \rangle - \langle V \rangle^2 = \frac{W^2}{12}$ . The random distribution function  $\tilde{P}(t)$  will be

$$\tilde{P}(t) = P(V) \frac{dV}{dt} \Leftrightarrow \tilde{P}(t) = \frac{1}{Wt}, \quad (2.2)$$

since  $t = e^V \in [e^{-W/2}, e^{W/2}]$ . The mean value is  $\langle t \rangle = \int_{e^{-W/2}}^{e^{W/2}} t \tilde{P}(t) dt = \frac{2}{W} \sinh(\frac{W}{2})$  and the variance is  $\sigma_t^2 = \langle t^2 \rangle - \langle t \rangle^2 = \frac{1}{W^2} (2 + W \sinh(W) - 2 \cosh(W))$ . The logarithmic distribution is chosen to ensure that all hoppings  $t$  will take positive non-zero values, which can become arbitrarily strong. For comparison, the uniform and logarithmic distributions alongside with the Gaussian(0,1) are plotted in Fig.2.1 for disorder strength  $W = 1$ .

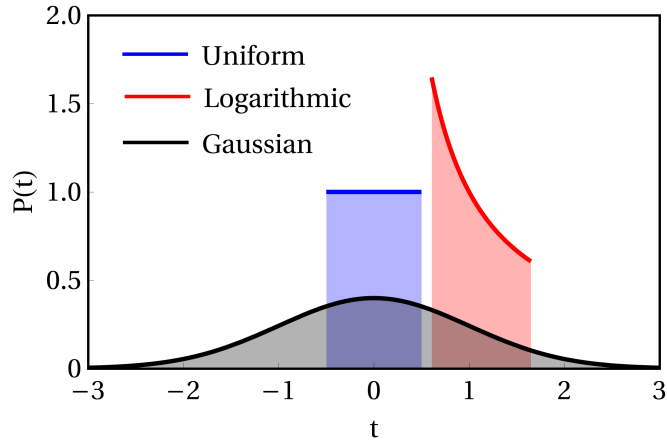


Figure 2.1: The random hopping distributions for  $W = 1$ , uniform (blue), logarithmic (red) and Gaussian (black). The mean is 0 and the variance is 1.

In order to illustrate the major features of even and odd lattice sizes, analytical results are presented for  $N = 2$  and  $N = 3$ . We found  $\rho(E)$ ,  $IPR(E)$  and level statistics  $P(S)$  near  $E = 0$ . For both cases, we choose the logarithmic distribution for the hoppings with  $W = 1$ .



Figure 2.2: (a)  $N=2$  and (b)  $N=3$ .

For  $N = 2$  (Fig.2.2(a)), in the discrete basis  $|n\rangle$  the Hamiltonian matrix is

$$H_{N=2} = \begin{pmatrix} 0 & t \\ t & 0 \end{pmatrix}.$$

The matrix has eigenvalues  $E_{\pm} = \pm t$  and normalized eigenvectors  $|\Psi_{E_{\pm}}\rangle = \frac{1}{\sqrt{2}} \begin{pmatrix} 1 \\ \pm 1 \end{pmatrix}$ .

The Inverse Participation Ratios are  $IPR_{\Psi_{E_+}} = IPR_{\Psi_{E_-}} = \sum_{i=1}^N |\Psi_i|^4 = (\frac{1}{\sqrt{2}})^4 + (\frac{1}{\sqrt{2}})^4 = \frac{1}{2}$ .

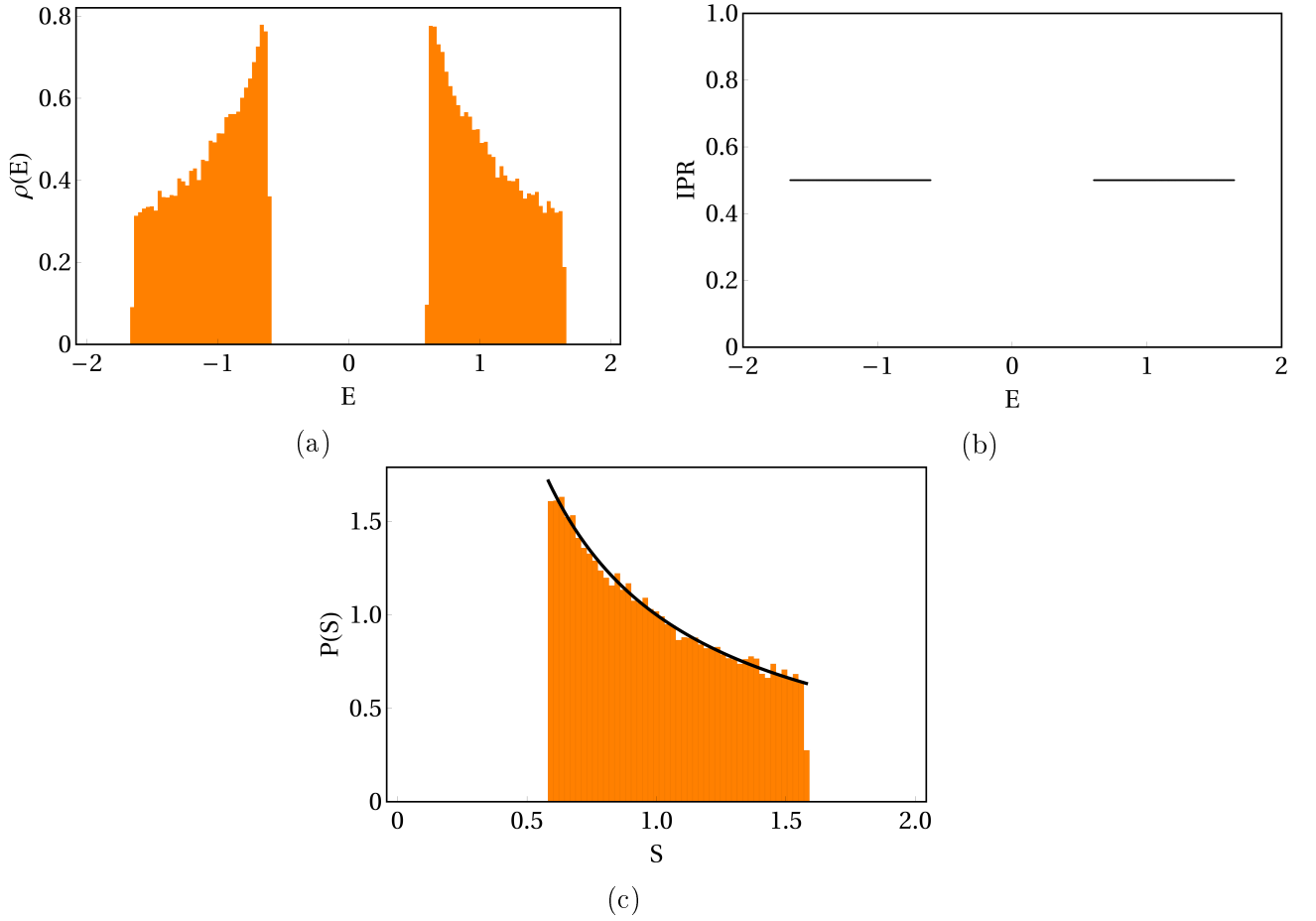


Figure 2.3:  $N = 2$ . (a)  $\rho(E)$  has a gap, (b)  $IPR(E)$  and (c)  $P(S)$ . In black is the analytic curve.  $IPR = 0.5$  means that the support of the states are on both the  $N = 2$  sites.

Considering many realizations, the density of states  $\rho(E)$  and  $\text{IPR}(E)$  are plotted in Fig.2.3(a),(b) and the level spacing distribution  $P(S)$  is plotted in Fig.2.3(c) with  $S = E_2 - E_1 = 2t$ . The black line denotes the analytic curve which is  $P(S) = \tilde{P}(t) \frac{dt}{dS} \Leftrightarrow \Leftrightarrow P(S) = \frac{1}{2t} = \frac{1}{S}$ .

For  $N = 3$  (Fig.2.10(b)) in the discrete basis  $|n\rangle$  the Hamiltonian matrix is

$$H_{N=3} = \begin{pmatrix} 0 & t_1 & 0 \\ t_1 & 0 & t_2 \\ 0 & t_2 & 0 \end{pmatrix}.$$

The matrix has eigenvalues  $E_1 = \sqrt{t_1^2 + t_2^2}$ ,  $E_2 = 0$  and  $E_3 = -\sqrt{t_1^2 + t_2^2}$ . The corresponding normalized eigenvectors are

$$|\Psi_{E_1}\rangle = \frac{t_2}{\sqrt{2t_1^2 + 2t_2^2}} \begin{pmatrix} t_1/t_2 \\ \sqrt{t_1^2+t_2^2} \\ 1 \end{pmatrix}, \quad |\Psi_{E_2}\rangle = \frac{t_2}{\sqrt{2t_1^2 + 2t_2^2}} \begin{pmatrix} 1 \\ 0 \\ -t_1/t_2 \end{pmatrix}, \quad |\Psi_{E_3}\rangle = \frac{t_2}{\sqrt{2t_1^2 + 2t_2^2}} \begin{pmatrix} t_1/t_2 \\ -\sqrt{t_1^2+t_2^2} \\ 1 \end{pmatrix}$$

The corresponding Inverse Participation Ratios are

$$\text{IPR}_{\Psi_{E_1}} = \text{IPR}_{\Psi_{E_3}} = \sum_{i=1}^N |\Psi_i|^4 = \frac{t_1^4 + t_2^4 + t_1^2 t_2^2}{2(t_1^2 + t_2^2)^2}, \quad \text{IPR}_{\Psi_{E_2}} = \frac{t_1^4 + t_2^4}{(t_1^2 + t_2^2)^2}$$

Considering many realizations, the calculated density of states  $\rho(E)$  and  $\text{IPR}(E)$  are plotted in Fig.2.4(a),(b).

For the level spacing distribution  $P(S)$  we have  $S = E_3 - E_2 = \sqrt{t_1^2 + t_2^2}$ . We use the Dirac Delta Transformation of random variables to compute the analytic relation as

$$P(S) = \int_{\frac{1}{\sqrt{e}}}^{\sqrt{e}} \int_{e^{-\frac{1}{2}}}^{e^{\frac{1}{2}}} \frac{1}{t_1 t_2} \delta(S - \sqrt{t_1^2 + t_2^2}) dt_1 dt_2 \Leftrightarrow$$

$$\Leftrightarrow P(S) = \begin{cases} \frac{\ln(eS^2-1)}{S} & , \quad 0.57 < S < 1.168 \\ \frac{1-\ln(S^2-e)}{S} & , \quad 1.168 < S < 1.55 \\ 0 & , \quad otherwise \end{cases} \quad (2.3)$$

The resulting piecewise curve for the  $P(S)$  distribution is plotted in Fig.2.4(c) with the two branches in blue and red color, respectively.

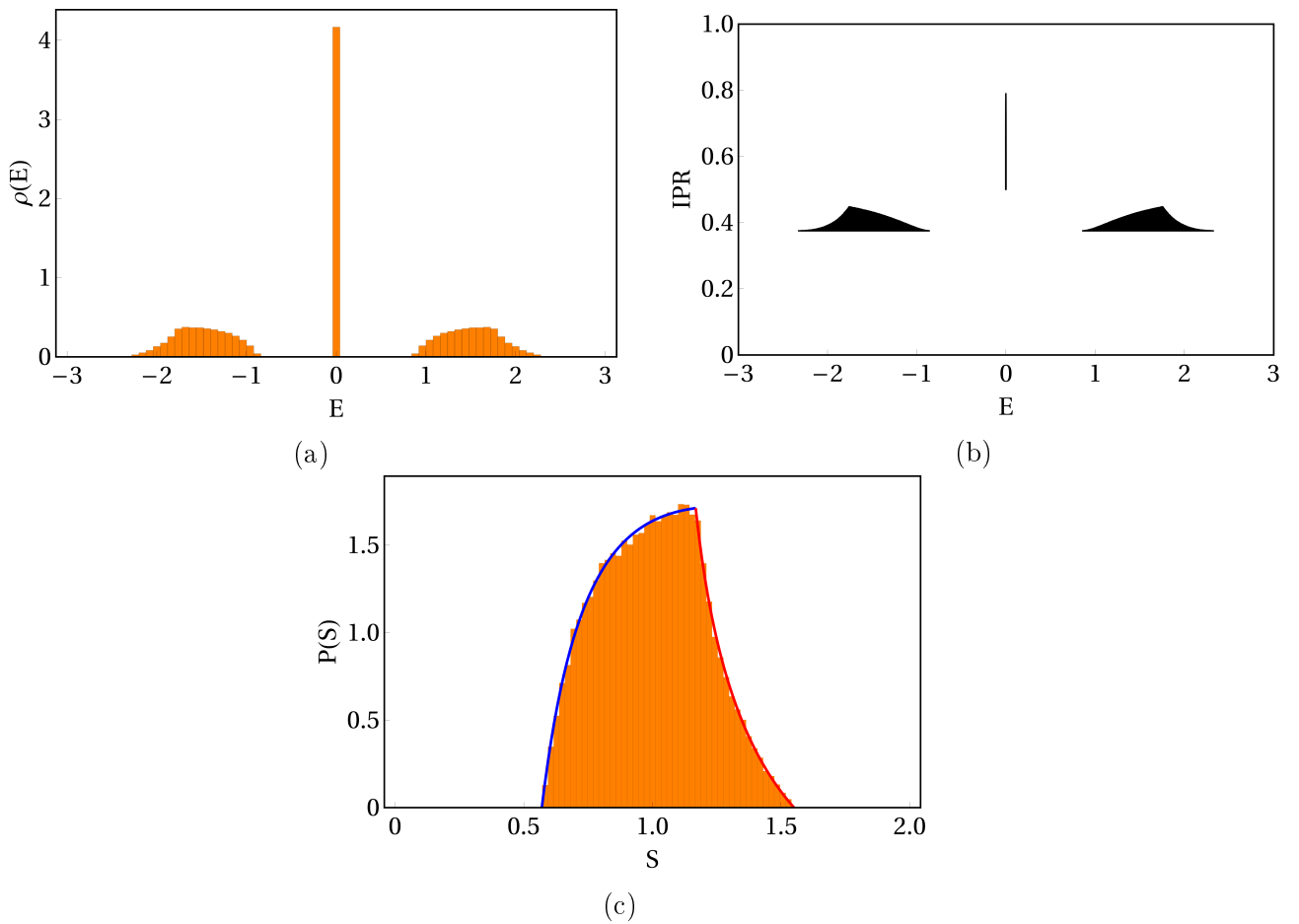


Figure 2.4:  $N = 3$ . (a)  $\rho(E)$ , (b)  $IPR(E)$ , (c) The piecewise  $P(S)$  function consists of two branches in blue and red color, respectively.

The crucial difference between the two cases is apparent. For the odd size  $N = 3$  the  $E = 0$  eigenstate has amplitudes only on odd sites. This  $E = 0$  state is not present in even size  $N = 2$ . This distinction also holds for larger system sizes and is closely related to an underlying even-odd symmetry even for large- $N$ .

Chiral symmetry is one of the basic discrete symmetries which has to do with the mirror symmetry [29, 30]. The prerequisite for chiral symmetry is the presence of a bipartite lattice (Fig.2.5), which contains two sublattices A and B where the hopping terms connect sites of sublattice A with sites of sublattice B [31, 32, 33]. The A's and B's may represent two different kinds of atoms. A typical example is a disordered lattice with random hopping connecting A to B and without on-site potentials. The diagonal disorder breaks chiral symmetry. The chiral Hamiltonian can be written in an off-diagonal block symmetric form in the A-B sublattice basis as

$$H = \sum_{i,j} t_{i,j}(c_i^\dagger c_j + h.c.) = \begin{pmatrix} 0 & H_{AB} \\ H_{AB}^\dagger & 0 \end{pmatrix},$$

where the matrix  $H_{AB}$  contains the hoppings which connect the two sublattices.

The Hamiltonian  $H$  satisfies the anticommutation relation  $\{H, \sigma_z\} = H\sigma_z + \sigma_z H = 0$ , where  $\sigma_z = \begin{pmatrix} 1 & 0 \\ 0 & -1 \end{pmatrix}$  is the Pauli matrix, and can be written as  $H = -\sigma_z H \sigma_z$ .

The state with energy  $E$  has a wavefunction  $|\Psi\rangle = \begin{pmatrix} \Psi_A \\ \Psi_B \end{pmatrix}$  and the Schrödinger equation is

$$\begin{aligned} H|\Psi\rangle &= E|\Psi\rangle \\ \Leftrightarrow -\sigma_z H \sigma_z |\Psi\rangle &= E|\Psi\rangle \\ \Leftrightarrow H(\sigma_z |\Psi\rangle) &= -E(\sigma_z |\Psi\rangle). \end{aligned} \tag{2.4}$$

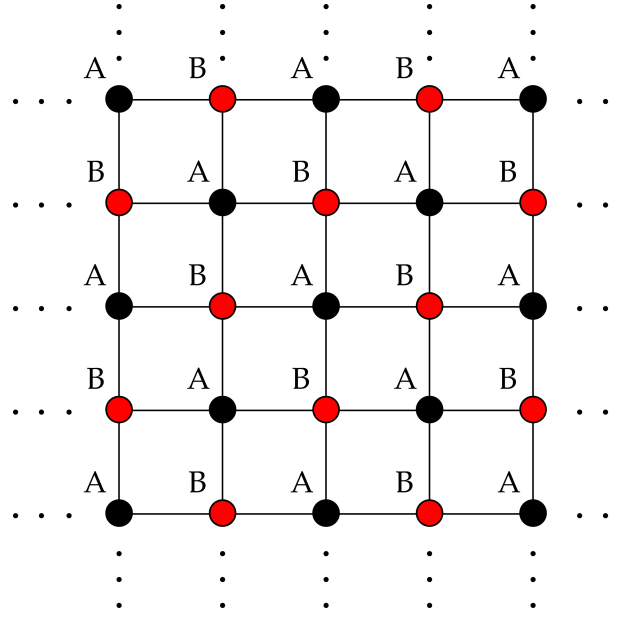


Figure 2.5: An example of a square lattice represented as a bipartite lattice, consisting of two interconnected sublattices, A with black and B with red.

From Eq.(2.4) the state with energy  $E$  and wavefunction  $|\Psi\rangle = \begin{pmatrix} \Psi_A \\ \Psi_B \end{pmatrix}$  is accompanied by a state with energy  $-E$  and wavefunction  $\sigma_z|\Psi\rangle = \begin{pmatrix} 1 & 0 \\ 0 & -1 \end{pmatrix} \begin{pmatrix} \Psi_A \\ \Psi_B \end{pmatrix} = \begin{pmatrix} \Psi_A \\ -\Psi_B \end{pmatrix}$ . The eigenvalues come in pairs  $E, -E$  around  $E = 0$  and the wavefunctions have the same amplitude in the sites of the A sublattice and opposite amplitudes in the B sublattice. The density of states is an even function of  $E$ ,  $\rho(E) = \rho(-E)$ . For an odd lattice of size  $N$  at least one  $E = 0$  state is always present. Moreover, if  $N_A$  are the number of sites for sublattice A and  $N_B$  for sublattice B then  $|N_A - N_B|$  zero modes exist.

Moreover, the presence of chiral symmetry efficiently reduces the size of corresponding matrices for diagonalization by half allowing less computational time. We have

$$H^2 = \begin{pmatrix} 0 & H_{AB} \\ H_{AB}^\dagger & 0 \end{pmatrix} \begin{pmatrix} 0 & H_{AB} \\ H_{AB}^\dagger & 0 \end{pmatrix} \Leftrightarrow H^2 = \begin{pmatrix} H_{AB}H_{AB}^\dagger & 0 \\ 0 & H_{AB}^\dagger H_{AB} \end{pmatrix}$$

since we can simply diagonalize the matrix  $H_{AB}H_{AB}^\dagger$  or the  $H_{AB}^\dagger H_{AB}$  giving the squared eigenvalues  $E_j^2$ ,  $j = 1, \dots, N$ .

## 2.2 1D Off-Diagonal Disorder

The simplest model which is guaranteed to have a eigenstate at  $E = 0$  (zero mode) is an odd-size  $N$  bipartite chain with off-diagonal disorder (Fig.2.6).

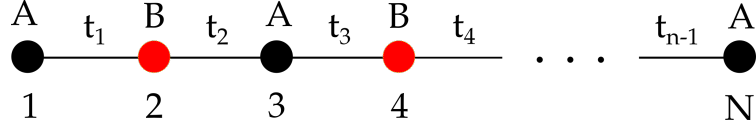


Figure 2.6: An example of a 1D bipartite lattice with two interconnected sublattices, A (black) and B (red) and random hoppings  $t_n$

The structure of the wavefunction for this state is calculated exactly. The Schrödinger equation for  $E = 0$  is  $H\Psi = 0$  and at

$$\text{even sites : } \Psi_{2n} = 0, \quad n = 1, 2, \dots, \frac{N-1}{2}, \quad (2.5)$$

$$\text{odd sites : } \Psi_{2n+1} = (-1)^n \prod_{m=1}^n \left( \frac{t_{2m-1}}{t_{2m}} \right) \Psi_1, \quad n = 1, 2, \dots, \frac{N-1}{2}.$$

We assume  $t_n = e^{V_n} \Leftrightarrow \ln t_n = V_n$ , where  $V_n$  are random numbers from a uniform distribution with  $\langle V_n \rangle = 0$  and  $\langle V_n^2 \rangle = \frac{W^2}{12}$ . The odd site amplitudes are

$$\Psi_{2n+1} = (-1)^n \prod_{m=1}^n e^{V_{2m-1} - V_{2m}} \Psi_1.$$

The exponents can be written

$$X_n = \sum_{m=1}^n (V_{2m-1} - V_{2m}) = \sum_{m=1}^n (\ln t_{2m-1} - \ln t_{2m}), \quad (2.6)$$

where  $X_n$  is an example of a random walk (discrete Brownian motion) so that the amplitudes become

$$\Psi_{2n+1} = (-1)^n e^{X_n} \Psi_1$$

Assuming independent random variables, the mean of  $X_n$  is

$$\langle X_n \rangle = \left\langle \sum_{m=1}^n (V_{2m-1} - V_{2m}) \right\rangle = \sum_{m=1}^n \langle (V_{2m-1} - V_{2m}) \rangle = \sum_{m=1}^n (\langle V_{2m-1} \rangle - \langle V_{2m} \rangle) = 0$$

and the variance is

$$\begin{aligned} \text{Var}(X_n) &= \langle X_n^2 \rangle - \langle X_n \rangle^2 = \left\langle \left( \sum_{m=1}^n (V_{2m-1} - V_{2m}) \right)^2 \right\rangle = \\ &= \sum_{m=1}^n \langle (V_{2m-1} - V_{2m})^2 \rangle = \sum_{m=1}^n (\langle V_{2m-1}^2 \rangle + \langle V_{2m}^2 \rangle) = n \frac{W^2}{6} = n(2\sigma_V^2). \end{aligned}$$

The standard deviation is  $\sqrt{\langle X_n^2 \rangle} = (\sqrt{2}\sigma_V)\sqrt{n}$  and setting  $\Psi_1 = 1$  the wavefunction becomes

$$|\Psi_{2n+1}| \sim e^{\pm(\sqrt{2}\sigma_V)\sqrt{n}}.$$

The  $E = 0$  wavefunction typically grows (decays) sub-exponentially as opposed to Anderson Localization exponential growth (decay)  $\sim e^{\pm\gamma|n|}$ ,  $\gamma = \frac{1}{\xi}$  is the Lyapunov exponent or the inverse localization length [34, 35].

The Inverse Participation Ratio (IPR) for the  $E = 0$  state is given by

$$IPR_{\Psi(E=0)} = \frac{1 + \sum_{n=1}^{(N-1)/2} |\Psi_{2n+1}|^4}{\left(1 + \sum_{n=1}^{(N-1)/2} |\Psi_{2n+1}|^2\right)^2}. \quad (2.7)$$

The scaling of  $IPR$  with the system size  $N$  indicates its multifractal behavior. We first calculate the  $\langle IPR \rangle$  over many realizations and then plot the  $\ln \langle IPR \rangle$  as a function of  $\ln N$ . The result is shown in Fig.2.7 for different values of disorder strength  $W$ .

For small sizes there is a linear scaling and a fractal dimension  $D_2$  exists. For small  $W$  we see a dimension close to 1. As we increase the disorder  $W$  the  $D_2$  clearly has non-integer values. For strong enough disorder the dimension would eventually approach 0 and the multifractal behavior will vanish.

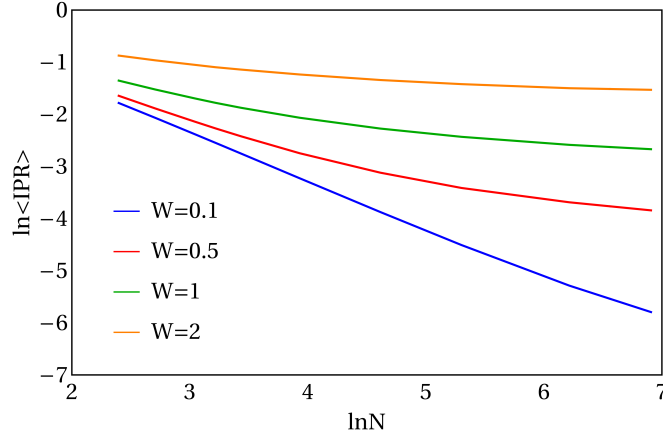


Figure 2.7: The scaling of  $\langle IPR \rangle$  with system size  $N$  at  $E = 0$ . A linear behavior can be observed for small sizes. An ensemble of  $10^5$  random realizations is considered.

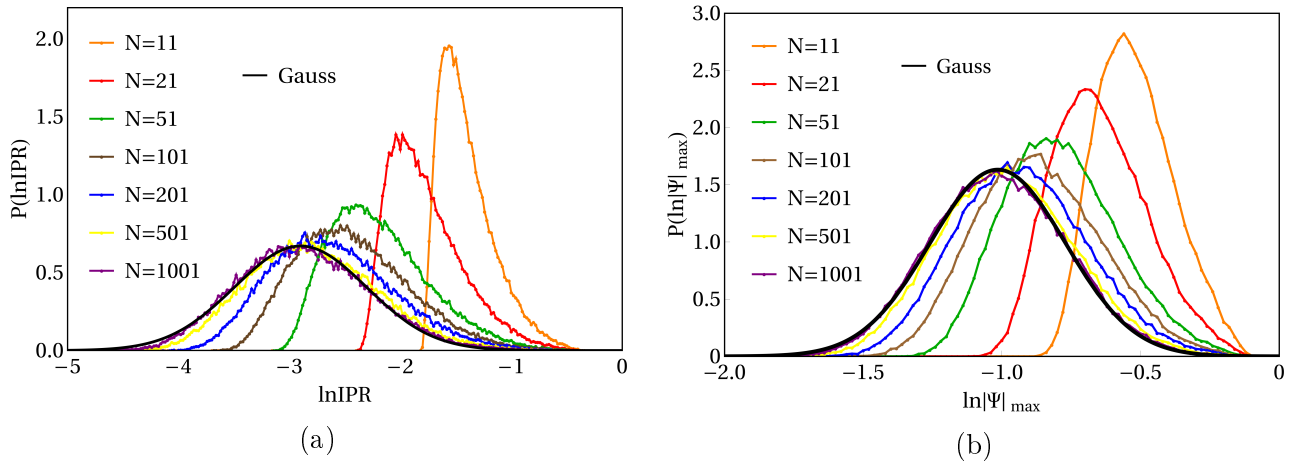


Figure 2.8: The probability distribution of (a)  $\ln IPR$  and (b)  $\ln |\Psi|_{max}$  at  $E = 0$  for different sizes  $N$ , disorder strength  $W = 1$  and an ensemble of  $10^5$  realizations.

In Fig.2.8 (a) we plot the probability distribution of  $\ln IPR$  for different sizes  $N$ . The disorder strength is  $W = 1$ . As we increase the size a fast convergence is apparent after about  $N = 101$ . The correlation dimension  $D_2$  exists only for small enough sizes.

In order to further check the convergence we calculated  $\ln|\Psi|_{max}$  and its scaling with the logarithm of size  $N$ . The result is shown in Fig. 2.8 (b). We clearly observe that the distribution of  $\ln|\Psi|_{max}$  is approaching a Gaussian with mean -1 and standard deviation of about 0.24. The result is in accordance to the random walk process exhibited by  $\ln|\Psi|$  (see Eq.2.6). Another measure that shows a similar behavior at  $E = 0$  is the Shannon Entropy

$$S = - \sum_{n=1}^N |\Psi_n|^2 \ln|\Psi_n|^2.$$

As we increase the system size  $N$  we also see a convergence of  $S$  to a Gaussian after  $N = 101$  and the existence of an information dimension  $D_1$  is obtained for small sizes. The result is plotted in Fig.2.9 for disorder strength  $W = 1$ .

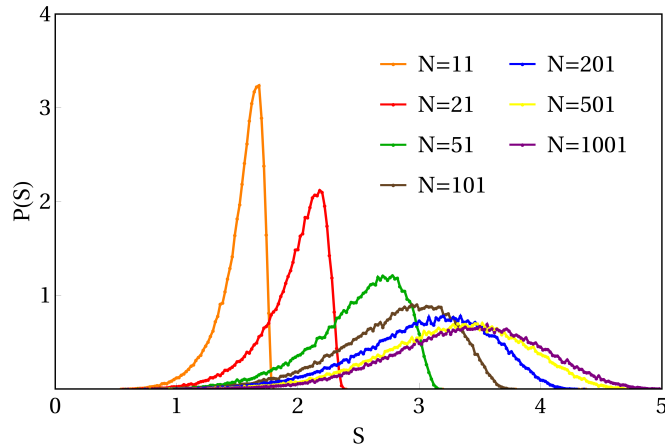


Figure 2.9: The probability distribution of the Shannon Entropy ( $S$ ) at  $E = 0$  for different sizes  $N$ , disorder strength  $W = 1$  and an ensemble of  $10^5$  realizations.

A picture of the  $E = 0$  wavefunction in 1D can be seen in Fig.2.10 (a) where the probability density is plotted versus a number of middle lattice sites for  $N = 5001$  and  $W = 0.5$ . In Fig.2.10 (b) the log-linear plot is presented and we can clearly see extreme fluctuations as they are revealed via the fractal structure.

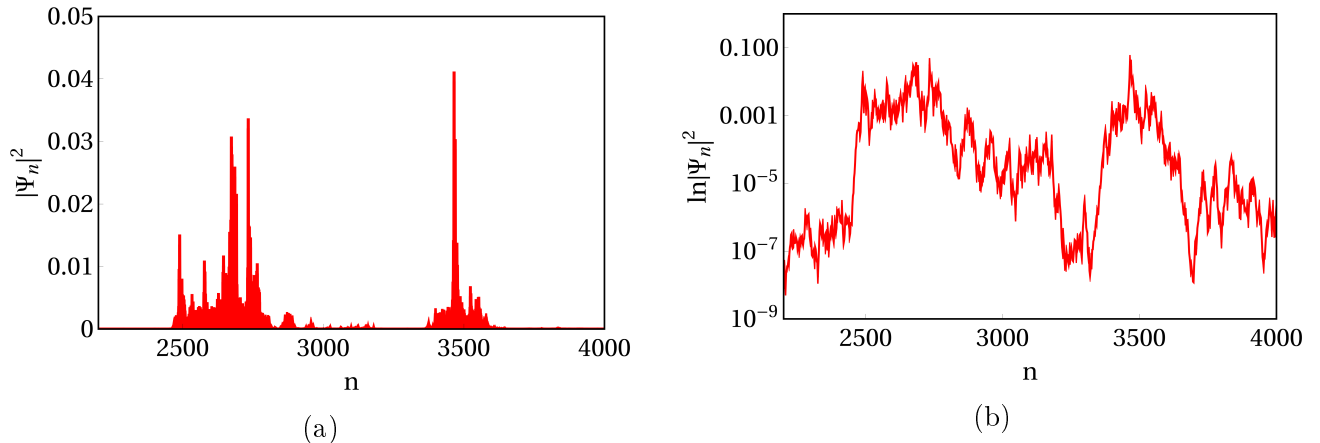


Figure 2.10: (a) The probability density  $|\Psi|^2$  for the  $E = 0$  state versus size, for  $N = 5001$  and  $W = 0.5$ . The range of sites is  $[2200, 4000]$  (b) The log-linear plot of (a).

We also study the effect of disorder on the correlation dimension  $D_2$  which is plotted as a function of  $W$  in Fig.2.11. For small values of  $W$  the  $D_2$  begins from 1 and approaches asymptotically to zero as  $W$  becomes larger. Besides the arithmetic mean  $\ln\langle IPR \rangle$ , we also provide results for the geometric mean  $e^{\langle \ln IPR \rangle}$  from the linear scaling of which  $\tilde{D}_2$  is calculated. The two curves are not the same and this is an implication that the  $E = 0$  state undergoes a "freezing" transition [36, 37]. For both cases, the fractal nature occurs for small sizes  $N$ .

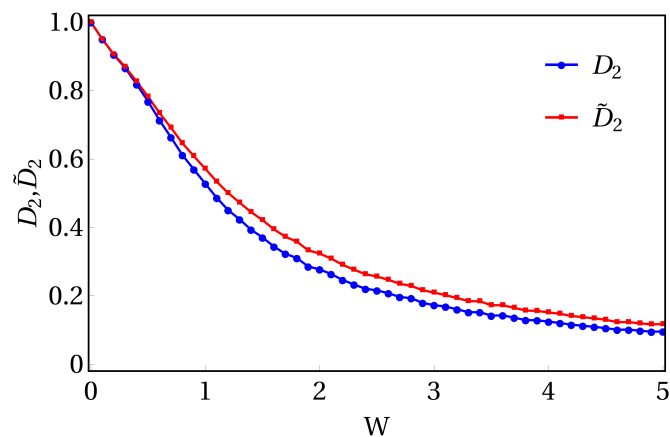


Figure 2.11: The correlation dimensions  $D_2$  and  $\tilde{D}_2$  as a function of disorder strength  $W$  for the  $E = 0$  state.

Multifractal analysis is an essential tool to study the wavefunction fluctuations near a critical regime [38, 13], e.g. at the critical point of the metal-insulator transition. In Fig.2.12 (a), we calculate the positive multifractal dimensions for  $q \in [0, 10]$  and  $a - f(a)$  spectra.

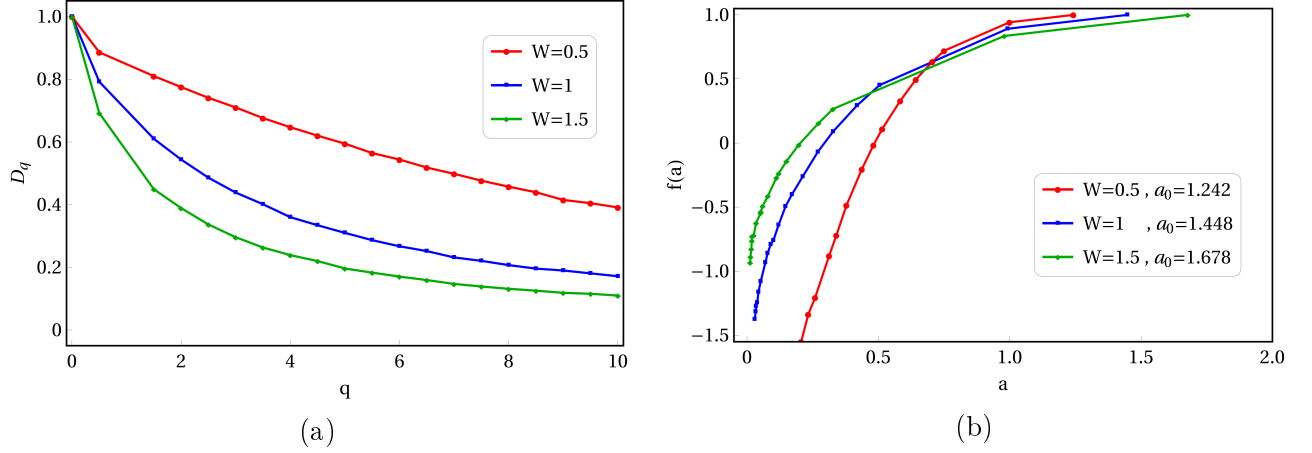


Figure 2.12: (a) The multifractal spectrum of dimensions  $D_q$ ,  $q \in [0, 10]$  for the  $E = 0$  state and  $W=0.5$  (red), 1 (blue), 1.5 (green). (b) The corresponding  $f(a)$  spectrum. It can also be seen how the position of the maxima  $a_0$  is affected by disorder.

For  $q = 0$ , we obtain the Hausdorff dimension  $D_0 = 1$  as expected for a 1D system. For  $q = 2$  we have the correlation dimension  $D_2$  we have already calculated explicitly. For larger values of  $q$ , we observe a decay towards  $D_q = 0$ . This behavior is more apparent when the disorder is further increased. We also describe the statistical properties of multifractal measures in terms of their singularity spectrum  $f(a)$  in Fig.2.12 (b) [39]. We define  $\tau_q = (q - 1)D_q$ . The  $f(a)$  and  $\tau_q$  are related by a Legendre transformation as

$$\tau_q = qa - f(a) \quad , \quad a = \frac{d\tau_q}{dq} \quad , \quad q = \frac{df(a)}{da} \quad , \quad (2.8)$$

where  $a$  is the Lipschitz-Hölder exponent and  $f(a_0) = D_0$ . For  $W = 1$ , the resulting exponent is  $a_0 \approx 1.45$ .

The level statistics at  $E_1$ , the closest energy near  $E = 0$ , is presented in the log-linear plot of Fig.2.13 (a),(b) for odd and even system sizes respectively. For odd sizes the consecutive level difference is  $S = E_1$  and for even sizes  $S = 2E_1$ . The Wigner curve is the dashed line whereas the Poisson is the solid black one. We observe that for the given disorder strength  $W = 1$  the system seems to follow the Wigner curve for  $N = 81$  and for  $N = 121$  ultimately reaches Poisson. Interestingly, a faster approach to localization and the Poisson limit is found for even sizes at  $N = 80$ . The system also passes from the Wigner curve at  $N = 20$ . This result indicates that the system briefly exhibits a quantum chaotic behavior (Wigner) for small sizes before reaching localization (Poisson). This crossover clearly is distinct for even and odd sizes  $N$ .

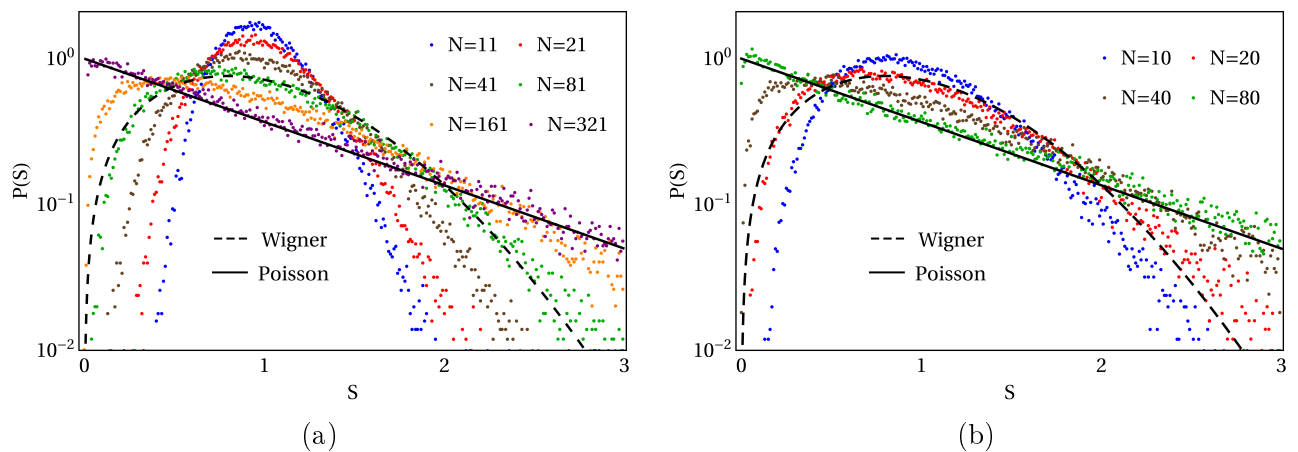


Figure 2.13: The distribution  $P(S)$  of the consecutive level spacing of the first positive energy  $E_1$  and  $W = 1$  in a log-linear plot for (a) odd sizes and (b) even sizes. An ensemble of 50000 realizations was considered.

## 2.3 2D Off-Diagonal Disorder

We now extend our model to a 2D square lattice [40, 41, 42, 43, 44] for two sublattices A and B and consider the vertical and horizontal random hoppings logarithmically distributed (Fig.2.5). The linear size of the lattices is  $L$  and  $N = L^2$ . When  $N$  is odd an  $E = 0$  mode always exists at the middle of the energy spectrum and the wavefunction has zero amplitude at the sites of B sublattice. A picture of a 2D wavefunction at  $E = 0$  is shown in Fig.2.14 where the logarithm of the wavefunction  $\ln|\Psi|$  is plotted for size  $N = 121^2 = 14641$  and various disorder strengths  $W = 0.1, 1, 2, 10$ .

It is apparent that the typical pictures of the 2D wavefunctions display fractal characteristics. For weak disorder ( $W = 0.1$ ), we observe an almost periodic distribution. For the intermediate values ( $W = 1, W = 2$ ) a fractal structure is obvious. For higher values of disorder ( $W = 10$ ) the amplitudes are extremely small and the wavefunction strongly decays. Moreover, these amplitudes are not concentrated in a small region of space but they seem scattered randomly over the lattice.

We study the multifractality of the  $E = 0$  state by scaling the  $\langle IPR \rangle$  with the linear size  $L$ . In Fig.2.15 (a) we plot the probability distribution of  $\ln IPR$  for various sizes and disorder  $W = 1$ . In contrast to the 1D case, we observe no convergence for the considered sizes.

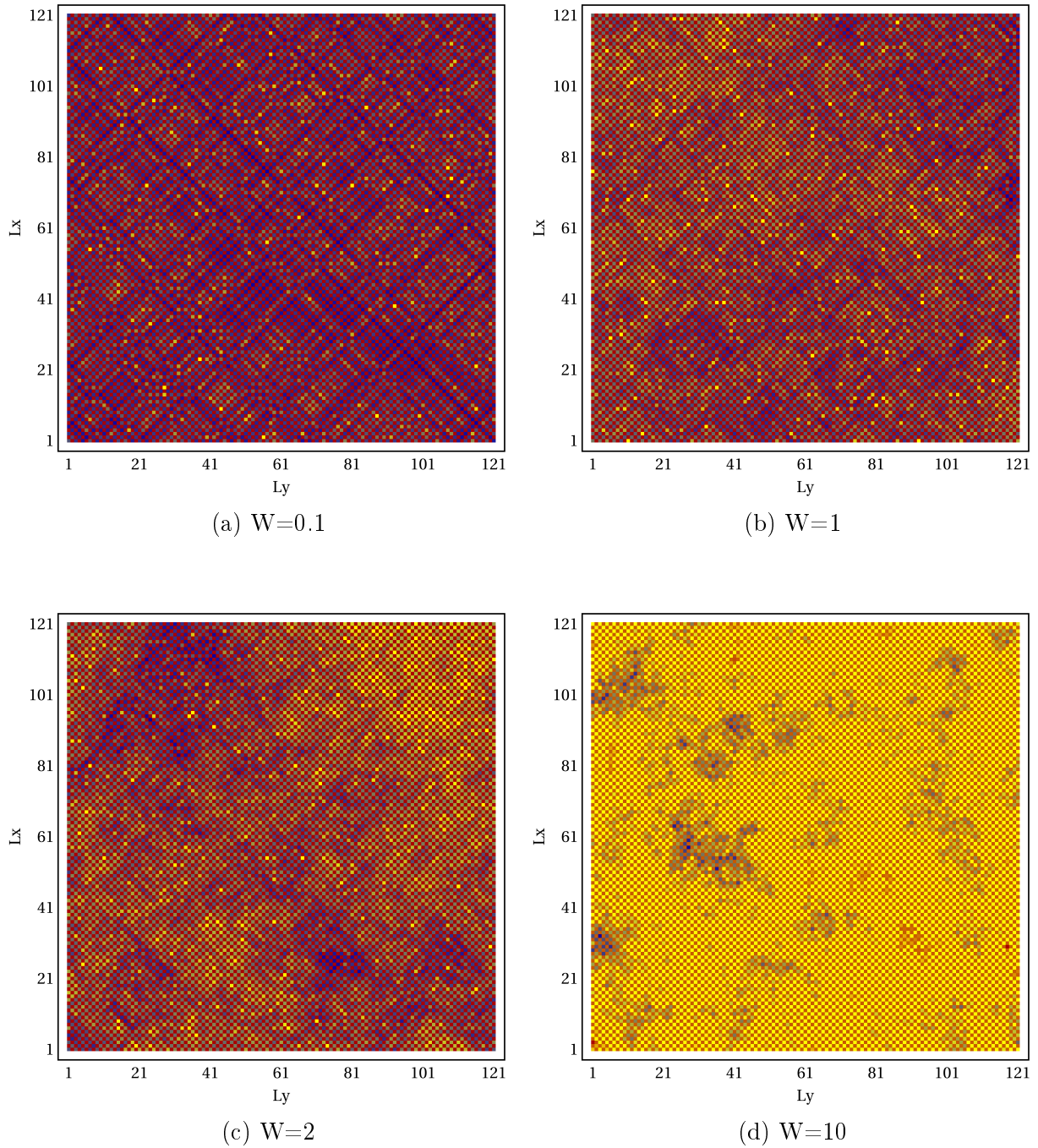


Figure 2.14:  $N = 121^2 = 14641$ . The logarithm of the  $E = 0$  wavefunction  $\ln|\Psi|$  for a 2D square lattice with random hopping and various disorder strengths, (a)  $W = 0.1$ , (b)  $W = 1$ , (c)  $W = 2$  and (d)  $W = 10$ . The purple areas represent the higher values and the dark yellow the lower values.

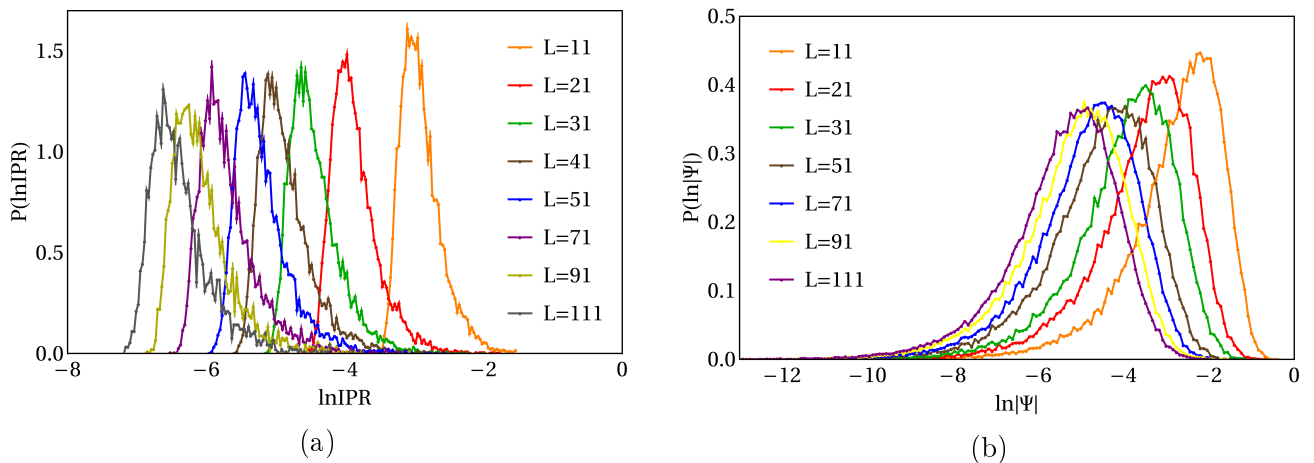


Figure 2.15: (a) The distribution  $P(\ln IPR)$  and (b) the logarithm of the  $E = 0$  wavefunction, for disorder strength  $W = 1$  and different sizes linear lengths  $L$ .

In Fig.2.15 (b) we plot the distribution of the logarithm of the  $E = 0$  wavefunction. For the sizes considered, it is not decisive whether we have convergence to a known distribution as in the 1D case. We also compute the scaling of arithmetic mean  $\langle \ln IPR \rangle$  and of geometric mean  $e^{\langle \ln IPR \rangle}$  with system size  $\ln N$ . From their linear scaling, we obtain the fractal dimensions  $D_2, \tilde{D}_2$ . The two curves are shown in Fig.2.16. Their difference again implies the existence of a "freezing" transition. We observe that for small values of  $W$ , the fractal dimension is almost 2 which means that the  $E = 0$  is a completely extended state covering all the available 2D space. For very large disorder ( $W > 10$ ) the  $D_2, \tilde{D}_2 \rightarrow 0$  and the wavefunction becomes localized. For intermediate values of disorder the dimension  $D_2, \tilde{D}_2$  acquire non-integer values and  $E = 0$  states exhibits a multifractal behavior.

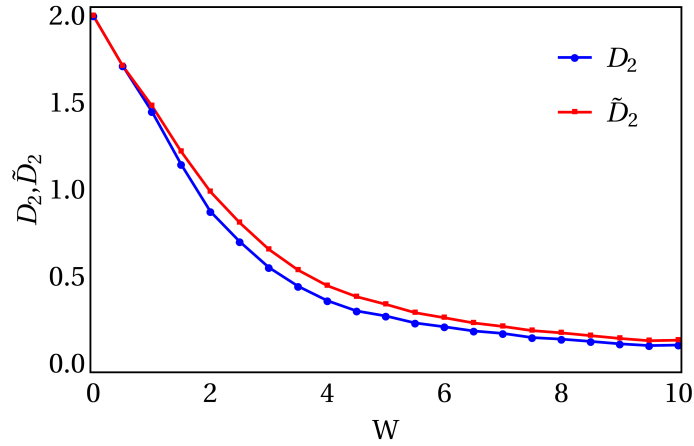


Figure 2.16: The fractal dimension  $D_2$  as a function of disorder strength  $W$  for the 2D  $E = 0$  wavefunction of the random hopping square lattice.

We further analyze the multifractal properties by calculating the multifractal spectrum  $D_q$ . We consider only positive multifractal dimensions with  $q \in [0, 10]$ . The results can be seen in Fig.2.17 (a).

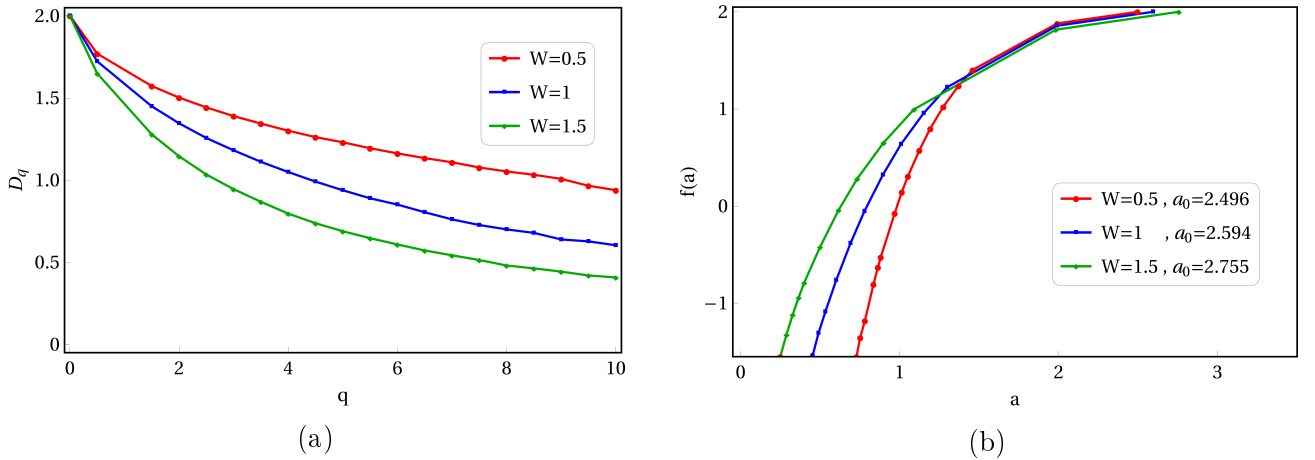


Figure 2.17: (a) The multifractal spectrum  $D_q$  for the  $E = 0$  state of the 2D random hopping model for  $W = 0.5$  (red), 1 (blue), 1.5 (green). (b) The corresponding  $f(a)$  spectrum.

For  $q = 0$ , the Hausdorff dimension  $D_0 = 2$  is obtained as expected for a 2D system. For  $q = 2$  we get the correlation dimension  $D_2$  as calculated before. For larger values of  $q$  a decay of  $D_q$  is observed. As  $W$  increases this behavior is even more quicker. We perform the Legendre transformation (Eq.2.8) to calculate the  $f(a)$  spectrum in Fig.2.17 (b). We

present how the multifractal spectrum scales with disorder and how the position of maximum is affected. For  $W = 1$ , the resulting exponent is  $a_0 \approx 2.6$ .

The level statistics of the  $E_1$ , the energy closest to  $E = 0$ , is presented in the log-linear plot of Fig.2.18.

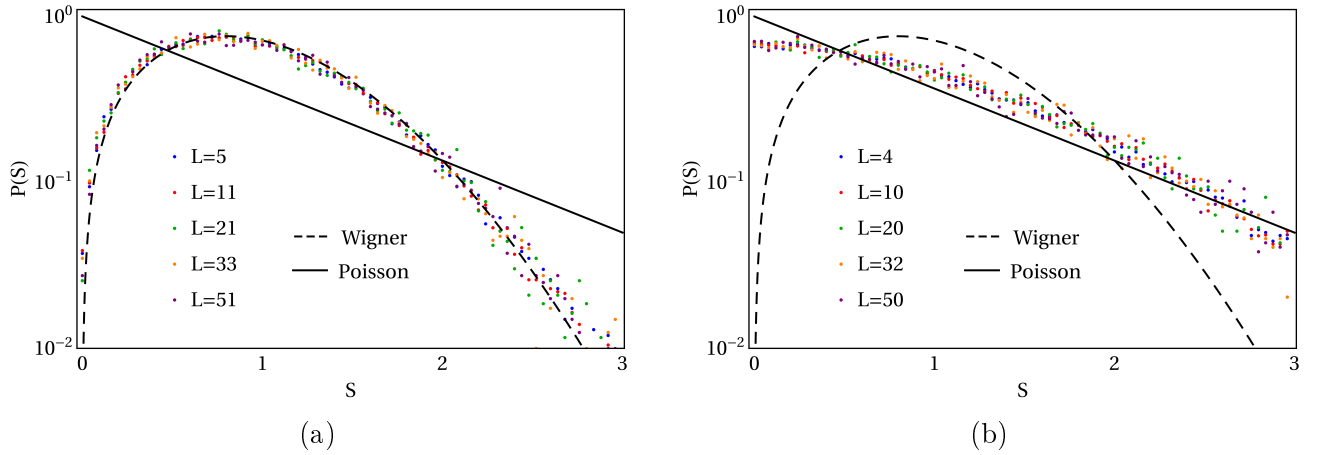


Figure 2.18: (a) The distribution  $P(S)$  of the consecutive level spacing for odd system sizes. (b) The distribution of the consecutive level spacing for even system sizes. In both cases the strength of disorder is  $W = 1$  and about  $10^4$  realizations are considered.

For odd sizes the consecutive level difference is  $S = E_1$  and for even sizes we have  $S = 2E_1$ . The Wigner curve is the dashed line whereas the Poisson is the solid black one. It is clear that  $P(S)$  follows closely the Wigner distribution in a scale-invariant way. For even sizes the behavior is rather different and neither Wigner nor Poisson is obtained. We have an intermediate behavior. The localization length in 2D is very large and a quantum chaotic behavior is expected for sizes way smaller than the localization length. For the sizes considered here, a clear distinction between even and odd sizes  $N$  exists.

## 2.4 Summary

In summary, we presented an analytical and numerical study for the effect of off-diagonal disorder in 1D and 2D systems. We focused mostly at the  $E = 0$  midband state which exists for finite lattices of odd size  $N$ .

In 1D, for even size  $N$  systems the corresponding level statistics of the first positive energy exhibits a faster approach to localization. On the contrary for odd size lattices Anderson localization occurs for larger values of  $N$ . The wavefunction of the random hopping chain is analytically calculated and is shown to be multifractal for small sizes (e.g.  $N < 100$  for  $W = 1$ ). More specifically, the correlation dimension  $D_2$  varies strongly with disorder as it ranges from space filling extended behavior ( $D_2 = 1$ ) for very weak disorder to point-like localized behavior ( $D_2 \rightarrow 0$ ) for very strong disorder. For intermediate values of disorder  $0 < D_2 < 1$ . The  $f(a)$  spectrum is also calculated and the position of the maximum for  $W = 1$  is found  $a_0 = 1.45$ .

In 2D, the level statistics for the first positive energy with odd size  $N$  is found to exhibit strong level repulsion and follow a scale-invariant Wigner distribution. For even sizes, we also find an invariance for the distribution which becomes intermediate to Wigner and Poisson. In 2D the  $E = 0$  wavefunction exhibits multifractal characteristics for sizes below the localization length. However, it is not decisive if a convergence to a known distribution exists as found in 1D. For small values of disorder  $D_2 = 2$  and the wavefunction is fully extended to the available space. For intermediate values disorder,  $0 < D_2 < 2$  and for very strong disorder  $D_2 \rightarrow 0$ . The calculated  $f(a)$  spectrum for  $W = 1$  shows a maximum at  $a_0 = 2.59$ .

In general, for large scales, chiral disordered systems behave like ordinary disordered systems except for the  $E = 0$  mode which shows a critical behavior. Recent experiments [45, 46, 47, 48, 49] concerning even-odd symmetry and zero modes are conducted with cold atoms, so it is of great importance to understand the nature of disorder and also how topological effects and interactions shape the features of such disordered systems.

# Chapter 3

## Topological Disordered Systems

Novel phases of matter and fascinating properties of materials have always been a main subject of research in condensed matter physics. In the last few decades, the role of topology in solid-state systems has attracted a lot of research interest. Topology is the branch of mathematics which studies abstract shapes and concerns quantities that remain intact invariant under continuous transformations, e.g. when we have a number of holes which remain although the shape might change. The topological phases are characterized by integer numbers which are called topological invariants, e.g. Chern numbers, winding numbers, etc. Two objects are topologically equivalent when they have the same topological invariant and can be continuously transformed into each other. A change in the topological invariant indicates a topological phase transition, e.g. by closing the holes or making the energy gap vanish for our systems.

Topological insulators are electronic materials that have insulating behavior in their interior (bulk) but conduct electricity on their surface. In other words, in the bulk the states can be Anderson localized due to disorder and in the surface conducting. In 3D we may have surface states, in 2D edge states and in 1D point-like states known as Majorana states. The topological states are robust and insensitive to smooth changes or small disorder. The first example of a topological insulator was the 2D Integer Quantum Hall Effect (IQHE)

discovered in the 1980's [50]. The Hall conductivity  $\sigma_{xy}$  for potential in the  $y$ -direction and current in the  $x$ -direction is quantized to integer values  $\frac{\nu e^2}{h}$ ,  $\nu$  is an integer with an accuracy of  $10^{-9}$ . The IQHE describes electrons moving on a 2D plane subjected to strong perpendicular magnetic field  $B$  and very low temperatures. According to classical mechanics electrons will follow circular orbits with radius  $\sim \frac{1}{B}$  and quantum mechanics replaces these orbits by quantized orbitals called Landau discrete energy levels  $E_n = (n + \frac{1}{2})\hbar\omega_c$ ,  $\omega_c = \frac{eB}{mc}$  is the cyclotron frequency. At the edges of a finite sample the electrons do not have enough space to complete a full circle and bounce off. This leads to "skipping orbits" which propagate along the edge in the direction determined by the magnetic field. These edge states are known to be chiral (one-way) and are responsible for the quantized Hall conductivity. The number of edge states defines the topological invariant called Chern number.

The theory developed for topological insulators can be generalized to topological superconductors. A superconductor is a material which below a very low critical temperature can conduct electricity without resistance. A topological superconductor has superconducting behavior in the bulk but hosts conducting states on the surface. In one-dimension the two point-like edge states corresponding to Majorana fermions are like particles being their own antiparticles [51, 52]. In a sense, they are halves of ordinary fermions and a fermionic state can be obtained as a superposition of two Majorana fermions. The Majorana fermions are well separated at the two ends of the chain and can be used to encode non-local quantum bits which perform error-resilient computation. The controlling and manipulating of these emergent properties of qubits poses a significant challenge as they are very fragile and prone to loss of their behavior via decoherence [53, 54, 55, 56].

In mid 90's, with the growing level of activity in disordered mesoscopic physics and superconductivity, an extension of the standard Wigner-Dyson universality classes was found by Altland and Zirnbauer [57] who introduced an expanded classification scheme based on generic symmetries which includes superconductors.

The time-reversal symmetry (TRS), the particle-hole symmetry (PHS) and their product chiral/sublattice symmetry (SLS) give the 10 universality classes shown in Table 1.1.

		TRS	PHS	SLS
standard (WD)	A (unitary)	0	0	0
	AI (orthogonal)	+1	0	0
	AII (symplectic)	-1	0	0
chiral (sublattice)	AIII (chiral unitary)	0	0	1
	BDI (chiral orthogonal)	+1	+1	1
	CII (chiral symplectic)	-1	-1	1
BdG	D	0	+1	0
	C	0	-1	0
	DIII	-1	+1	1
	CI	+1	-1	1

Table 3.1: Ten symmetry classes of single particle quantum Hamiltonian classified in terms of time-reversal symmetry (TRS), particle-hole symmetry (PHS) and chiral (or sublattice) symmetry (SLS).

The first 3 universality classes are the standard "Wigner-Dyson" classes used in quantum chaotic systems. The next 3 classes have the addition of chiral symmetry. A paradigmatic model with chiral symmetry is a bipartite lattice with off-diagonal disorder discussed in Ch.2. The last 4 classes are relevant to superconductors for Bogoliubov-deGennes quasi-particles in the presence of disorder [58, 59, 60, 61].

In the following sections we study the topological properties of one-dimensional superconducting chain with p-wave pairing and show how the presence of disorder affects the behavior of the  $E = 0$  Majorana modes. This work initiated in [62] where the effect of disorder in the Kitaev chain was considered.

### 3.1 1D p-wave Superconductor

We consider the toy model introduced by A.Kitaev [63, 64] which describes a 1D spinless p-wave superconductor supporting Majorana fermions. The spinless Hamiltonian is

$$H = \mu \sum_{j=1}^L c_j^\dagger c_j + t \sum_{j=1}^{L-1} (c_j^\dagger c_{j+1} + c_{j+1}^\dagger c_j) + \Delta \sum_{j=1}^{L-1} (c_j^\dagger c_{j+1}^\dagger + c_{j+1} c_j), \quad (3.1)$$

where  $c_j^\dagger(c_j)$  are the electron creation (annihilation) operator at site  $j$ ,  $t$  is the hopping,  $\mu$  the chemical potential and  $\Delta$  is the p-wave pairing amplitude. We assume  $\mu, t, \Delta$  to acquire real and positive values,  $L$  denotes the system size and we set the lattice constant equal to 1. We note that the p-wave pairing is unconventional in that the electrons pair in a triplet state with parallel spins in contrast to the conventional s-wave pairing of the Bardeen-Cooper-Schrieffer (BCS) mean-field theory [65] which only couples electrons with opposite spins in a singlet state [66, 67]. Nevertheless, in the p-wave model we consider each site to be either occupied or empty by an effectively spinless fermion and the superconducting term creates Cooper pairs in adjacent lattice sites. The Pauli exclusion principle forbids a site to be doubly occupied.

Due to the inherent particle-hole symmetry in superconducting systems, we can conveniently split the chain into two interconnected chains one for electrons and one for holes (see Fig.3.1).

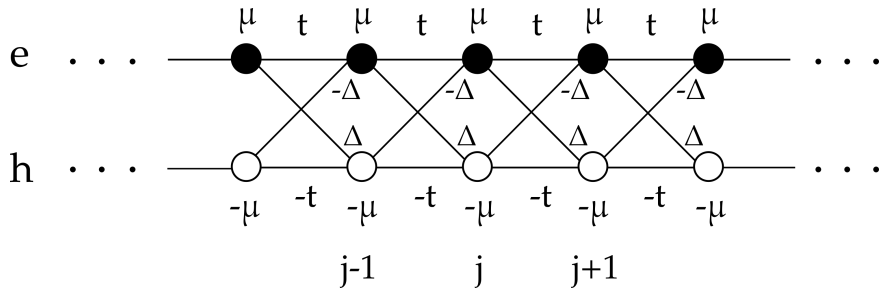


Figure 3.1: 1D chain with real p-wave pairing  $\Delta$ . The electron(hole) chain sites are depicted by full(empty) circles,  $j$  denotes the site.

The Schrödinger difference equations for the  $j$ -th unit cell are

$$\begin{aligned} E\Psi_j^e &= \mu\Psi_j^e + t\Psi_{j+1}^e + t\Psi_{j-1}^e + \Delta\Psi_{j+1}^h - \Delta\Psi_{j-1}^h \\ E\Psi_j^h &= -\mu\Psi_j^h - t\Psi_{j+1}^h - t\Psi_{j-1}^h - \Delta\Psi_{j+1}^e + \Delta\Psi_{j-1}^e. \end{aligned}$$

We take into account the periodicity of the lattice via the Bloch's theorem by assuming plane wave solutions  $\Psi_j^e = \Psi_e e^{ikj}$ ,  $\Psi_j^h = \Psi_h e^{ikj}$  for electrons and holes, respectively. We obtain

$$\begin{aligned} (E - \mu - te^{ik} - te^{-ik})\Psi_e - \Delta(e^{ik} - e^{-ik})\Psi_h &= 0 \\ \Delta(e^{ik} - e^{-ik})\Psi_e + (E + \mu + te^{ik} + te^{-ik})\Psi_h &= 0 \end{aligned}$$

and we find the eigenvalues

$$\begin{vmatrix} E - 2t\cos k - \mu & -2i\Delta\sin k \\ 2i\Delta\sin k & E + 2t\cos k + \mu \end{vmatrix} = 0 \Leftrightarrow (E - 2t\cos k - \mu)(E + 2t\cos k + \mu) - 4\Delta^2 \sin^2 k = 0$$

$$\Leftrightarrow E_{\pm}(k) = \pm\sqrt{(2t\cos k + \mu)^2 + (2\Delta\sin k)^2}, \quad k \in [-\pi, \pi]. \quad (3.2)$$

The energy dispersion relation for the 1D p-wave superconductor (Eq.3.2) consists of two energy bands, one for the electron and one for the hole. The Hamiltonian of spinless electrons in the momentum space can be written in the Bogoliubov-deGennes (BdG) form

$$H = \frac{1}{2} \sum_{k \in [-\pi, \pi]} \Psi_k^\dagger \mathcal{H}(k) \Psi_k, \quad \mathcal{H}(k) = \begin{pmatrix} -2t\cos k - \mu & -2i\Delta\sin k \\ 2i\Delta\sin k & 2t\cos k + \mu \end{pmatrix}, \quad (3.3)$$

where  $\Psi_k^\dagger = (c_k^\dagger \ c_{-k})$  is the two-component Nambu vector [68, 69]. The matrix  $\mathcal{H}(k)$  is a 2x2 Hermitian matrix written as

$$\begin{aligned}\mathcal{H}(k) &= \vec{d}(k) \cdot \vec{\sigma} = \\ &= (-2t\cos k - \mu)\sigma_z + (2\Delta\sin k)\sigma_y,\end{aligned}\tag{3.4}$$

in terms of the identity matrix  $\mathcal{I}$  and Pauli matrices  $\vec{\sigma} = (\sigma_x, \sigma_y, \sigma_z)$ , where the vector  $\vec{d}(k) = (d_x, d_y, d_z) = (0, 2\Delta\sin k, -2t\cos k - \mu)$ . The diagonalization of  $\mathcal{H}(k)$  gives the energy dispersion  $E_{\pm}(k)$  we have found, and the corresponding normalized eigenvectors which are

$$|\pm\rangle = \frac{d_y}{\sqrt{d_y^2 + (\sqrt{d_z^2 + d_y^2} \pm d_z)^2}} \begin{pmatrix} \frac{\pm i(\sqrt{d_z^2 + d_y^2} \pm d_z)}{d_y} \\ 1 \end{pmatrix}\tag{3.5}$$

In terms of the components of the vector  $\vec{d}(k)$  the energy dispersion can be rewritten as  $E_{\pm}(k) = \pm\sqrt{d_z^2 + d_y^2}$ . The gap closes when both

$$\begin{aligned}d_z &= 2t\cos k + \mu = 0 \\ d_y &= 2\Delta\sin k = 0\end{aligned}$$

are satisfied. This happens at  $k = 0$  for  $\mu = -2t$  and at  $k = \pi$  for  $\mu = 2t$ . Thus, we have 3 quantum phases,  $\mu < -2t$ ,  $-2t < \mu < 2t$ ,  $\mu > 2t$ . Since we initially assumed that  $\mu, t, \Delta \geq 0$ , the phase diagram  $(\frac{\Delta}{t}, \frac{\mu}{2t})$  of the 1D p-wave superconductor is plotted in Fig.3.2(a). In Fig.3.2(b-e), we show the energy dispersions  $E(k)$  at the exact points denoted with the red stars in Fig.3.2(a). When  $\mu$  varies from 0 to 3, the energy gap closes and reopens showing the band inversion mechanism characteristic to topological insulators and superconductors.

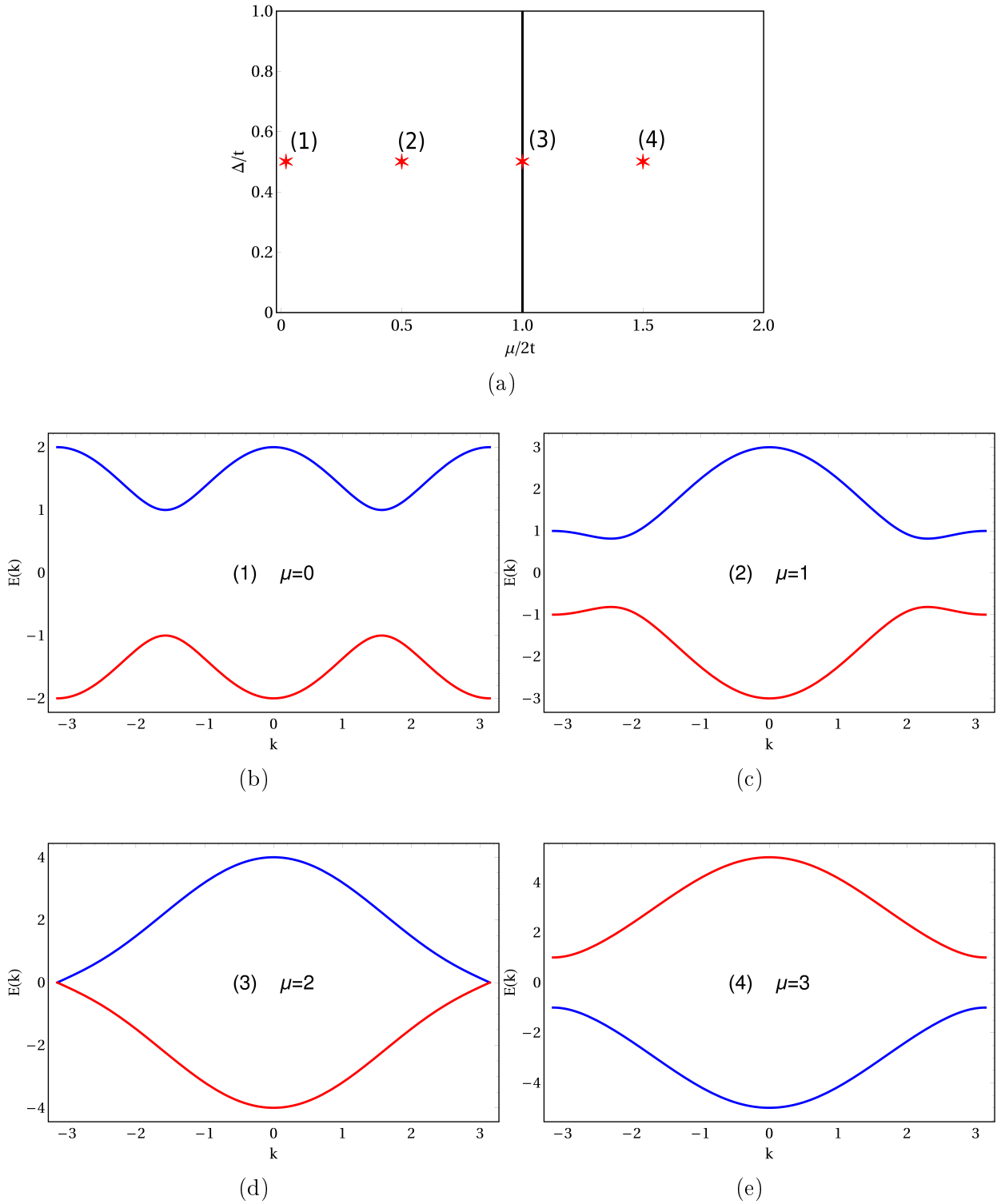


Figure 3.2: (a) The phase diagram  $(\frac{\Delta}{t}, \frac{\mu}{2t})$  of the 1D p-wave superconducting chain. The red stars indicate the special points for the energy dispersion (b)  $\mu = 0$ , (c)  $\mu = 1$ , (d)  $\mu = 2$  and (e)  $\mu = 3$ . In Fig.3.2(b)-(e) we have  $t = 1$  and  $\Delta = 0.5$ .

The topological aspects of this model are obtained by calculating the winding number  $\nu \in \mathbb{Z}$  which is an example of a topological invariant [70, 71]. The winding number defines the total number of times that a curve winds counterclockwise around a given point. In our case the curve follows the movement of the tip of the vector  $\vec{d}(k) = (0, 2\Delta \sin k, -2t \cos k - \mu)$  when  $k$  changes from  $-\pi$  to  $\pi$ . The tip moves around an ellipse on y-z plane with center at  $-\mu$ . For  $\mu = 0 < 2t$ , the origin of  $\vec{d}(k)$  is inside the elliptic loop and  $\nu = 1$  (Fig.3.2(b)). For  $\mu = 2t$ , the loop crosses the origin, the energy gap vanishes and  $\nu$  cannot be defined (Fig.3.2(d)). Finally, for  $\mu = 3 > 2t$ , the origin is outside the loop and  $\nu = 0$  (Fig.3.2(e)). The three cases are shown in the parametric plot of Fig.3.3. in blue, red and green, respectively.

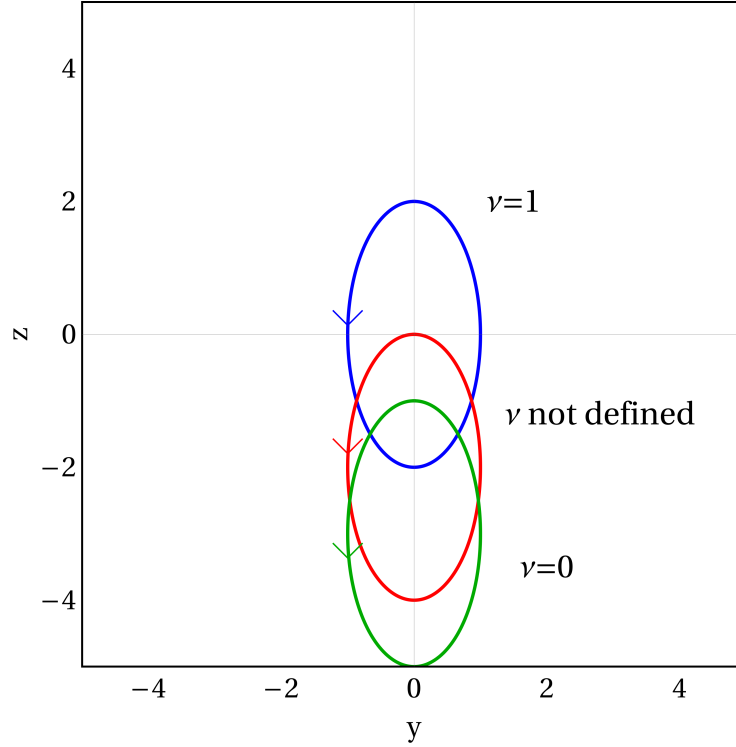


Figure 3.3: The winding number for the (a) non-trivial topological case  $\mu = 0$  (blue), (b) the topological phase transition point  $\mu = 2$  (red), (c) the trivial topological case  $\mu = 3$  (green). We set  $t = 1$  and  $\Delta = 0.5$ .

### 3.2 Disordered 1D p-wave Superconductor

Our aim is to study the Kitaev model in the presence of disorder. We focus our attention to systems of finite size  $L$ . The hopping  $t$  is a random variable from the uniform distribution  $[-\frac{W}{2}, \frac{W}{2}]$ ,  $W$  is the strength of the disorder. The pairing  $\Delta$  is a real positive number and  $\mu = 0$ . The Hamiltonian matrix for electrons and holes has dimension  $\dim(H) = 2L$  and open boundary conditions are considered. First, we study the sizes  $L = 2$  and  $L = 3$  which have the even-odd distinction.

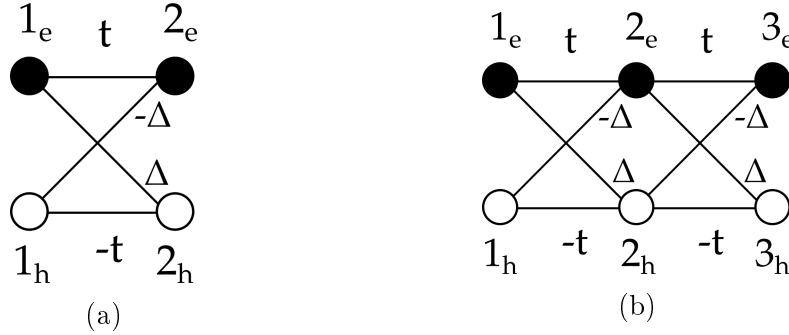


Figure 3.4: (a) Linear size  $L=2$  even and (b)  $L=3$  odd.

For  $L = 2$  (Fig.3.4 (a)), in the discrete basis  $\{|j\rangle, j = 1e, 2e, 1h, 2h\}$  the Hamiltonian matrix is

$$H_{L=2} = \begin{pmatrix} 0 & t & 0 & \Delta \\ t & 0 & -\Delta & 0 \\ 0 & -\Delta & 0 & -t \\ \Delta & 0 & -t & 0 \end{pmatrix}.$$

The matrix has eigenvalues  $E_1 = -t - \Delta$ ,  $E_2 = -t + \Delta$ ,  $E_3 = t - \Delta$ ,  $E_4 = t + \Delta$  and normalized eigenvectors

$$|\Psi_{E_1}\rangle = \frac{1}{2} \begin{pmatrix} -1 \\ 1 \\ 1 \\ 1 \end{pmatrix}, \quad |\Psi_{E_2}\rangle = \frac{1}{2} \begin{pmatrix} 1 \\ -1 \\ 1 \\ 1 \end{pmatrix}, \quad |\Psi_{E_3}\rangle = \frac{1}{2} \begin{pmatrix} -1 \\ -1 \\ -1 \\ 1 \end{pmatrix}, \quad |\Psi_{E_4}\rangle = \frac{1}{2} \begin{pmatrix} 1 \\ 1 \\ -1 \\ 1 \end{pmatrix} \quad (3.6)$$

The Inverse Participation Ratios of the corresponding eigenstates are  $IPR_{\Psi_{E_1}} = IPR_{\Psi_{E_2}} = IPR_{\Psi_{E_3}} = IPR_{\Psi_{E_4}} = \sum_{i=1}^N |\Psi_i|^4 = 4(\frac{1}{2})^4 = 0.25$ . For many realizations with disorder  $W = 1$  we calculated the density of states  $\rho(E)$  and  $IPR(E)$ . The plots are shown in Fig.3.5(a),(b).

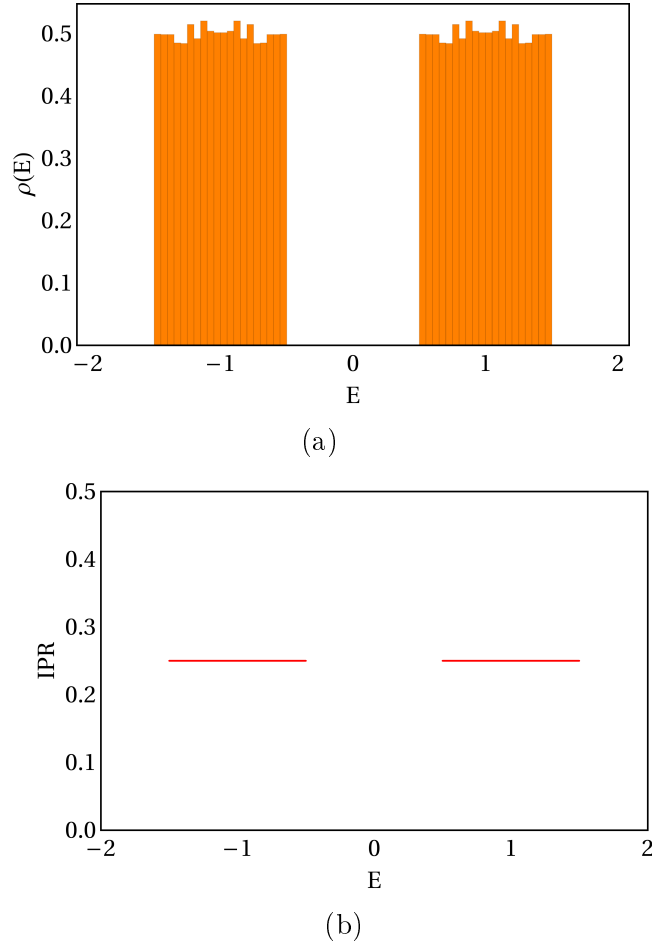


Figure 3.5:  $L = 2$ . (a) Density of states  $\rho(E)$  and (b) Inverse Participation Ratio  $IPR(E)$ . The pairing  $\Delta = 1$ .

For  $L = 3$  (Fig.3.4(b)), in the discrete basis  $\{|j\rangle, j = 1e, 2e, 3e, 1h, 2h, 3h\}$  the Hamiltonian matrix is

$$H_{L=3} = \begin{pmatrix} 0 & t & 0 & 0 & \Delta & 0 \\ t & 0 & t & -\Delta & 0 & \Delta \\ 0 & t & 0 & 0 & -\Delta & 0 \\ 0 & -\Delta & 0 & 0 & -t & 0 \\ \Delta & 0 & -\Delta & -t & 0 & -t \\ 0 & \Delta & 0 & 0 & -t & 0 \end{pmatrix}$$

The matrix has 3 doubly degenerate eigenvalues  $E_{1,2} = -\sqrt{2}(t^2 + \Delta^2)$ ,  $E_{3,4} = 0$ ,  $E_{5,6} = \sqrt{2}(t^2 + \Delta^2)$  and the normalized eigenvectors are

$$\begin{aligned} |\Psi_{E_1}\rangle &= \frac{1}{N} \begin{pmatrix} t/\Delta \\ -\frac{\sqrt{2(t^2+\Delta^2)}}{\Delta} \\ t/\Delta \\ -1 \\ 0 \\ 1 \end{pmatrix}, & |\Psi_{E_2}\rangle &= \frac{1}{N} \begin{pmatrix} -\frac{\sqrt{t^2+\Delta^2}}{\sqrt{2}\Delta} \\ t/\Delta \\ \frac{\Delta^2-t^2}{\Delta\sqrt{2(t^2+\Delta^2)}} \\ \frac{\sqrt{2}t}{\sqrt{t^2+\Delta^2}} \\ 1 \\ 0 \end{pmatrix}, & |\Psi_{E_3}\rangle &= \frac{1}{N} \begin{pmatrix} \frac{t}{2\Delta} - \frac{\Delta}{2t} \\ 0 \\ -\frac{t^2+\Delta^2}{2t\Delta} \\ 0 \\ 0 \\ 1 \end{pmatrix} \\ |\Psi_{E_4}\rangle &= \frac{1}{N} \begin{pmatrix} \frac{t^2+\Delta^2}{2t\Delta} \\ 0 \\ -\frac{t}{2\Delta} + \frac{\Delta}{2t} \\ 1 \\ 0 \\ 0 \end{pmatrix}, & |\Psi_{E_5}\rangle &= \frac{1}{N} \begin{pmatrix} t/\Delta \\ \frac{\sqrt{2(t^2+\Delta^2)}}{\Delta} \\ t/\Delta \\ -1 \\ 0 \\ 1 \end{pmatrix}, & |\Psi_{E_6}\rangle &= \frac{1}{N} \begin{pmatrix} \frac{\sqrt{t^2+\Delta^2}}{\sqrt{2}\Delta} \\ t/\Delta \\ \frac{t^2-\Delta^2}{\Delta\sqrt{2(t^2+\Delta^2)}} \\ -\frac{\sqrt{2}t}{\sqrt{t^2+\Delta^2}} \\ 1 \\ 0 \end{pmatrix}, \end{aligned}$$

$N$  is the normalization. Considering many realizations with disorder  $W = 1$  we calculated the density of states  $\rho(E)$  and  $IPR(E)$  shown in Fig.3.6(a),(b).

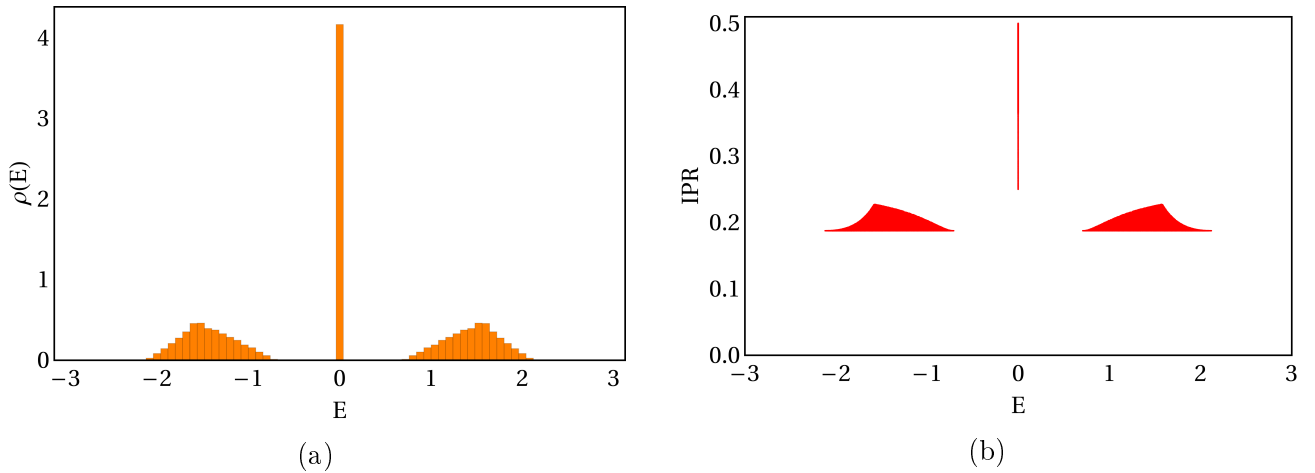


Figure 3.6:  $L = 3$ . (a) Density of states  $\rho(E)$  and (b) Inverse Participation Ratio  $IPR(E)$ . The pairing  $\Delta = 1$ .

We observe an important difference between the two cases in analogy to the  $\Delta = 0$  case studied in Ch.2. For odd linear size  $L = 3$  degenerate  $E = 0$  modes exist (Fig.3.6(a)) which are not present in even  $L = 2$  system (Fig.3.5(a)). The  $E = 0$  states are the Majorana modes. This even-odd distinction which is apparent in very small sizes also holds true for larger  $L$ . In Fig.3.7 we show the  $E = 0$  doubling for  $L = 20$  (even) and  $L = 21$  (odd) where  $W = 1$ .

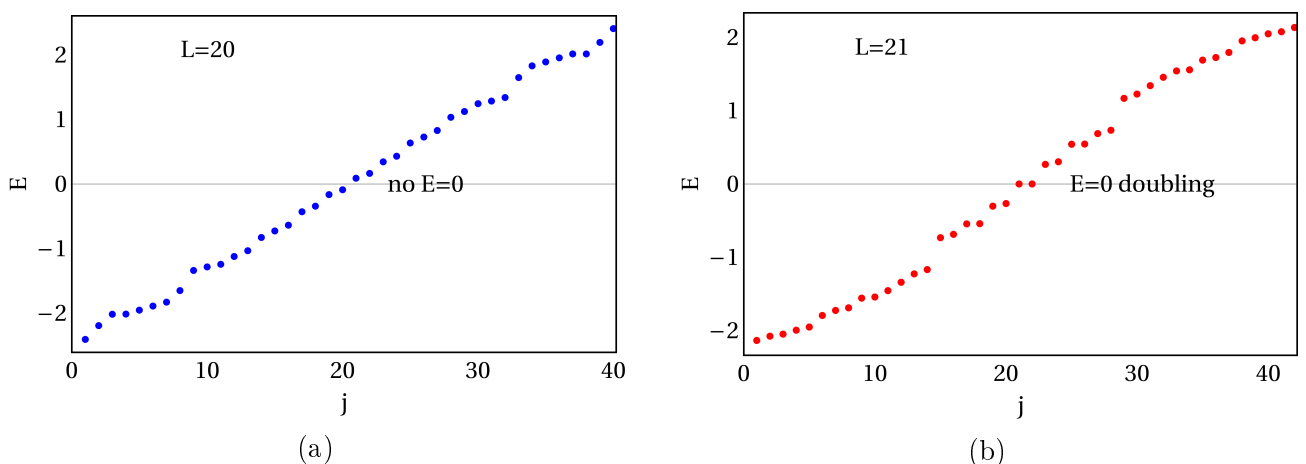
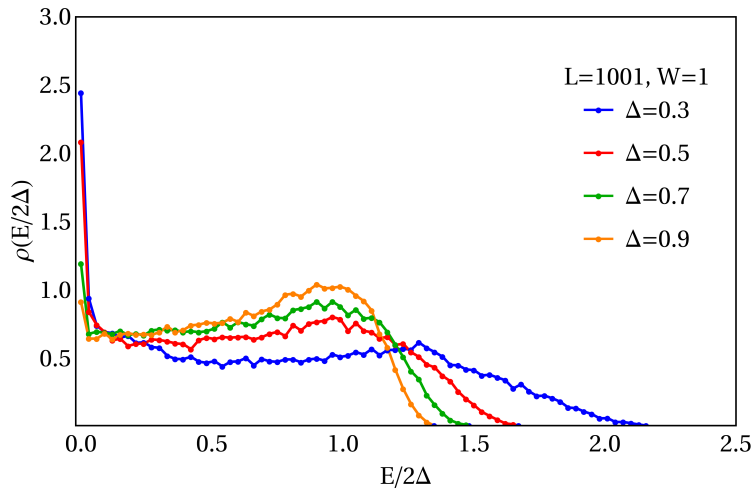


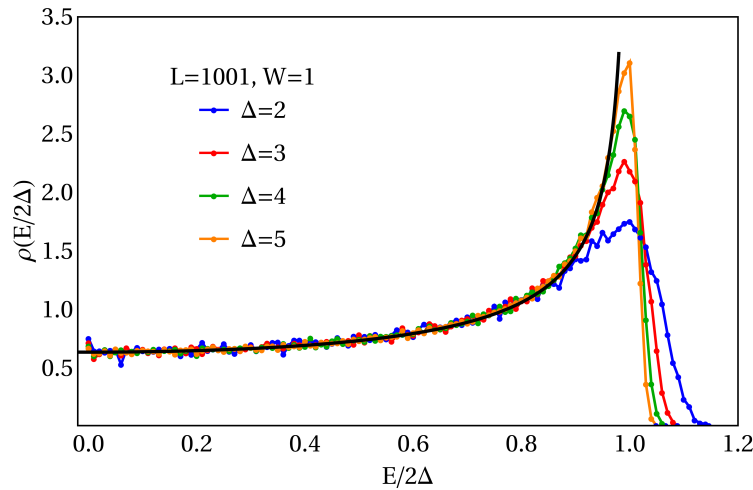
Figure 3.7: The  $E = 0$  doubling for sizes (a)  $L = 20$  and (b)  $L = 21$  for  $\Delta = 1$  and  $W = 1$ . The index  $j$  numbers the eigenvalues.

### 3.3 Level Statistics

In order to further study the Kitaev model near  $E = 0$  we plot the density of states  $\rho(E)$  for size  $L = 1001$  with fixed off-diagonal disorder  $W = 1$ . We vary  $\Delta$  from smaller than 1 to larger than 1 values. The two limits are shown in Fig.3.8.



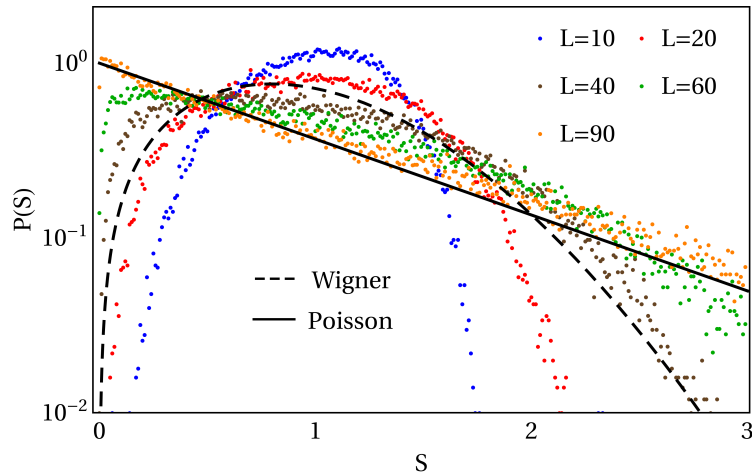
(a)



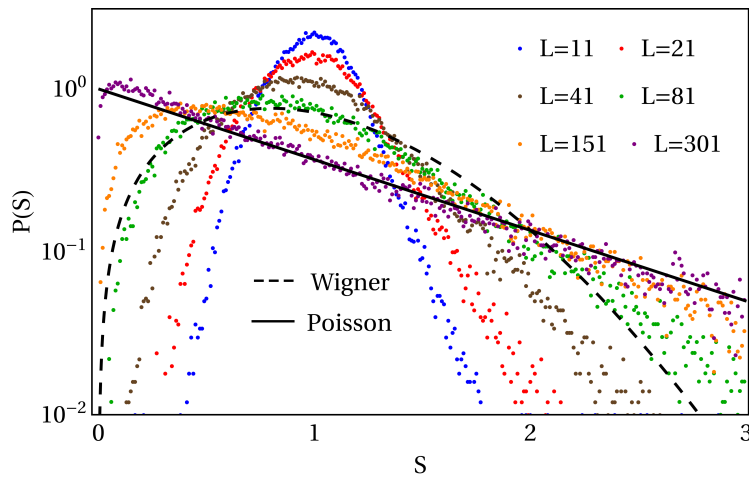
(b)

Figure 3.8: The density of states  $\rho(E)$  for  $W = 1$  and (a)  $\Delta < 1$  and (b)  $\Delta > 1$ . The linear size is  $L = 1001$ . The solid black curve is the density of states  $\rho(E)$  in 1D for  $W = 0$  (Ch.1.1).

We observe a peak at  $E = 0$  when  $\Delta$  approaches zero in the "localization" limit  $W \gg \Delta$ . On the contrary, when  $\Delta$  increases  $W \ll \Delta$  and the density of states behaves much more like the 1D system in the absence of disorder represented by a solid black curve in Fig.3.8(b).



(a)



(b)

Figure 3.9: The distribution  $P(S)$  of the consecutive level spacing of the first positive energy  $E_1$ ,  $W = 1$  and  $\Delta = 1$  for (a) even sizes and (b) odd sizes. An ensemble of 50000 realizations is considered. The dashed curve is the Wigner distribution and the solid line is the Poisson distribution.

In order to study the energy level statistics near  $E = 0$ , we employ the spacings between consecutive levels  $S = 2E_1$  for even  $L$  and  $S = E_1$  for odd  $L$ . We set  $W = 1$  and  $\Delta = 1$  fixed. The resulting log-linear plots are shown in Fig.3.9(a),(b). We find a faster approach to Poisson limit for even size systems than for odd sizes in accordance with 1D lattices with  $\Delta = 0$  studied in Ch.2.

### 3.4 Majorana Mode Multifractality

We now focus on the wavefunction statistics of the  $E = 0$  Majorana modes in the presence of disorder. For  $W = 0$  ( $t = 1$ ),  $\Delta \neq 0$  and odd linear size  $L$ , we find two Majorana modes localized at the two edges of the 1D chain. They are shown in Fig.3.10 with blue and red color respectively.

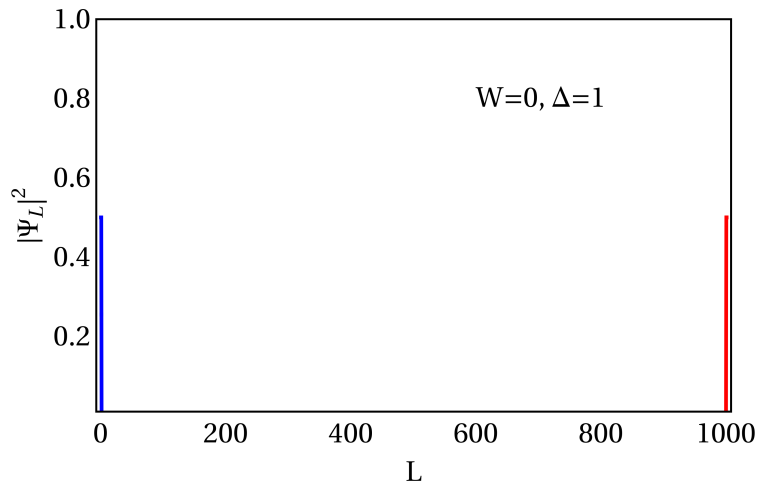


Figure 3.10: The two Majorana modes localized at the edges for the linear size  $L = 1001$ .

For  $W \neq 0$  ( $t$  random) the situation changes. The two Majorana modes become delocalized and spread inside the whole lattice. In Fig.3.11 we show the structure of one Majorana mode (blue) for various values of disorder  $W$  and fixed  $\Delta = 1$ . The linear size is  $L = 1001$ .

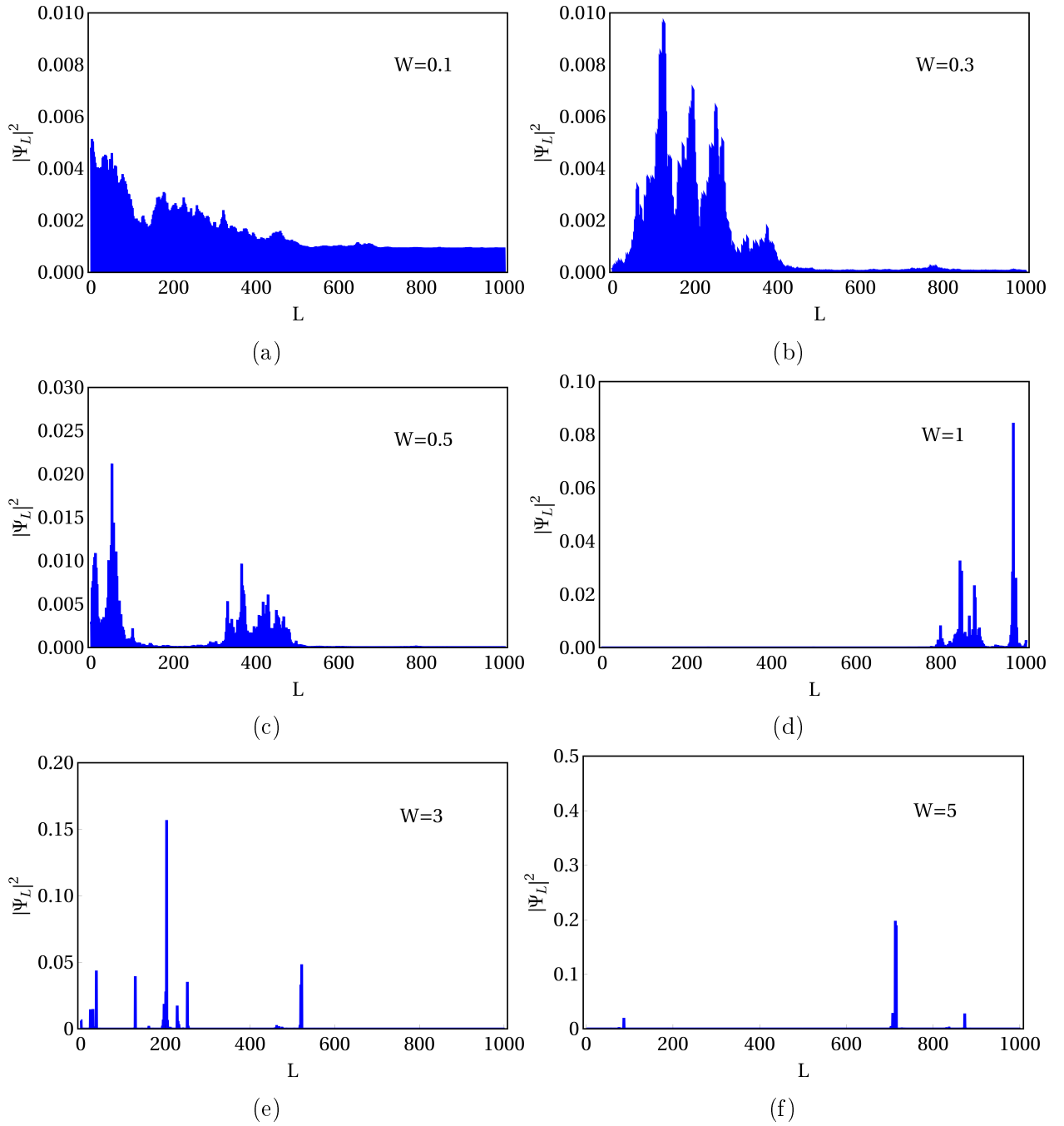


Figure 3.11: The spread of the 1D Majorana mode for various values of disorder  $W$  (a)-(f).

The  $E = 0$  Majorana mode in the presence of off-diagonal disorder can be treated via a recursive relation without diagonalizing the Hamiltonian. The amplitude on each site is calculated by a product of transfer matrices. The first iteration is shown in Fig.3.12. The system size is denoted by  $L$  and  $M = \frac{L+1}{2}$  is the number of e-h pairs.

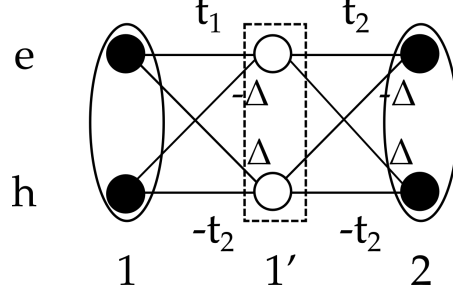


Figure 3.12: The representation of the transfer matrix for  $L = 3$ . The  $E = 0$  wavefunction has non-zero amplitudes at the filled circles and zero at the empty ones.

The Schrödinger difference equations for the e-h pair  $1'$  are

$$\begin{aligned} t_1 \Psi_1^e + t_2 \Psi_2^e - \Delta \Psi_1^h + \Delta \Psi_2^h &= 0 \\ -t_1 \Psi_1^h - t_2 \Psi_2^h + \Delta \Psi_1^e - \Delta \Psi_2^e &= 0 \end{aligned}$$

$$\Leftrightarrow \begin{pmatrix} t_1 & -\Delta \\ \Delta & -t_1 \end{pmatrix} \begin{pmatrix} \Psi_1^e \\ \Psi_1^h \end{pmatrix} = \begin{pmatrix} -t_2 & -\Delta \\ \Delta & t_2 \end{pmatrix} \begin{pmatrix} \Psi_2^e \\ \Psi_2^h \end{pmatrix}$$

$$\Leftrightarrow \begin{pmatrix} \Psi_2^e \\ \Psi_2^h \end{pmatrix} = \begin{pmatrix} -t_2 & -\Delta \\ \Delta & t_2 \end{pmatrix}^{-1} \begin{pmatrix} t_1 & -\Delta \\ \Delta & -t_1 \end{pmatrix} \begin{pmatrix} \Psi_1^e \\ \Psi_1^h \end{pmatrix}$$

$$\Leftrightarrow \begin{pmatrix} \Psi_2^e \\ \Psi_2^h \end{pmatrix} = \frac{1}{\Delta^2 - t_2^2} \begin{pmatrix} \Delta^2 + t_1 t_2 & -\Delta(t_1 + t_2) \\ -\Delta(t_1 + t_2) & \Delta^2 + t_1 t_2 \end{pmatrix} \begin{pmatrix} \Psi_1^e \\ \Psi_1^h \end{pmatrix}.$$

The recursive relation is expressed as

$$\Leftrightarrow \begin{pmatrix} \Psi_M^e \\ \Psi_M^h \end{pmatrix} = \prod_{j=M-1}^1 \frac{1}{\Delta^2 - t_{2j}^2} \begin{pmatrix} \Delta^2 + t_{2j-1}t_{2j} & -\Delta(t_{2j-1} + t_{2j}) \\ -\Delta(t_{2j-1} + t_{2j}) & \Delta^2 + t_{2j-1}t_{2j} \end{pmatrix} \begin{pmatrix} \Psi_1^e \\ \Psi_1^h \end{pmatrix}$$

We calculate the  $\langle IPR \rangle$  for large  $L$  over many realizations and plot the  $\ln \langle IPR \rangle$  as a function of  $\ln N$ . The result is shown in Fig.3.13(a) for different values of disorder  $W$ .

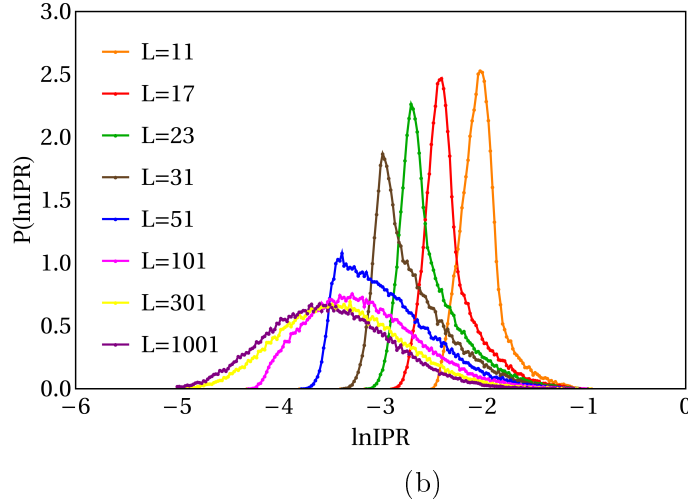
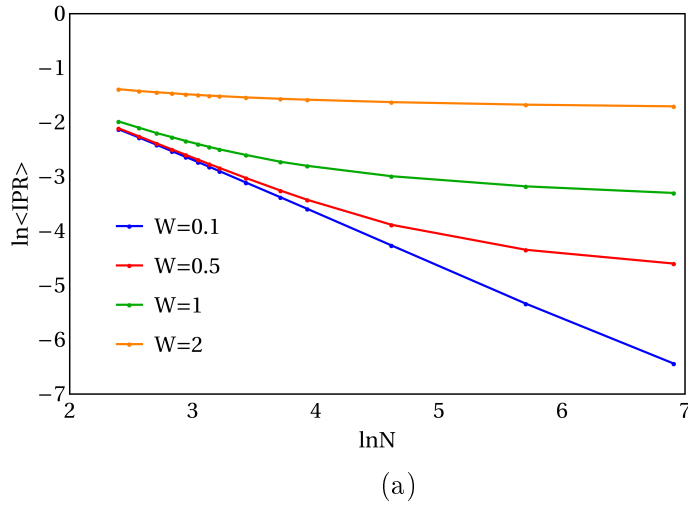


Figure 3.13: (a) The scaling of  $\langle IPR \rangle$  with system size  $L$  at  $E = 0$  for  $\Delta = 1$ . The ensemble consists of  $10^5$  realizations. An almost linear behavior is observed for small sizes and small values of disorder. (b) For  $W = 1$  and  $\Delta = 1$  the probability distribution of  $\ln IPR$  for several sizes  $L$  approaches a Gaussian as found in Ch.2.

We observe a linear scaling for small values of disorder  $W$  so that a fractal dimension  $D_2$  can be defined. As we increase  $W$  the slope becomes constant with the size and  $D_2 \rightarrow 0$  which implies localized states. In Fig.3.13(b) we plot the probability distribution of  $\ln IPR$  for different sizes  $L$  and disorder strength  $W = 1$ . As we increase the size, a fast convergence is apparent for sizes larger than  $L = 101$ . This gives a correlation dimension  $D_2$  only for small enough sizes since the linear fit vanishes for larger  $L$ .

The effect of disorder on the correlation dimension  $D_2$  is shown in Fig.3.14. We highlight that for  $W = 0$  the  $D_2 = 0$ . This is because the Majorana mode is strongly localized and it has no fractal dimension. As we increase  $W$  the  $D_2$  acquires non-integer values and for strong enough disorder  $D_2 \rightarrow 0$ . The geometric mean  $e^{\langle \ln IPR \rangle}$  from the linear scaling gives the dimension  $\tilde{D}_2$ . The  $D_2$  and  $\tilde{D}_2$  differ so that a kind of freezing transition exists.

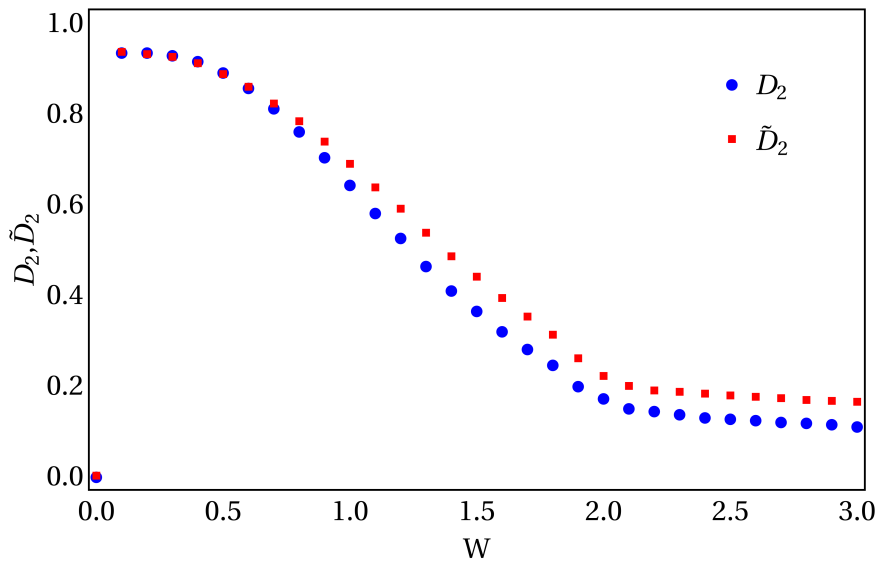


Figure 3.14: The correlation dimension  $D_2$  and  $\tilde{D}_2$  of the Majorana mode with  $\Delta = 1$  as a function of disorder  $W$ .

### 3.5 Summary

The p-wave superconductor in one dimension without disorder demonstrates interesting topological properties via the appearance of two Majorana modes localized at the two ends of the chain. We add hopping disorder in the chain to examine the fate of the Majorana topological modes. We find an even-odd asymmetry as in Ch.2. A double degeneracy at  $E = 0$  occurs only for odd systems. At the vicinity of  $E = 0$  the calculation of level statistics shows a faster approach to localization for even  $L$  sizes in comparison to odd  $L$  systems, as in the case of disorder only ( $\Delta = 0$ ) studied in Ch.2. We have derived a recurrence relation for the  $E = 0$  state by using the product of transfer matrices. The scaling of the  $\ln\langle IPR \rangle$  and the  $\langle \ln IPR \rangle$  with the logarithm of the system size gives the correlation dimension  $D_2$  and  $\tilde{D}_2$ , respectively. For  $W = 0$  the Majorana mode is localized and has  $D_2 = \tilde{D}_2 = 0$ . For  $W \neq 0$ , the state spreads inside the lattice and acquires non-zero  $D_2, \tilde{D}_2$  which indicate a multifractal character. For very strong disorder, the state becomes localized with correlation dimensions  $D_2, \tilde{D}_2 \rightarrow 0$ .

# Chapter 4

## Many-Body Localization

### 4.1 Thermalization .vs. Localization

We have seen how the presence of disorder and topology affect the behavior of quantum condensed matter systems. The addition of interactions makes the problem highly complicated due to the required exponentially large Hilbert space. In general, a disordered many-body system can either thermalize (ergodic) or become many-body localized (MBL). Thermalization means that a state will cover all the available Hilbert space and the system will achieve uniform temperature and equipartition of energy occurs. MBL, instead, means that a state will be confined in a finite region of the many-body Hilbert space. MBL is a quantum phenomenon related with the absence of ergodicity in the system and denotes its failure to thermally equilibrate.

A closed quantum system that is isolated from the environment will unitary evolve in time according to the Schrödinger equation. If the system is initially in a quantum state  $|\Psi_0\rangle$  it will reach a thermal Gibbs state. In order for this to happen the system has to be able to act as its own reservoir. The thermal state contains no information about the initial state, but according to the laws of Thermodynamics, information itself cannot be erased. The system has no memory and in a sense hides the quantum information. On the

contrary, the Anderson localized systems cannot act as their own reservoirs and therefore do not exhibit thermalization. This raises the fundamental question whether a many-body system thermalizes or not. The system with MBL avoids scrambling of stored quantum information and can be used for quantum computing. A quantum manifestation of thermal behavior is the Eigenstate Thermalization Hypothesis (ETH) [19, 20] which explains when a quantum system can be described by equilibrium statistical mechanics. It states that the mean value of the local observables at long times will follow the microcanonical ensemble. MBL systems seem to violate the hypothesis of quantum thermalization.

Over the last few years [72], numerous works have revealed several interesting properties of MBL. For recent reviews, see [24, 73, 74]. The main result is the existence of a disordered-induced dynamical transition between a thermal (ergodic) phase and a localized (non-ergodic) phase [21, 75]. There is also evidence that for weak disorder the states are ergodic and obey Wigner statistics, i.e. chaotic with level repulsion. For strong disorder the MBL eigenstates are non-ergodic and obey Poisson statistics like integrable systems. In the intermediate region the states can be extended non-ergodic [76].

The topic of MBL continues to attract much attention and experimental methods have been developed, mostly with ultracold atoms. These atoms are well isolated from the environment exhibiting high level of quantum coherence. They are stored in optical lattices, i.e. crystals made of light which are used to trap atoms at very low temperatures [77, 78]. The disorder is introduced by special modulated laser beams which can localize the spins in space probing the features of MBL.

The problem presents a tedious computational task because of the exponentially large dimension of many-body Hilbert space. We choose the method of exact diagonalization [72] and we get the phase diagram for a many-body disordered system by examining level statistics. We also pursue an eigenstate analysis. Several computational methods [79] are also employed, such as decimation schemes [80] and machine learning techniques [81, 82]

which help to distinguish many-body localized from ergodic eigenstates.

## 4.2 The Model

We study an isolated and static system of interacting spinless electrons at half-filling [83].

The Hamiltonian of the system in a one-dimensional disordered lattice is

$$H = t \sum_j (c_j^\dagger c_{j+1} + c_{j+1}^\dagger c_j) + \sum_j V_j \left( n_j - \frac{1}{2} \right) + \sum_j U_j \left( n_j - \frac{1}{2} \right) \left( n_{j+1} - \frac{1}{2} \right), \quad (4.1)$$

where  $t$  is the hopping matrix element,  $V_j$  is the on-site random potential,  $U_j$  is the random interaction strength and  $n_j = c_j^\dagger c_j$  is the occupation number operator. This fermionic model can be exactly mapped to the Heisenberg XXZ quantum spin chain via the Jordan-Wigner Transformation [84]

$$c_j^\dagger = S_j^+ e^{-i\pi \sum_{m=1}^{j-1} S_m^+ S_m^-}, \quad c_j = e^{i\pi \sum_{m=1}^{j-1} S_m^+ S_m^-} S_j^-. \quad (4.2)$$

The spin-1/2 particles are fermions and we use the analogy that the spin "down" state can be seen as an empty lattice site, whereas the spin "up" state can be seen as a site occupied by a single fermion. We can now calculate each term of the Hamiltonian. The hopping term between two neighbors  $j, j + 1$  is

$$\begin{aligned} c_j^\dagger c_{j+1} &= S_j^+ e^{-i\pi \sum_{m=1}^{j-1} S_m^+ S_m^-} e^{i\pi \sum_{m=1}^j S_m^+ S_m^-} S_{j+1}^- = \\ &= S_j^+ e^{i\pi S_m^+ S_m^-} S_{j+1}^- \\ &= -2S_j^+ S_j^z S_{j+1}^- \\ &= -2\left(-\frac{1}{2}S_j^+\right)S_{j+1}^- \\ &= S_j^+ S_{j+1}^-, \end{aligned} \quad (4.3)$$

where we have used the relation  $e^{\pm i\pi S_j^+ S_j^-} = e^{\pm i\pi(\frac{1}{2} + S_j^z)} = -2S_j^z$ . Similarly, we have  $c_{j+1}^\dagger c_j = S_j^- S_{j+1}^+$  for the complex conjugate part.

The on-site  $j$  term is

$$\begin{aligned} c_j^\dagger c_j &= S_j^+ e^{-i\pi \sum_{m=1}^j S_m^+ S_m^-} e^{i\pi \sum_{m=1}^j S_m^+ S_m^-} S_j^- = \\ &= S_j^+ S_j^- \\ &= \frac{1}{2} + S_j^z. \end{aligned} \quad (4.4)$$

The Hamiltonian of Eq.(4.1) becomes

$$H = t \sum_j (S_j^+ S_{j+1}^- + S_{j+1}^- S_j^+) + \sum_j V_j \left( S_j^+ S_j^- - \frac{1}{2} \right) + \sum_j U_j \left( S_j^+ S_j^- - \frac{1}{2} \right) \left( S_{j+1}^+ S_{j+1}^- - \frac{1}{2} \right).$$

We set  $t = \frac{J_{xy}}{2}$ ,  $V_j = h_j$ ,  $U_j = \Delta_j$  and we obtain

$$H_{XXZ} = \frac{J_{xy}}{2} \sum_j (S_j^+ S_{j+1}^- + S_j^- S_{j+1}^+) + \sum_j h_j S_j^z + \sum_j \Delta_j S_j^z S_{j+1}^z. \quad (4.5)$$

The exchange interaction is  $J_{xy}$ ,  $h$  is the transverse magnetic field and  $\Delta$  is the strength of interaction. The interacting fermionic (spin independent) problem has been mapped to a model of interacting spins. The number of sites  $N$  is equal to the number of spins.

The spin operators  $S^z, S^\pm$  are expressed as

$$S^z |s, m_s\rangle = \hbar m_s |s, m_s\rangle \quad , \quad S^\pm |s, m_s\rangle = \hbar \sqrt{s(s+1) - m_s(m_s \pm 1)} |s, m_s \pm 1\rangle. \quad (4.6)$$

For  $s = \frac{1}{2}$ ,  $m = \pm \frac{1}{2}$  and  $\hbar = 1$  we have

$$S^z |m\rangle = m |m\rangle \quad , \quad S^+ |m\rangle = \left( \frac{1}{2} - m \right) |m+1\rangle \quad , \quad S^- |m\rangle = \left( \frac{1}{2} + m \right) |m-1\rangle. \quad (4.7)$$

In general, the matrix elements given in [72] are

$$\begin{aligned}
 \frac{J}{2} \langle m_j m_{j+1} | S_j^+ S_{j+1}^- | m'_j m'_{j+1} \rangle &= \\
 &= \frac{J}{2} \langle m_j | S_j^+ | m'_j \rangle \langle m_{j+1} | S_{j+1}^- | m'_{j+1} \rangle \\
 &= \frac{J}{2} \left( \frac{1}{2} - m'_j \right) \left( \frac{1}{2} + m'_{j+1} \right) \delta_{m_j, m'_j+1} \delta_{m_{j+1}, m'_{j+1}-1},
 \end{aligned} \tag{4.8}$$

$$\begin{aligned}
 \frac{J}{2} \langle m_j m_{j+1} | S_j^- S_{j+1}^+ | m'_j m'_{j+1} \rangle &= \\
 &= \frac{J}{2} \langle m_j | S_j^- | m'_j \rangle \langle m_{j+1} | S_{j+1}^+ | m'_{j+1} \rangle \\
 &= \frac{J}{2} \left( \frac{1}{2} + m'_j \right) \left( \frac{1}{2} - m'_{j+1} \right) \delta_{m_j, m'_j-1} \delta_{m_{j+1}, m'_{j+1}+1},
 \end{aligned} \tag{4.9}$$

$$\begin{aligned}
 J \langle m_j m_{j+1} | S_j^z S_{j+1}^z | m'_j m'_{j+1} \rangle &= \\
 &= J \langle m_j | S_j^z | m'_j \rangle \langle m_{j+1} | S_{j+1}^z | m'_{j+1} \rangle \\
 &= J m'_j m'_{j+1} \delta_{m_j, m'_j} \delta_{m_{j+1}, m'_{j+1}},
 \end{aligned} \tag{4.10}$$

where  $\delta$  here is the Dirac Delta function.

As an example, we solve the case of  $N = 2$  sites/spins. For simplicity, we set  $h_j = 0$  and  $J_{xy} = \Delta_j = J$ . The total number of configurations is  $2^N = 4$ :  $\{ | \uparrow\uparrow \rangle, | \uparrow\downarrow \rangle, | \downarrow\uparrow \rangle, | \downarrow\downarrow \rangle \}$ . Working in the subsector where  $\mathcal{S}^z = 0$ , the possible configurations are now reduced to  $M = N!/(N/2)!^2 = 2$ , namely:  $\{ | \uparrow\downarrow \rangle, | \downarrow\uparrow \rangle \}$ .

For the case of  $N = 2$  spins we have  $m_1 = m'_1 = \frac{1}{2}$  and  $m_2 = m'_2 = -\frac{1}{2}$ . The matrix elements are

$$\begin{aligned}\langle \uparrow\downarrow | H | \uparrow\downarrow \rangle &= -\frac{J}{4} = H_{11} \\ \langle \downarrow\uparrow | H | \downarrow\uparrow \rangle &= -\frac{J}{4} = H_{22} \\ \langle \uparrow\downarrow | H | \downarrow\uparrow \rangle &= \frac{J}{2} = H_{12} \\ \langle \downarrow\uparrow | H | \uparrow\downarrow \rangle &= \frac{J}{2} = H_{21}.\end{aligned}$$

The Hamiltonian in the spin configuration basis becomes

$$H_{(N=2)} = \begin{pmatrix} H_{11} & H_{12} \\ H_{21} & H_{22} \end{pmatrix} = \frac{J}{4} \begin{pmatrix} -1 & 2 \\ 2 & -1 \end{pmatrix},$$

with eigenvalues  $E_j = \{-0.75J, 0.25J\}$

In this work, to study MBL we explored the case where the magnetic field  $h$  and the interaction strength  $\Delta$  are random variables [85, 86]. The first kind of disorder corresponds to static magnetic fields of amplitude  $h_j$ , where  $h_j$  are random numbers from a uniform distribution  $[-W, W]$ ,  $W$  is the strength of disorder. The second disorder corresponds to varying interaction  $\Delta_j$ , where  $\Delta_j$  are random numbers from a distribution  $[0, \delta]$ ,  $\delta$  is the strength of the interaction. The total spin in the z-direction is conserved,  $\mathcal{S}^z = \sum_j S_j^z = 0$  and we choose for our analysis the largest subsector,  $(\mathcal{S}^z = 0)$  with dimension  $M = N!/(N/2)!^2$ . Open boundary conditions are considered for  $N$  sites and equal number of spins.

We perform exact diagonalization of the Hamiltonian for even sizes  $N$ , from  $N = 8$  to  $N = 16$ . We examine the full many-body spectrum at the "infinite temperature limit" where the energy density is higher. We keep the 10% of the states at the centre of the spectrum to search for the existence of the transition. Table 4.1 contains the numerical data of our calculations.

sites/spins $N$	$\dim(H) = 2^N$	$\dim(H_{\text{subsector}}) = N!/(N/2)!^2$	$E_{\text{kept}}$	realizations
8	256	70	8	14000
10	1024	252	24	4200
12	4096	924	92	1100
14	16384	3432	344	290
16	65536	12870	1288	77

Table 4.1: The numerical data including the system size  $N$ , the dimension of many-body Hilbert space, the dimension  $M$  of the used subsector, the number of levels from the centre of the spectrum and the number of realizations. The ensemble contains approximately  $10^5$  configuration data.

### 4.3 Level Statistics

The first and more natural distinction between ergodicity and localization is to calculate the spectral statistics between the energy eigenvalues. Instead of examining the many-body energy spacings  $S$  and their distribution  $P(S)$ , we focus on the recently proposed  $P(r)$  distribution [87, 88]. The reason is that we need to perform an unfolding transformation for the energies because their density is not everywhere the same. It is possible to circumvent this difficulty by introducing a new quantity to describe the energy levels. Let  $\{E_n\}$  be the set of the many-body energies in ascending order and  $S_n = E_{n+1} - E_n \geq 0$ , the nearest-neighbor spacings. We define the adjacent gap ratio as

$$r_n = \frac{S_{n+1}}{S_n}. \quad (4.11)$$

This quantity requires no unfolding since the ratios of adjacent level spacings are independent of the local density of states and therefore a practical measure of level fluctuations. The  $P(r)$  distribution for the GOE matrix ensemble is

$$P_{GOE}(r) = \frac{27}{8} \frac{r + r^2}{(1 + r + r^2)^{5/2}}, \quad (4.12)$$

whereas for the Poisson distribution is

$$P_{Poisson}(r) = \frac{1}{(1 + r)^2}. \quad (4.13)$$

The two distributions are plotted in Fig.4.1.

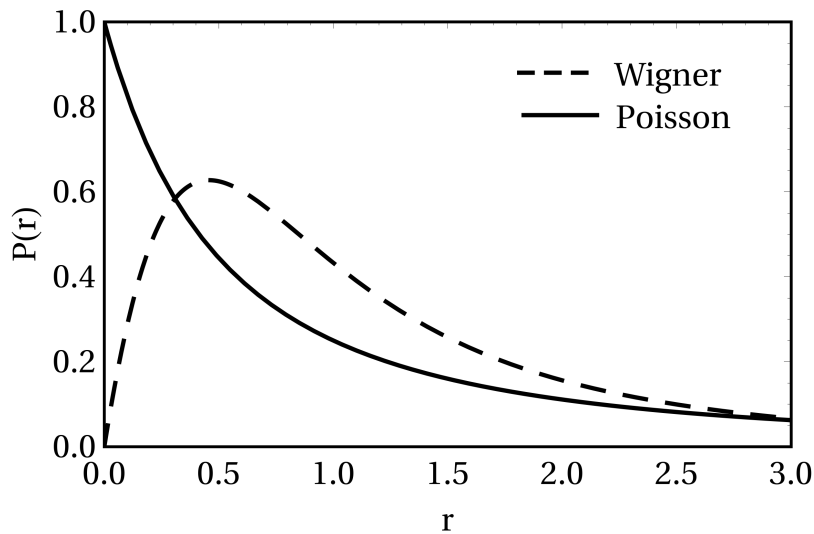


Figure 4.1:  $P(r)$  distributions for Wigner-Dyson (dashed line) and Poisson (solid line).

In addition to  $r_n$ , one can calculate the distribution of  $\tilde{r}_n$  where:

$$\tilde{r}_n = \frac{\min(S_n, S_{n-1})}{\max(S_n, S_{n-1})} = \min\left(r_n, \frac{1}{r_n}\right). \quad (4.14)$$

It is particularly useful to consider the averages of  $r_n$  and  $\tilde{r}_n$ . For GOE  $\langle r_n \rangle = 1.75$  and for Poisson  $\langle r_n \rangle = \infty$ . Moreover, we have  $\langle \tilde{r}_n \rangle = 4 - 2\sqrt{3} = 0.536$  for GOE and  $\langle \tilde{r}_n \rangle = 2\ln 2 - 1 = 0.386$  for Poisson.

We begin our analysis for the level statistics with the phase diagram of  $\langle \tilde{r}_n \rangle$  in Fig.4.2 when the disorder strengths  $W$  and  $\delta$  are varying.

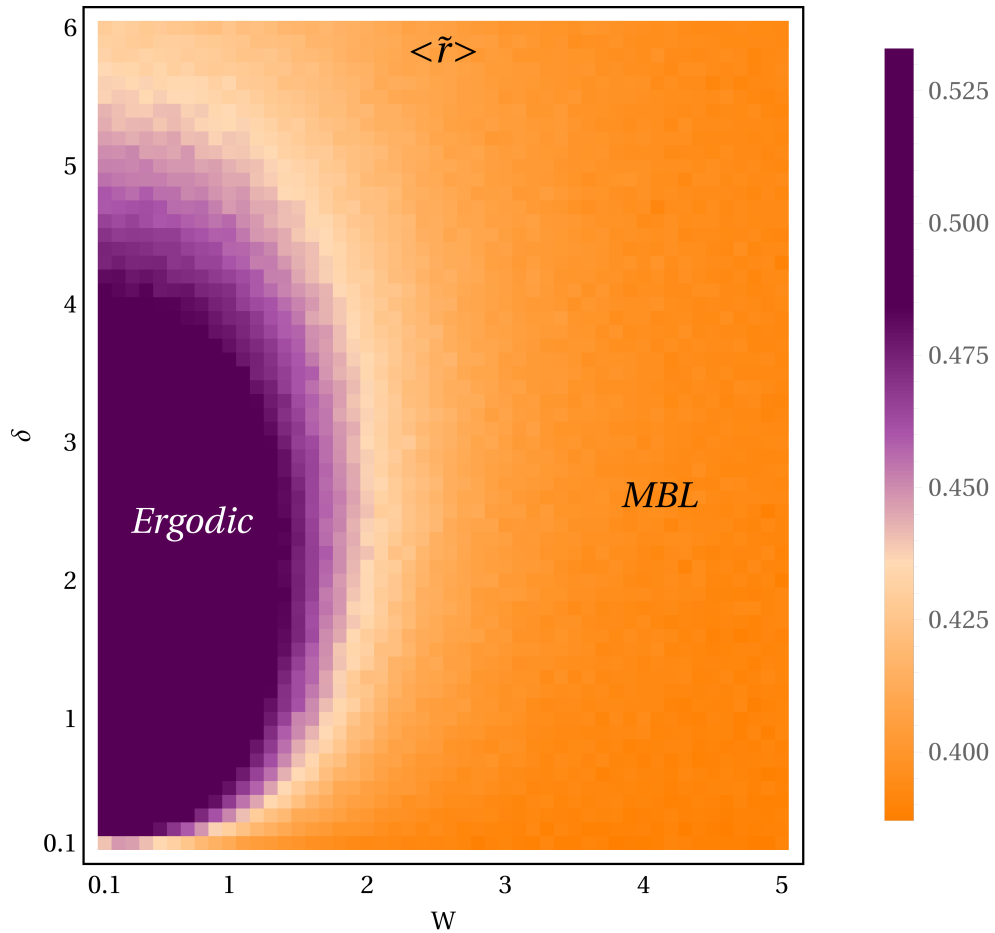


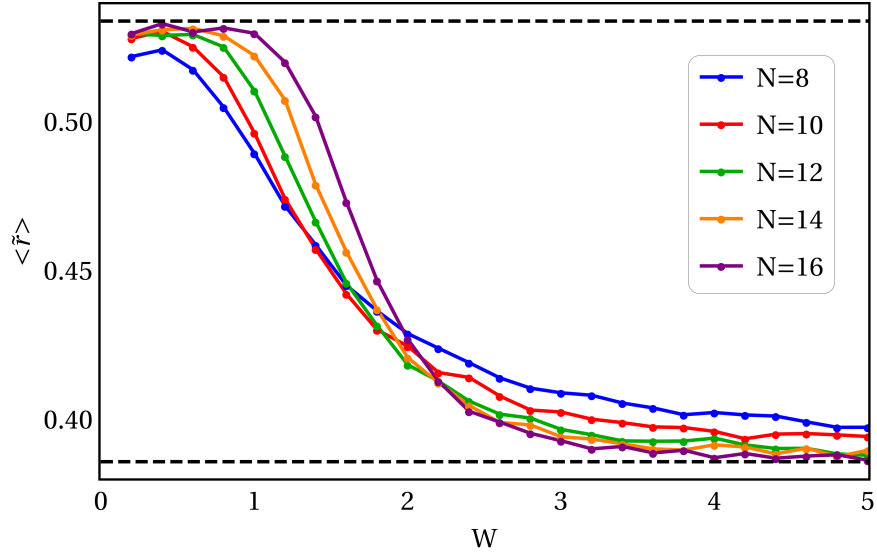
Figure 4.2: Phase diagram of  $\langle \tilde{r}_n \rangle$  as a function of  $W$  and  $\delta$  for a spin chain of size  $N=12$ .

Our simulations suggest the existence of two clearly distinct regions. The ergodic region (purple color) and the MBL region (orange color). For the current system size ( $N=12$ ), we observe that the two regions separate at a disorder strength  $W \approx 2$  when moving across the x-direction and a disorder strength  $\delta \approx 6$  when moving across y-direction.

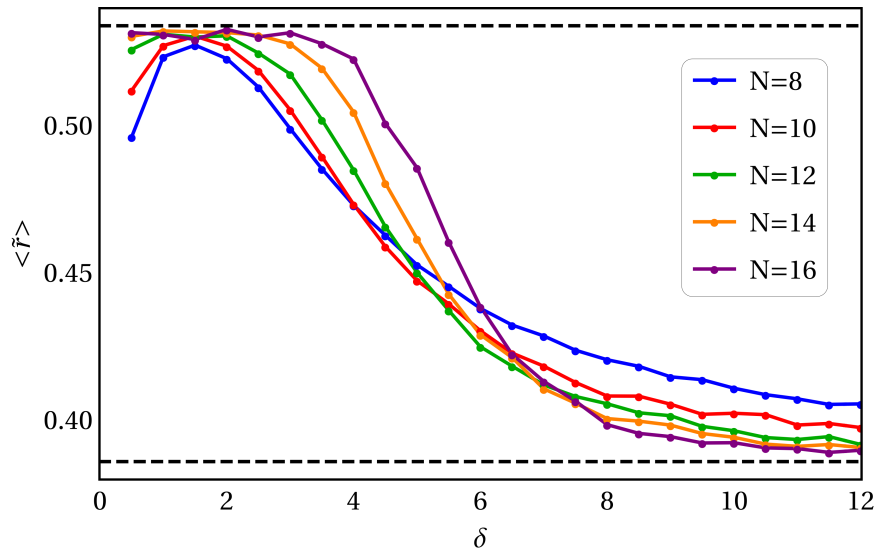
We then perform finite size scaling in order to better locate the transition. The sizes considered vary from  $N = 8$  to  $N = 16$ . The latter is the "computational limit" of exact diagonalization in these systems. In Fig.4.3(a) we show level statistics by setting  $\delta = 1$  and varying  $W$ , whereas in Fig.4.3(b),  $W = 0.5$  and  $\delta$  varies.

The crossings in both cases give a rough estimate of the locations  $W_c$  and  $\delta_c$  of the transitions. As can be seen from the figures, we get  $W_c \in [1.5, 2.5]$  and  $\delta_c \in [5.5, 7.5]$ . We observe a kind of drifting towards larger values of  $W$  and  $\delta$  as the size  $N$  increases. At the largest size considered  $N = 16$ , we clearly see the crossings around  $W_c \approx 2.4$  and  $\delta_c \approx 7$  respectively.

The results are close to those calculated for the "standard model" of MBL [21]. In that model, a 1D spin-1/2 chain is considered with random magnetic fields  $h_i \in [-W, W]$ . The strength of interaction is constant  $\Delta = 1$  and periodic boundary conditions are imposed. For these parameters this model is supposed to exhibit an MBL transition at  $W_c \approx 3.6$ . In our work, additionally to random magnetic field, we choose the interaction strength random and always positive with  $\Delta \in [0, \delta]$ . In that sense, the system has two kinds of disorder and thus we expect a more localized behavior.



(a)



(b)

Figure 4.3: The finite size scaling of the level statistics for (a)  $\delta = 1$ ,  $W$  varies and (b)  $W = 0.5$ ,  $\delta$  varies. The dashed lines are the Wigner-Dyson limit ( $\langle \tilde{r}_n \rangle = 0.536$ ) and the Poisson limit ( $\langle \tilde{r}_n \rangle = 0.386$ ) respectively.

## 4.4 Statistics of Eigenstates

In addition to eigenvalue statistics, information about the system can be received from the eigenstates and their structure [89, 90]. We consider a many-body wavefunction  $|\Psi\rangle = \sum_{j=1}^M \psi_j |j\rangle$  expressed in the basis of the z components of each spin,  $|j\rangle = |S_1 \dots S_N\rangle$  where  $M$  is the dimension of the many-body Hilbert space. The central quantities of our research are the Rényi entropies  $S_q$  for the wavefunction  $|\Psi\rangle$  expressed as

$$S_q = -\frac{1}{q-1} \ln \left( \sum_{j=1}^M |\psi_j|^{2q} \right), \quad q \in (-\infty, \infty). \quad (4.15)$$

In the limit  $M \rightarrow \infty$ , we obtain the multifractal dimensions  $D_q$  defined in Eq.1.12.

For  $q = 2$  the Rényi entropy  $S_2 = -\ln(IPR)$  includes the known inverse participation ratio (IPR) defined in Eq.1.15 which measures the delocalization of a many-body state in the many-body Hilbert space. In the case considered here, we observe states of 3 different kinds,

- *Ergodic states:*  $IPR \propto M^{-1}$
- *Extended non-Ergodic states:*  $IPR \propto M^{-D_2}$ ,  $D_2 < 1$
- *Localized states:*  $IPR \propto \mathcal{O}(1)$

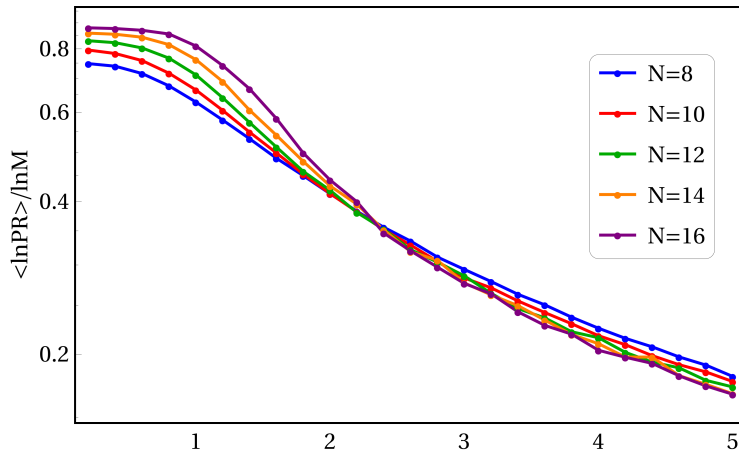
For the special case with  $q \rightarrow 1$ ,  $S_1$  is the Rényi entropy which coincides with the Shannon Entropy ( $S$  or  $S_{SH}$ )

$$S_{SH} = -\sum_{j=1}^M |\psi_j|^2 \ln |\psi_j|^2, \quad (4.16)$$

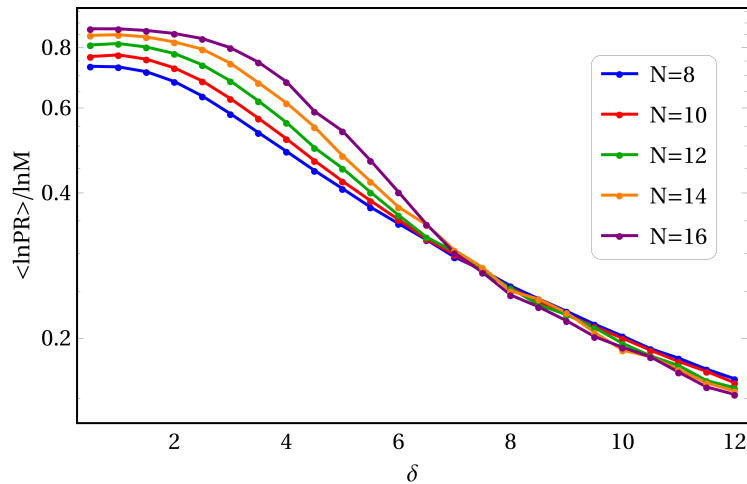
another measure for the localization.

### 4.4.1 Participation Ratio

In this section we provide numerical results for the Participation Ratio (PR). For a fully localized many-body eigenstate we have  $PR = 1$  and if  $|\Psi\rangle$  is a fully ergodic state, then  $PR = M$ . In particular, we study the scaling of the quantity  $\frac{\langle \ln PR \rangle}{\ln M}$  as a function of disorder strength  $W$  and  $\delta$ , respectively by varying the system size  $N$ . The results are shown in Fig.4.4.



(a)



(b)

Figure 4.4: The finite size scaling  $\frac{\langle \ln PR \rangle}{\ln M}$  for (a)  $\delta = 1$ ,  $W$  varies and (b)  $W = 0.5$ ,  $\delta$  varies.

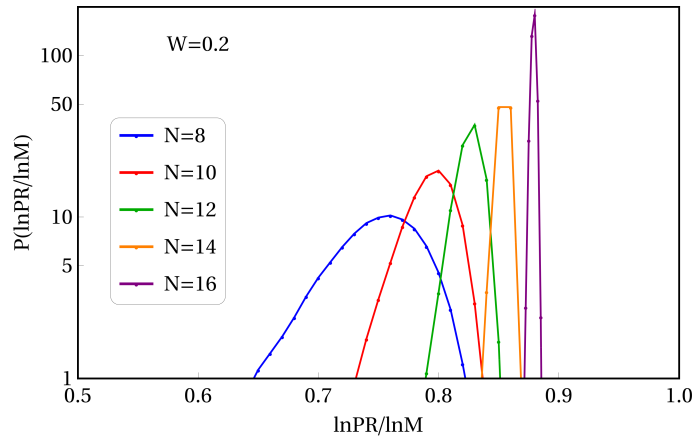
We observe a crossing point around the neighborhood of the critical disordered strength  $W_c = 2.4$  and  $\delta = 7$  respectively which strongly supports our findings from the level statistics. To better visualize and understand the behavior on both sides of the crossings we studied the distribution of  $\ln PR$  for  $W = 0.2$  in the ergodic region and for  $W = 5$  in the localization region. We also did the same for the argued critical disordered strength  $W = 2.4$ . Disorder strength  $\delta = 1$  fixed. The results are shown in Fig.4.5.

The same procedure is repeated when  $\delta$  varies and  $W = 0.5$  fixed. We plot the distribution of  $\ln PR$  for  $\delta = 1$  in the ergodic region, for  $\delta = 12$  in the localized region and for  $\delta = 7$  at the second estimated critical point. The results are presented in Fig.4.6. From Fig.4.5 (a) and (c) we clearly observe a different behavior between the ergodic and the localized regions. For the critical region in Fig.4.5 (b) a somehow intermediate picture is obtained. There also exist quantitative finite size effects that may not be taken under consideration. The same behavior is observed in Fig.4.6 where the finite size effects also exist.

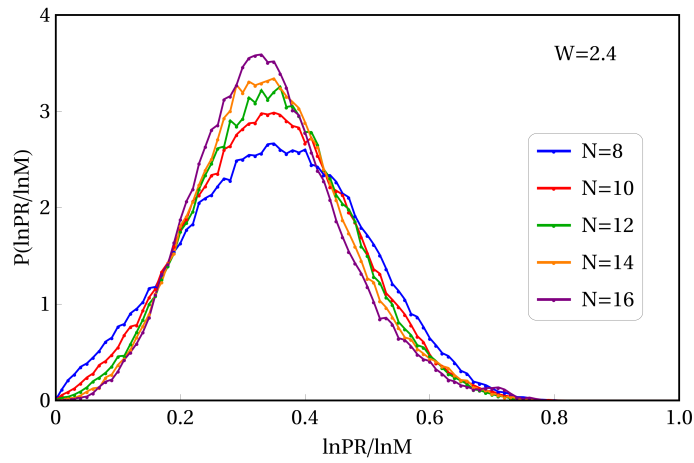
We also study the variance of  $\ln PR$  given by the relation

$$Var(\ln PR) = \langle (\ln PR)^2 \rangle - \langle \ln PR \rangle^2. \quad (4.17)$$

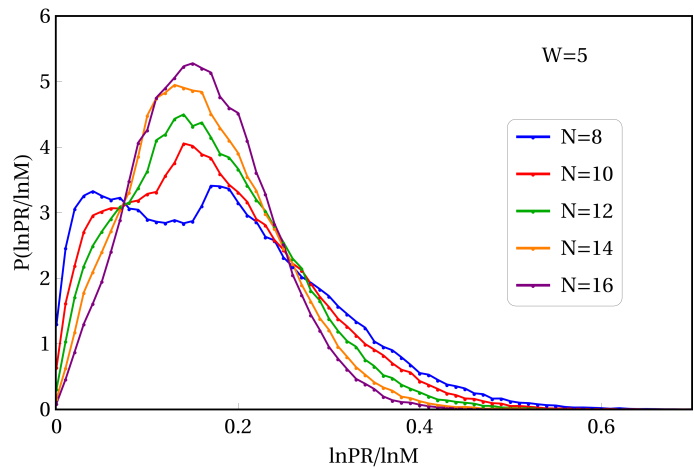
This quantity should vanish in a strongly delocalized or localized region but is expected to have a peak near the crossover point due to the coexistence of ergodic and non-ergodic states [91]. This is also true in our case where the peak is drifting closer to the critical point as the size  $N$  increases. However, the variance does not completely vanishes at the localized region up to the considered strengths  $W, \delta$ .



(a)



(b)



(c)

Figure 4.5: The distribution of  $\ln PR$  for sizes  $N=8,10,12,14,16$  and  $\delta = 1$ . (a) ergodic region for  $W = 0.2$ , (b) estimated critical point  $W \approx 2.4$ , (c) localized region for  $W = 5$

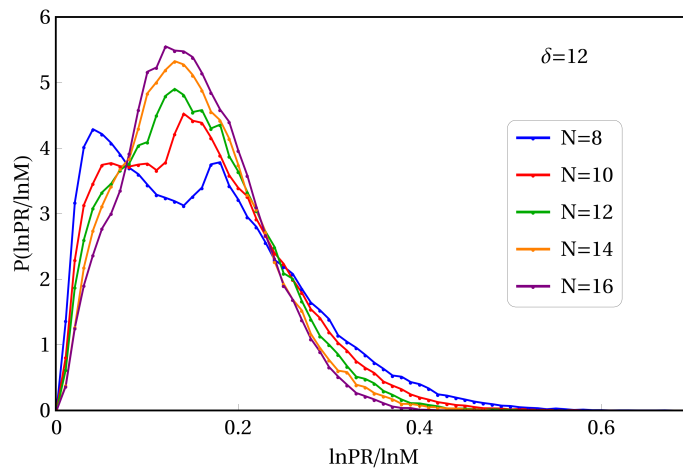
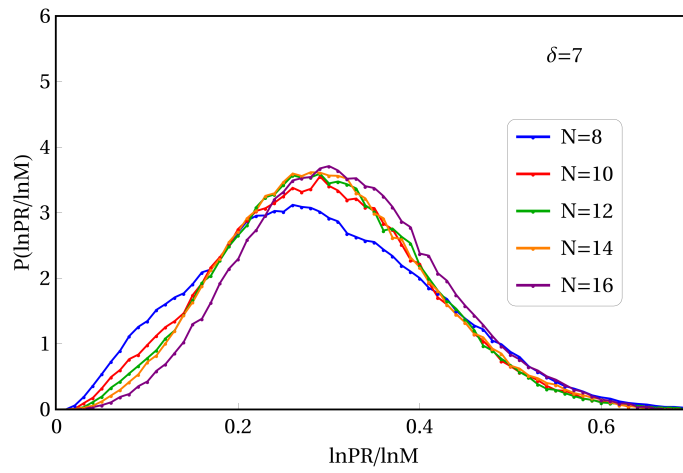
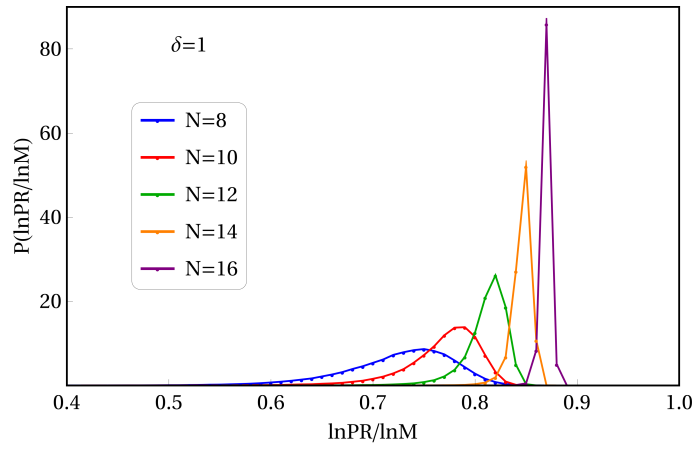
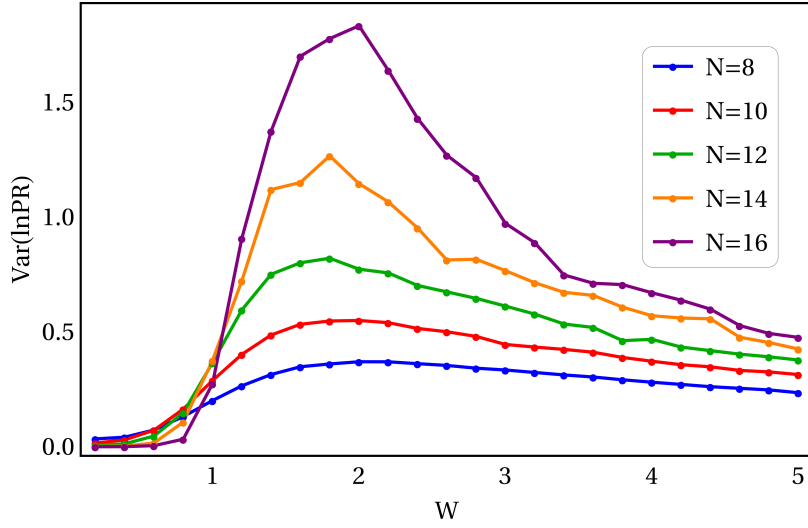
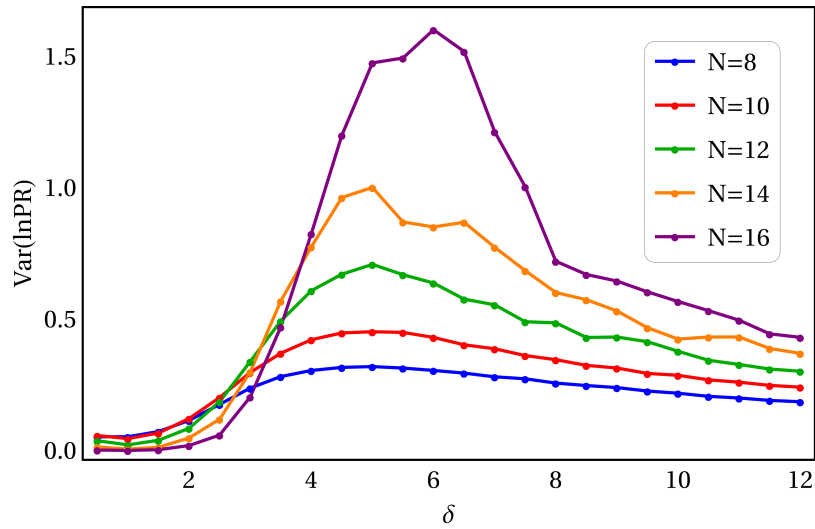


Figure 4.6: The distribution of  $\ln PR$  for sizes  $N=8,10,12,14,16$  and  $\delta = 1$ . (a) ergodic region for  $\delta = 1$ , (b) estimated critical point  $\delta \approx 7$ , (c) localized region for  $\delta = 12$



(a)

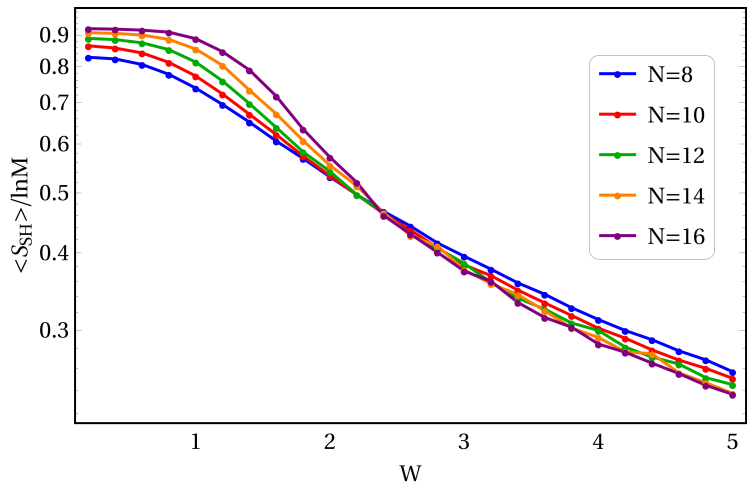


(b)

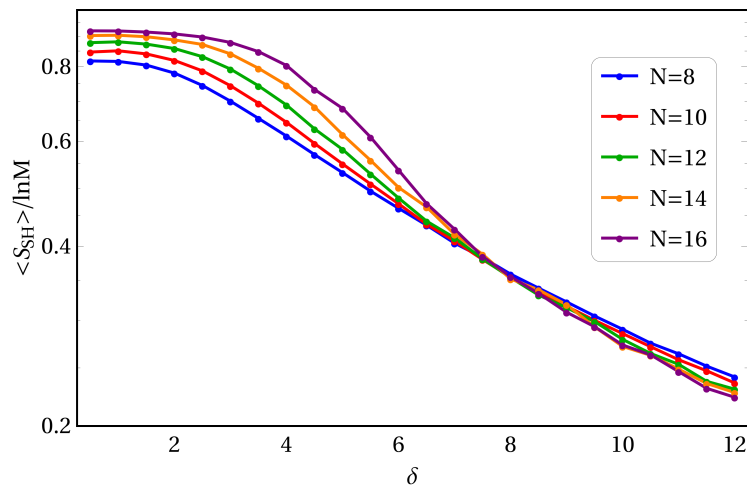
Figure 4.7: The  $\text{Var}(\ln PR)$  of Eq.4.17 for  $N=8, 10, 12, 14, 16$  when (a)  $\delta = 1$ ,  $W$  varies and (b)  $W = 0.5$ ,  $\delta$  varies.

### 4.4.2 Shannon Entropy

In Fig.4.8(a) and (b) we present the numerical results for the scaled Shannon entropy  $\frac{\langle S_{SH} \rangle}{\ln M}$  as a function of  $W$  and  $\delta$ , respectively, for different system sizes  $N$ . As it is stressed here [76], the computational advantage of Shannon entropy makes it a preferable option giving similar results as the von Neumann entanglement entropy which is widely used in the MBL problem.



(a)



(b)

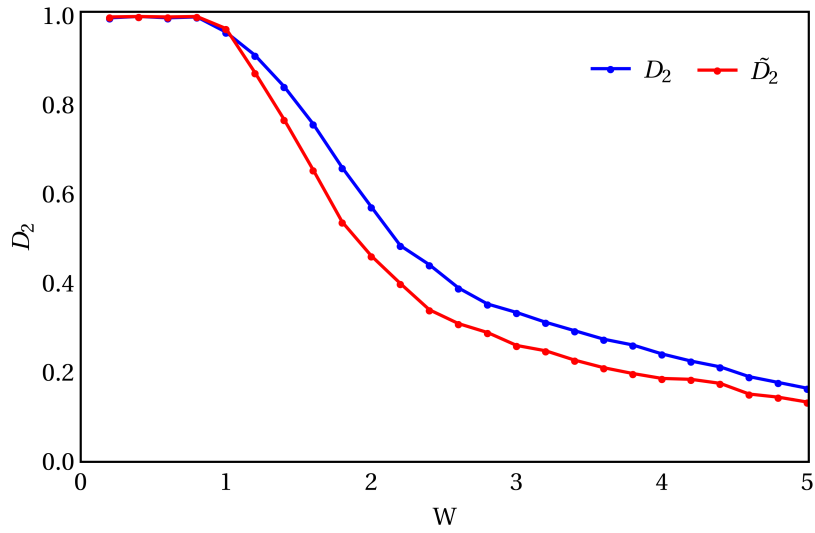
Figure 4.8: The scaled Shannon entropy  $\frac{\langle S_{SH} \rangle}{\ln M}$  for  $N=8,10,12,14,16$  when (a)  $\delta = 1$ ,  $W$  varies and (b)  $W = 0.5$ ,  $\delta$  varies.

The results are quite similar to those of the previously calculated participation ratio. In Fig.4.8(a) the crossings happen at  $W_c \approx 2.4$ . In Fig.4.8(b) we rather observe a slight difference with the crossings taking place to value closer to  $\delta \approx 7.5$ . There is a small shift of the previously argued crossing point of  $\delta \approx 7$ .

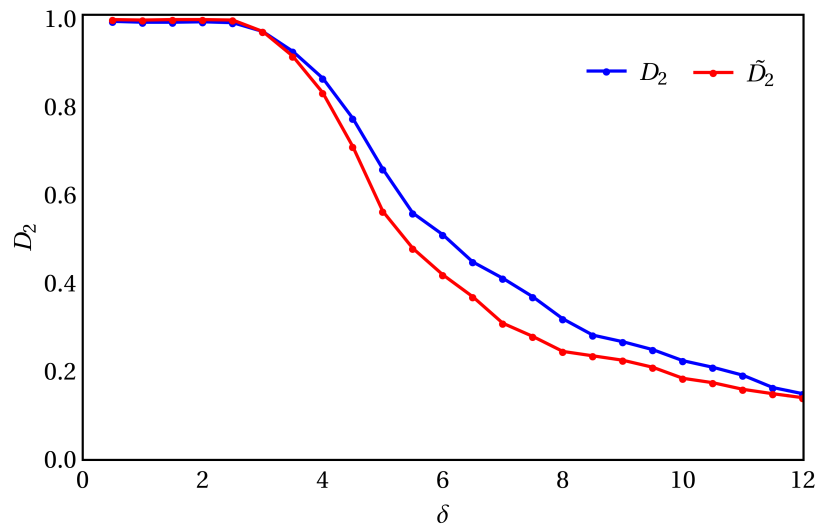
### 4.4.3 Multifractality

To further explore the effect of both kinds of disorder on the correlation dimension  $D_2$  we plot it as a function of  $W$  and  $\delta$ . The result is shown in Fig.4.9. The fractal dimension  $D_2$  will approach asymptotically to zero as  $W$  and  $\delta$  becomes very large. Besides the  $\langle IPR \rangle$ , we also calculate for the  $e^{\langle IPR \rangle}$  from which the fractal dimension  $\tilde{D}_2$  is calculated. The two curves are not the same and this is an implication that the system undergoes a "freezing" transition. Moreover, in both cases it is apparent that the two dimensions  $D_2$  and  $\tilde{D}_2$  vary the most at the neighborhood of the critical point. Therefore, we argue that the states in this region are extended but non-ergodic, as they are not being able to cover the whole many-body space.

In Fig.4.9(a) we observe that for  $W < 1$  the two fractal dimensions are equal,  $D_2 = \tilde{D}_2 = 1$ . For  $W > 1$ , as we leave the strongly ergodic phase, we reach the intermediate critical region where  $D_2 = \tilde{D}_2 \approx 0.5$ . For larger  $W$ , the values seem to decrease significantly but they do not vanish at least until the disorder value considered. In Fig.4.9(b), the fully ergodic region exists for  $\delta < 3$  for both dimensions, whereas near the critical point  $D_2 = \tilde{D}_2 = 0.4$ . For larger values of  $\delta$ , the dimensions  $D_2, \tilde{D}_2$  are getting closer to each other both approaching zero.



(a)



(b)

Figure 4.9: The multifractal dimension  $D_2$  and  $\tilde{D}_2$  (a)  $\delta = 1$ ,  $W$  varies and (b)  $W = 0.5$ ,  $\delta$  varies.

## 4.5 Summary

We have analyzed the static properties for a finite 1D spin-1/2 chain with random magnetic fields and random interaction. For the random magnetic field, we identified a critical disorder strength  $W_c \approx 2.4$  and for the random interaction a critical disorder strength  $\delta_c \approx 7$ . These points separate two totally distinct regions, the ergodic and the many-body localized, respectively. The calculation of level statistics for different sizes gives an indication of where the ergodic and MBL phases separate. The ergodic phase is characterized by Wigner-Dyson level statistics whereas the MBL phase has Poisson level statistics. We performed finite size scaling of the participation ratio and the Shannon entropy to better locate the crossing points based on the structure of many-body wavefunctions. Our results support those from the studied level statistics. We also examined the multifractal dimensions  $D_2$  and  $\tilde{D}_2$  of the many-body wavefunctions. We observe that near the critical disorder strengths the states are extended but non-ergodic with  $0 < D_2, \tilde{D}_2 < 1$ .



# Chapter 5

## Conclusions

This thesis studies the effect of disorder in specific condensed matter systems. The work is separated into three main parts.

The first part concerns the presence of bond disorder which preserves chiral (or sublattice) symmetry. We focus on the behavior of the  $E = 0$  state which exists only for odd system sizes  $N$ . We treat it both analytically and numerically. The  $\Psi_{E=0}$  state decays subexponentially opposed to the phenomenon of Anderson localization where under disorder a wavefunction shows an exponential decay. The scaling with the logarithm of the system size  $N$  of the  $\ln\langle IPR \rangle$  and  $\langle \ln IPR \rangle$  gives the correlation fractal dimensions  $D_2$  and  $\tilde{D}_2$ , respectively. The dimensions  $D_2$  and  $\tilde{D}_2$  measure the spatial extent of the wavefunction and define its multifractal character. For weak disorder ( $W \rightarrow 0$ )  $E = 0$  state is extended ( $D_2, \tilde{D}_2 \rightarrow 1$ ) and for very strong disorder it is localized ( $D_2, \tilde{D}_2 \rightarrow 0$ ). For intermediate values of disorder the correlation dimensions are intermediate to 0 and 1 and signify the multifractality of the  $E = 0$  state. The energy level statistics of the system near the specific  $E = 0$  energy is also studied. Interestingly, we find a faster approach to localization for even  $N$  system sizes in comparison with the odd  $N$  sizes.

For a square lattice the  $\Psi_{E=0}$  state exhibits multifractal characteristics for sizes below the large localization length. For weak disorder ( $W \rightarrow 0$ ), the  $E = 0$  state is extended

( $D_2, \tilde{D}_2 \rightarrow 2$ ) and for very strong disorder it is localized ( $D_2, \tilde{D}_2 \rightarrow 0$ ). For intermediate values of disorder, we find  $0 < D_2, \tilde{D}_2 < 2$ . We have also calculated the energy level statistics near  $E = 0$ . For odd  $L$  system sizes a scale-invariant Wigner distribution is obtained whereas for even  $N$  systems a distribution intermediate to Wigner and Poisson is found. The even-odd asymmetry and zero modes in disordered systems are important for understanding the nature of the critical  $E = 0$  mode.

The second part shows the interplay between disorder and topology. We consider a p-wave superconductor with bond disorder in one dimension. This kind of system has been proposed for use in quantum computing. In the absence of disorder, this system hosts two topologically protected Majorana modes localized at the two ends of the chain. Our motivation is to study the fate of the special Majorana states under disorder. Due to the inherent particle-hole symmetry of the superconductor, the system consists of two chains, one for electrons and one for holes. We first find an even-odd asymmetry between even  $L$  and odd  $L$  chains. A double degeneracy at  $E = 0$  exists for the odd case only and not for the even case. The calculation of level statistics near the  $E = 0$  again reveals a faster approach to localization for even  $L$  and not for odd  $L$  systems. Our results resemble the case of off-diagonal disorder ( $\Delta = 0$ ) studied in Ch.2. Moreover, an analytical expression for the wavefunction of the  $E = 0$  state was derived via the transfer matrix method. The scaling with the logarithm of the system size  $L$  of  $\ln\langle IPR \rangle$  and  $\langle \ln IPR \rangle$  gives the correlation dimension  $D_2, \tilde{D}_2$ . In the absence of disorder the Majorana modes are localized at the two ends of the chain with  $D_2 = \tilde{D}_2 = 0$ . As disorder increases the Majorana states lose their topological protection and spread into the lattice.

The third part is focused on the interplay of disorder and interactions. We study a many-body problem in a lattice of randomly interacting fermions in the presence of a random

potential. This problem is equivalent to a spin-1/2 chain with random magnetic fields of strength  $W$  and random interactions of strength  $\delta$ . The motivation is to study the phenomenon known as Many-Body Localization (MBL) which occurs in the presence of both interactions and disorder. Due to the exponentially large Hilbert space of the many-body system the problem poses a computational challenge. We perform exact diagonalization and examine the centre of the many-body spectrum where the energy density of states is higher. The level statistics is calculated. Our simulations suggest the existence of a transition between two clearly distinct phases. An ergodic phase characterized by Wigner statistics and a many-body localized (MBL) phase characterized by Poisson statistics. In the considered kinds of disorder we identify two critical points, one at  $W_c \approx 2.4$  for the random magnetic field and another at  $\delta_c \approx 7$  for the random interaction. We also study the statistics of the many-body eigenstates. The finite size scaling of the  $\langle \ln IPR \rangle$  supports the findings from the eigenvalue statistics concerning the estimated values for the critical points. Moreover, at the critical points we study the whole distributions  $P(\ln IPR)$  which are almost scale-invariant. Finally, we examine the correlation dimensions  $D_2$  and  $\tilde{D}_2$ . For weak disorder  $W$  the states are fully ergodic and near the critical point they are multifractal resulting in intermediate correlation dimensions  $0 < D_2, \tilde{D}_2 < 1$ . For weak disorder  $\delta$  the states again are fully ergodic and near the critical point they become multifractal with intermediate correlation dimensions.

#### *Future Outlook*

First, it will be interesting to study the effect of disorder in other kinds of topological systems involving different symmetries e.g. in the presence of spin-orbit interaction. The disordered systems this thesis dealt with are realized in the laboratory with ultracold atoms and laser techniques which create the disorder with modulated beams [45, 46, 49, 47]. This leads to the engineering of new materials for quantum information processing and technol-

ogy. Moreover, the problem of many-body localization considered here can be generalized in higher dimensions where the situation is currently unclear [92, 93, 94]. The questions concerning the very nature and the existence of the ergodic to MBL transition remain unanswered. The many-body Hilbert space is exponentially large and there is a research interest in statistical methods for spectra and wavefunctions to distinguish between ergodicity and localization. Finally, we could explore other directions in the numerical part by developing new and/or more efficient algorithms in order to reduce the computational cost and improve the current precision. In the last few years, novel techniques involving supervised/unsupervised machine learning and neural network training have begun to contribute in the field by exploring exotic phases of matter and predict differences between them [95, 96, 97, 98, 99].

# Bibliography

- [1] P. W. Anderson, “Absence of diffusion in certain random lattices,” *Phys. Rev.*, vol. 109, pp. 1492–1505, 1958.
- [2] E. Abrahams, *50 Years of Anderson Localization*. WORLD SCIENTIFIC, 2010.
- [3] E. Abrahams, P. W. Anderson, D. C. Licciardello, and T. V. Ramakrishnan, “Scaling theory of localization: Absence of quantum diffusion in two dimensions,” *Phys. Rev. Lett.*, vol. 42, pp. 673–676, 1979.
- [4] E. Wigner, “Random matrices in physics,” *SIAM Review*, vol. 9, no. 1, pp. 1–23, 1967.
- [5] F. J. Dyson, “The threefold way. algebraic structure of symmetry groups and ensembles in quantum mechanics,” *Journal of Mathematical Physics*, vol. 3, no. 6, pp. 1199–1215, 1962.
- [6] M. V. Berry and M. Tabor, “Level clustering in the regular spectrum,” *Proceedings of the Royal Society of London. Series A, Mathematical and Physical Sciences*, vol. 356, no. 1686, pp. 375–394, 1977.
- [7] O. Bohigas, M. J. Giannoni, and C. Schmit, “Characterization of chaotic quantum spectra and universality of level fluctuation laws,” *Phys. Rev. Lett.*, vol. 52, pp. 1–4, 1984.

- [8] M. Imada, A. Fujimori, and Y. Tokura, “Metal-insulator transitions,” *Rev. Mod. Phys.*, vol. 70, pp. 1039–1263, 1998.
- [9] H. Aoki, “Fractal dimensionality of wave functions at the mobility edge: Quantum fractal in the landau levels,” *Phys. Rev. B*, vol. 33, pp. 7310–7313, 1986.
- [10] V. I. Falko and K. B. Efetov, “Statistics of prelocalized states in disordered conductors,” *Phys. Rev. B*, vol. 52, pp. 17413–17429, 1995.
- [11] V. I. Falko and K. B. Efetov, “Multifractality: Generic property of eigenstates of 2d disordered metals,” *Europhysics Letters (EPL)*, vol. 32, pp. 627–632, dec 1995.
- [12] S. N. Evangelou, “Multifractal wavefunctions at the mobility edge,” *Journal of Physics A: Mathematical and General*, vol. 23, pp. L317–L323, apr 1990.
- [13] A. D. Mirlin and F. Evers, “Multifractality and critical fluctuations at the anderson transition,” *Phys. Rev. B*, vol. 62, pp. 7920–7933, 2000.
- [14] A. D. Mirlin, Y. V. Fyodorov, A. Mildenberger, and F. Evers, “Exact relations between multifractal exponents at the anderson transition,” *Phys. Rev. Lett.*, vol. 97, p. 046803, 2006.
- [15] A. Rodriguez, L. J. Vasquez, K. Slevin, and R. A. Römer, “Multifractal finite-size scaling and universality at the anderson transition,” *Phys. Rev. B*, vol. 84, p. 134209, 2011.
- [16] B. B. Mandelbrot, *The fractal geometry of nature*. San Francisco, CA: Freeman, 1982.
- [17] T. C. Halsey, M. H. Jensen, L. P. Kadanoff, I. Procaccia, and B. I. Shraiman, “Fractal measures and their singularities: The characterization of strange sets,” *Phys. Rev. A*, vol. 33, pp. 1141–1151, 1986.

- [18] D. Basko, I. Aleiner, and B. Altshuler, “Metal–insulator transition in a weakly interacting many-electron system with localized single-particle states,” *Annals of Physics*, vol. 321, no. 5, pp. 1126 – 1205, 2006.
- [19] J. M. Deutsch, “Quantum statistical mechanics in a closed system,” *Phys. Rev. A*, vol. 43, pp. 2046–2049, 1991.
- [20] M. Srednicki, “Chaos and quantum thermalization,” *Phys. Rev. E*, vol. 50, pp. 888–901, 1994.
- [21] A. Pal and D. A. Huse, “Many-body localization phase transition,” *Phys. Rev. B*, vol. 82, p. 174411, 2010.
- [22] R. Nandkishore and D. A. Huse, “Many-body localization and thermalization in quantum statistical mechanics,” *Annual Review of Condensed Matter Physics*, vol. 6, no. 1, pp. 15–38, 2015.
- [23] D. A. Abanin and Z. Papić, “Recent progress in many-body localization,” *Annalen der Physik*, vol. 529, no. 7, p. 1700169, 2017.
- [24] D. J. Luitz and Y. B. Lev, “The ergodic side of the many-body localization transition,” *Annalen der Physik*, vol. 529, no. 7, p. 1600350, 2017.
- [25] G. Theodorou and M. H. Cohen, “Extended states in a one-dimensional system with off-diagonal disorder,” *Phys. Rev. B*, vol. 13, pp. 4597–4601, 1976.
- [26] P. Markoš, “The one dimensional anderson model with off diagonal disorder: band centre anomaly,” *Zeitschrift für Physik B Condensed Matter*, vol. 73, no. 1, pp. 17–21, 1988.
- [27] R. Gade and F. Wegner, “The  $n = 0$  replica limit of  $u(n)$  and  $u(n)so(n)$  models,” *Nuclear Physics B*, vol. 360, no. 2, pp. 213 – 218, 1991.

- [28] P. W. Brouwer, E. Racine, A. Furusaki, Y. Hatsugai, Y. Morita, and C. Mudry, “Zero modes in the random hopping model,” *Phys. Rev. B*, vol. 66, p. 014204, 2002.
- [29] P. W. Brouwer, A. Furusaki, C. Mudry, and S. Ryu, “Disorder-induced critical phenomena—new universality classes in Anderson localization,” *arXiv e-prints*, pp. cond-mat/0511622, 2005.
- [30] F. Evers and A. D. Mirlin, “Anderson transitions,” *Rev. Mod. Phys.*, vol. 80, pp. 1355–1417, 2008.
- [31] M. Inui, S. A. Trugman, and E. Abrahams, “Unusual properties of midband states in systems with off-diagonal disorder,” *Phys. Rev. B*, vol. 49, pp. 3190–3196, 1994.
- [32] S. N. Evangelou and D. E. Katsanos, “Spectral statistics in chiral-orthogonal disordered systems,” *Journal of Physics A: Mathematical and General*, vol. 36, no. 12, pp. 3237–3254, 2003.
- [33] A. M. García-García and E. Cuevas, “Anderson transition in systems with chiral symmetry,” *Phys. Rev. B*, vol. 74, p. 113101, 2006.
- [34] P. L. Krapivsky and J. M. Luck, “Dynamics of a quantum particle in low-dimensional disordered systems with extended states,” *Journal of Statistical Mechanics: Theory and Experiment*, vol. 2011, no. 02, p. P02031, 2011.
- [35] Q. Zhao and J. Gong, “From disordered quantum walk to physics of off-diagonal disorder,” *Phys. Rev. B*, vol. 92, p. 214205, 2015.
- [36] G. Paladin and A. Vulpiani, “Anomalous scaling laws in multifractal objects,” *Physics Reports*, vol. 156, no. 4, pp. 147 – 225, 1987.
- [37] Y. V. Fyodorov, “Multifractality and freezing phenomena in random energy landscapes: An introduction,” *Physica A: Statistical Mechanics and its Applications*, vol. 389,

- no. 20, pp. 4229 – 4254, 2010. Proceedings of the 12th International Summer School on Fundamental Problems in Statistical Physics.
- [38] H. E. Roman, “Multifractal analysis of eigenstates in systems with off-diagonal disorder,” *Phys. Rev. B*, vol. 38, pp. 2948–2951, 1988.
- [39] E. Cuevas, “ $f(\alpha)$  multifractal spectrum at strong and weak disorder,” *Phys. Rev. B*, vol. 68, p. 024206, 2003.
- [40] S.-J. Xiong and S. N. Evangelou, “Power-law localization in two and three dimensions with off-diagonal disorder,” *Phys. Rev. B*, vol. 64, p. 113107, 2001.
- [41] A. Eilmes and R. A. Römer, “Exponents of the localization length in the 2d anderson model with off-diagonal disorder,” *physica status solidi (b)*, vol. 241, no. 9, pp. 2079–2088, 2004.
- [42] P. Markoš and L. Schweitzer, “Disordered two-dimensional electron systems with chiral symmetry,” *Physica B: Condensed Matter*, vol. 407, no. 20, pp. 4016 – 4022, 2012. Proceedings of the conference - Wave Propagation: From Electrons to Photonic Crystals and Metamaterials.
- [43] E. J. König, P. M. Ostrovsky, I. V. Protopopov, and A. D. Mirlin, “Metal-insulator transition in two-dimensional random fermion systems of chiral symmetry classes,” *Phys. Rev. B*, vol. 85, p. 195130, 2012.
- [44] P. M. Ostrovsky, I. V. Protopopov, E. J. König, I. V. Gornyi, A. D. Mirlin, and M. A. Skvortsov, “Density of states in a two-dimensional chiral metal with vacancies,” *Phys. Rev. Lett.*, vol. 113, p. 186803, 2014.
- [45] L. Martin, G. D. Giuseppe, A. Perez-Leija, R. Keil, F. Dreisow, M. Heinrich, S. Nolte, A. Szameit, A. F. Abouraddy, D. N. Christodoulides, and B. E. A. Saleh, “Ander-

- son localization in optical waveguide arrays with off-diagonal coupling disorder,” *Opt. Express*, vol. 19, no. 14, pp. 13636–13646, 2011.
- [46] Y. Lahini, Y. Bromberg, Y. Shechtman, A. Szameit, D. N. Christodoulides, R. Morandotti, and Y. Silberberg, “Hanbury brown and twiss correlations of anderson localized waves,” *Phys. Rev. A*, vol. 84, p. 041806, 2011.
- [47] E. Fratini and S. Pilati, “Anderson localization in optical lattices with correlated disorder,” *Phys. Rev. A*, vol. 92, p. 063621, 2015.
- [48] X. Shi, X. Chen, B. A. Malomed, N. C. Panoiu, and F. Ye, “Anderson localization at the subwavelength scale for surface plasmon polaritons in disordered arrays of metallic nanowires,” *Phys. Rev. B*, vol. 89, p. 195428, 2014.
- [49] I. D. Vatnik, A. Tikan, G. Onishchukov, D. V. Churkin, and A. A. Sukhorukov, “Anderson localization in synthetic photonic lattices,” *Scientific Reports*, vol. 7, no. 1, p. 4301, 2017.
- [50] K. v. Klitzing, G. Dorda, and M. Pepper, “New method for high-accuracy determination of the fine-structure constant based on quantized hall resistance,” *Phys. Rev. Lett.*, vol. 45, pp. 494–497, 1980.
- [51] E. Majorana, “Teoria simmetrica dell’elettrone e del positrone,” *Il Nuovo Cimento (1924-1942)*, vol. 14, no. 4, p. 171, 2008.
- [52] F. Wilczek, “Majorana returns,” *Nature Physics*, vol. 5, no. 9, pp. 614–618, 2009.
- [53] M. Leijnse and K. Flensberg, “Introduction to topological superconductivity and majorana fermions,” *Semiconductor Science and Technology*, vol. 27, no. 12, p. 124003, 2012.

- [54] C. Beenakker, “Search for majorana fermions in superconductors,” *Annual Review of Condensed Matter Physics*, vol. 4, no. 1, pp. 113–136, 2013.
- [55] F. Hassler, “Majorana Qubits,” *arXiv e-prints*, p. arXiv:1404.0897, 2014.
- [56] S. D. Sarma, M. Freedman, and C. Nayak, “Majorana zero modes and topological quantum computation,” *Npj Quantum Information*, vol. 1, pp. 15001 EP –, 2015. Review Article.
- [57] A. Altland and M. R. Zirnbauer, “Nonstandard symmetry classes in mesoscopic normal-superconducting hybrid structures,” *Phys. Rev. B*, vol. 55, pp. 1142–1161, 1997.
- [58] F. Haake, *Quantum Signatures of Chaos*. Physics and astronomy online library, Springer, 2001.
- [59] A. P. Schnyder, S. Ryu, A. Furusaki, and A. W. W. Ludwig, “Classification of topological insulators and superconductors in three spatial dimensions,” *Phys. Rev. B*, vol. 78, p. 195125, 2008.
- [60] S. Ryu, A. P. Schnyder, A. Furusaki, and A. W. W. Ludwig, “Topological insulators and superconductors: tenfold way and dimensional hierarchy,” *New Journal of Physics*, vol. 12, no. 6, p. 065010, 2010.
- [61] C.-K. Chiu, J. C. Y. Teo, A. P. Schnyder, and S. Ryu, “Classification of topological quantum matter with symmetries,” *Rev. Mod. Phys.*, vol. 88, p. 035005, 2016.
- [62] G. T. Stamatiou, D. Manolas, and S. N. Evangelou unpublished, 2009.
- [63] A. Y. Kitaev, “Unpaired majorana fermions in quantum wires,” *Physics-Uspokhi*, vol. 44, no. 10S, pp. 131–136, 2001.
- [64] L. Fidkowski and A. Kitaev, “Topological phases of fermions in one dimension,” *Phys. Rev. B*, vol. 83, p. 075103, 2011.

- [65] J. Bardeen, L. N. Cooper, and J. R. Schrieffer, “Theory of superconductivity,” *Phys. Rev.*, vol. 108, pp. 1175–1204, 1957.
- [66] A. Mackenzie and Y. Maeno, “p-wave superconductivity,” *Physica B: Condensed Matter*, vol. 280, no. 1, pp. 148 – 153, 2000.
- [67] E. F. Talantsev, K. Iida, T. Ohmura, T. Matsumoto, W. P. Crump, N. M. Strickland, S. C. Wimbush, and H. Ikuta, “p-wave superconductivity in iron-based superconductors,” *Scientific Reports*, vol. 9, no. 1, p. 14245, 2019.
- [68] M. Z. Hasan and C. L. Kane, “Colloquium: Topological insulators,” *Rev. Mod. Phys.*, vol. 82, pp. 3045–3067, 2010.
- [69] S. Shen, *Topological Insulators: Dirac Equation in Condensed Matter*. Springer Series in Solid-State Sciences, Springer Singapore, 2017.
- [70] J. Alicea, “New directions in the pursuit of majorana fermions in solid state systems,” *Reports on Progress in Physics*, vol. 75, no. 7, p. 076501, 2012.
- [71] L. Li, C. Yang, and S. Chen, “Topological invariants for phase transition points of one-dimensional z2 topological systems,” *The European Physical Journal B*, vol. 89, no. 9, p. 195, 2016.
- [72] S. N. Evangelou, “The numerical analysis of the quantum antiferromagnetic chain: A many-body matrix diagonalization.” Lecture notes and computer programs, 1996.
- [73] F. Alet and N. Laflorencie, “Many-body localization: An introduction and selected topics,” *Comptes Rendus Physique*, vol. 19, no. 6, pp. 498 – 525, 2018. Quantum simulation / Simulation quantique.
- [74] D. A. Abanin, E. Altman, I. Bloch, and M. Serbyn, “Colloquium: Many-body localization, thermalization, and entanglement,” *Rev. Mod. Phys.*, vol. 91, p. 021001, 2019.

- [75] D. J. Luitz, N. Laflorencie, and F. Alet, “Many-body localization edge in the random-field heisenberg chain,” *Phys. Rev. B*, vol. 91, p. 081103, 2015.
- [76] E. J. Torres-Herrera and L. F. Santos, “Extended nonergodic states in disordered many-body quantum systems,” *Annalen der Physik*, vol. 529, no. 7, p. 1600284, 2017.
- [77] M. Schreiber, S. S. Hodgman, P. Bordia, H. P. Lüschen, M. H. Fischer, R. Vosk, E. Altman, U. Schneider, and I. Bloch, “Observation of many-body localization of interacting fermions in a quasirandom optical lattice,” *Science*, vol. 349, no. 6250, pp. 842–845, 2015.
- [78] J. Smith, A. Lee, P. Richerme, B. Neyenhuis, P. W. Hess, P. Hauke, M. Heyl, D. A. Huse, and C. Monroe, “Many-body localization in a quantum simulator with programmable random disorder,” *Nature Physics*, vol. 12, pp. 907 EP –, 2016.
- [79] F. Pietracaprina, N. Macé, D. J. Luitz, and F. Alet, “Shift-invert diagonalization of large many-body localizing spin chains,” *SciPost Phys.*, vol. 5, p. 45, 2018.
- [80] F. Pietracaprina and N. Laflorencie, “Hilbert Space Fragmentation and Many-Body Localization,” *arXiv e-prints*, p. arXiv:1906.05709, 2019.
- [81] E. V. H. Doggen, F. Schindler, K. S. Tikhonov, A. D. Mirlin, T. Neupert, D. G. Polyakov, and I. V. Gornyi, “Many-body localization and delocalization in large quantum chains,” *Phys. Rev. B*, vol. 98, p. 174202, 2018.
- [82] W. Zhang, L. Wang, and Z. Wang, “Interpretable machine learning study of the many-body localization transition in disordered quantum ising spin chains,” *Phys. Rev. B*, vol. 99, p. 054208, 2019.
- [83] Y. Bar Lev, G. Cohen, and D. R. Reichman, “Absence of diffusion in an interacting system of spinless fermions on a one-dimensional disordered lattice,” *Phys. Rev. Lett.*, vol. 114, p. 100601, 2015.

- [84] C. D. Batista and G. Ortiz, “Generalized jordan-wigner transformations,” *Phys. Rev. Lett.*, vol. 86, pp. 1082–1085, 2001.
- [85] R. Vasseur, A. J. Friedman, S. A. Parameswaran, and A. C. Potter, “Particle-hole symmetry, many-body localization, and topological edge modes,” *Phys. Rev. B*, vol. 93, p. 134207, 2016.
- [86] P. Sierant, D. Delande, and J. Zakrzewski, “Many-body localization due to random interactions,” *Phys. Rev. A*, vol. 95, p. 021601, 2017.
- [87] V. Oganesyan and D. A. Huse, “Localization of interacting fermions at high temperature,” *Phys. Rev. B*, vol. 75, p. 155111, 2007.
- [88] Y. Y. Atas, E. Bogomolny, O. Giraud, and G. Roux, “Distribution of the ratio of consecutive level spacings in random matrix ensembles,” *Phys. Rev. Lett.*, vol. 110, p. 084101, 2013.
- [89] Y. Y. Atas and E. Bogomolny, “Multifractality of eigenfunctions in spin chains,” *Phys. Rev. E*, vol. 86, p. 021104, 2012.
- [90] N. Macé, F. Alet, and N. Laflorencie, “Multifractal scalings across the many-body localization transition,” *Phys. Rev. Lett.*, vol. 123, p. 180601, 2019.
- [91] W. Buijsman, V. Gritsev, and V. Cheianov, “Many-body localization in the Fock space of natural orbitals,” *SciPost Phys.*, vol. 4, p. 38, 2018.
- [92] J.-y. Choi, S. Hild, J. Zeiher, P. Schauß, A. Rubio-Abadal, T. Yefsah, V. Khemani, D. A. Huse, I. Bloch, and C. Gross, “Exploring the many-body localization transition in two dimensions,” *Science*, vol. 352, no. 6293, pp. 1547–1552, 2016.
- [93] T. B. Wahl, A. Pal, and S. H. Simon, “Signatures of the many-body localized regime in two dimensions,” *Nature Physics*, vol. 15, no. 2, pp. 164–169, 2019.

- [94] H. Théveniaut, Z. Lan, and F. Alet, “Many-body localization transition in a two-dimensional disordered quantum dimer model,” *arXiv e-prints*, p. arXiv:1902.04091, 2019.
- [95] J. Carrasquilla and R. G. Melko, “Machine learning phases of matter,” *Nature Physics*, vol. 13, pp. 431 EP –, 2017.
- [96] D.-L. Deng, X. Li, and S. Das Sarma, “Machine learning topological states,” *Phys. Rev. B*, vol. 96, p. 195145, 2017.
- [97] P. Zhang, H. Shen, and H. Zhai, “Machine learning topological invariants with neural networks,” *Phys. Rev. Lett.*, vol. 120, p. 066401, 2018.
- [98] E. V. H. Doggen, F. Schindler, K. S. Tikhonov, A. D. Mirlin, T. Neupert, D. G. Polyakov, and I. V. Gornyi, “Many-body localization and delocalization in large quantum chains,” *Phys. Rev. B*, vol. 98, p. 174202, 2018.
- [99] Y.-T. Hsu, X. Li, D.-L. Deng, and S. Das Sarma, “Machine learning many-body localization: Search for the elusive nonergodic metal,” *Phys. Rev. Lett.*, vol. 121, p. 245701, 2018.



*"Vires acquirit eundo"*

Virgil

© Copyright

2020